ROAD TO SEAMLESS POSITIONING: HYBRID POSITIONING SYSTEM COMBINING GPS AND TELEVISION SIGNALS

A DISSERTATION
SUBMITTED TO THE DEPARTMENT OF ELECTRICAL ENGINEERING
AND THE COMMITTEE ON GRADUATE STUDIES
OF STANFORD UNIVERSITY
IN PARTIAL FULFILLMENT OF THE REQUIREMENTS
FOR THE DEGREE OF
DOCTOR OF PHILOSOPHY

Ju-Yong Do
May 2008

I certify that I have read this dissertation and that, in my opinion, it is fully adequate in scope and quality as a dissertation for the degree of Doctor of Philosophy.

Per Enge
(Electrical Engineering) Principal Adviser

I certify that I have read this dissertation and that, in my opinion, it is fully adequate in scope and quality as a dissertation for the degree of Doctor of Philosophy.

Teresa Meng
(Electrical Engineering)

I certify that I have read this dissertation and that, in my opinion, it is fully adequate in scope and quality as a dissertation for the degree of Doctor of Philosophy.

Matthew Rabinowitz
(Aeronautics and Astronautics)

Approved for the University Committee on Graduate Studies.

Abstract

A new type of positioning system that combines the Global Positioning System (GPS) and a television positioning system (TPS) is introduced. GPS is a satellite-based positioning system and has been widely used in navigation systems since its introduction in the 1970s. TPS is a relatively new system introduced in the 2000s which utilizes ground-based broadcast television stations as ranging sources.

In this dissertation, these two positioning systems, GPS and TPS, are combined to achieve seamless positioning service. Seamless coverage includes open spaces and obstructed spaces, urban and rural areas, outdoors, and indoors. GPS provides a global service, good for outdoor activities, but suffers in dense urban and indoor areas. In contrast, although TPS is successful in metropolitan areas, TPS has weaker coverage in rural areas. Because GPS and TPS are complementary in their coverage, an integrated hybrid GPS and TPS positioning system is expected to provide enhanced positioning coverage over the individual systems.

The development and demonstration of the hybrid positioning system is conducted through a comparison of pseudorange formats, a fault detection and exclusion algorithm implementation, a hybrid system implementation, and field tests. First, pseudorange formats, time of arrival (TOA) and a time difference of arrival (TDOA), are compared. Pseudoranges (range measurements with a clock bias) can be represented either in a TOA format or in a TDOA format. TOA is used in GPS while TDOA is used in TPS. Although it is known that there is no difference in positioning accuracy between TOA and TDOA, TOA-based position estimation is shown to provide more robust results under inaccurate measurement statistics and suboptimal system implementation. Thus, TOA is used for both GPS and TPS.

Second, a fault detection and exclusion algorithm is developed. Due to multipath effects in urban canyons and indoors and clock drifts in television transmitters, there exist a large number of outliers, in particular, in TPS pseudoranges. To detect and exclude these outliers, a multi-fault tolerant receiver autonomous integrity monitoring (RAIM) algorithm is proposed. The proposed RAIM combines and implements iterative steps of the multi-hypothesis solution separation (MHSS) test for fault detection and the maximum likelihood test for fault exclusion which are, respectively, based on the algorithms by Pervan and Sturza [70], [72].

Third, a hybrid positioning system which combines GPS and TPS is constructed. The hybrid system is composed of a GPS receiver, a TPS receiver, and Matlab-based position estimation software. Based on pseudorange measurements from the GPS and TPS receivers, the hybrid positioning software estimates a user position and executes the multi-fault tolerant RAIM for outlier removal.

Lastly, the hybrid system is tested through an extensive field test campaign. Thirty nine sites are selected from the San Francisco Bay Area which include outdoors, indoors, urban, suburban, residential, and rural areas. At each location, one hour of stationary data is collected and processed by the hybrid positioning system.

The field test results of the hybrid system (after exclusion of two zero availability urban indoor sites) show substantially improved availability compared to the individual GPS or TPS results. While the GPS availability is fifty-one percent and the TPS availability eighty-two percent, the hybrid system is available ninety percent of the time at the tested locations. Also, after further improvement by time domain filtering and local optimization of RAIM parameters, this availability reaches over ninety-nine percent outdoors and ninety-five percent indoors. The high availability illustrates the potential of the hybrid GPS and TV positioning system as a "road to seamless positioning service." However, the low accuracy in a few harsh environments and the existence of two zero availability sites (out of thirty nine sites) reveal the challenge in urban and indoor areas. These remain as future work.

Acknowledgements

I would like to thank my mother, my wife, Younju, and my two sons, Wonho and Wonyoung, for their love and limitless support.

Contents

List of Tables

List of Figures

Chapter 1

Introduction

GPS is a satellite-based radio positioning system providing both time and position information. However, GPS has not been able to provide seamless coverage. It suffers in urban canyons and indoor areas in spite of huge demands. Hence, to augment GPS and penetrate into these challenging environments, for universal coverage we seek a solution from land-based radio signals [2], [3].

1.1 Motivation and Background

Figure 1.1 illustrates a transition during which mechanical time and position references (traditional wrist watches and compasses) are being replaced by electrical references (GPS positioners). GPS, with enhanced accuracy (tens of meters in position and sub-microseconds in time) allows a solid grasp of our lives in four dimensional space and time. There are numerous examples of GPS applications around us. Internet websites encourages us to post travel photos with GPS tags and present them on a map so that your friends can share your travel experience with a good sense of when and where we have been. Gordon Bell at Microsoft Research Labs has been recording his life with a life-logging device composed of a camera, a microphone and a GPS receiver [9]. The "life-logger," worn by him during most of his day, takes photos and records conversations. These data are time-and-space tagged by the GPS receiver so that the researcher can go back and search a certain part of his life by specifying a

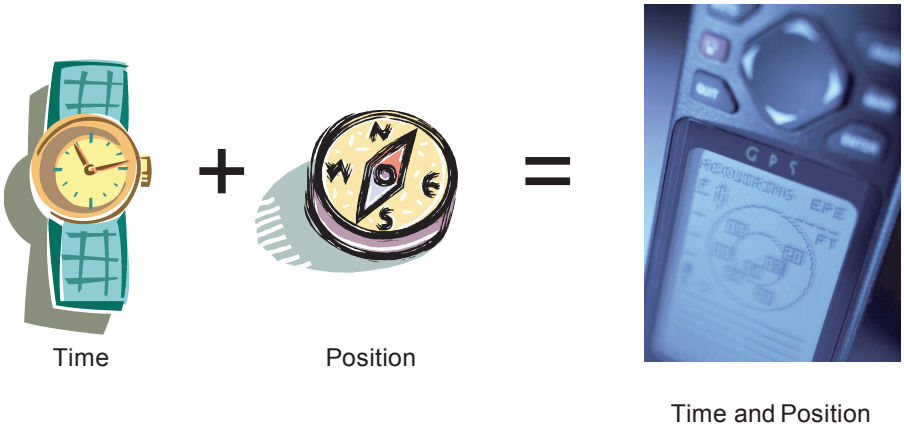

Figure 1.1: Time and position reference

location or a time instance.

Social infrastructures are also increasingly dependent on GPS information. Communication networks, financial systems, and transportation systems are so dependent on GPS location or time information that a GPS outage could jeopardize their operations. Obviously, other nations' ventures into new satellite navigation systems—Galileo (European Union), Compass (China) and QZSS (Japan)—in spite of astronomical price tags, are motivated by the appreciations of personal, social, and national values of a uniform time and position reference [18], [19].

Mindful of these benefits, we seek a positioning service that is continuous in time and space. The biggest challenge to seamless positioning lies in indoor areas and urban canyons where the majority of the population spends most of its time. Multipath and building obstructions make indoor areas and urban canyons an obstacle to seamless positioning service.

A quick comparison with cell phone service—more formally, wireless positioning versus wireless communication—indicates why it is difficult to provide positioning service in urban and indoor environments. Why does a GPS receiver not work everywhere a cell phone works? Both positioning and communication devices commonly use handheld platforms based on wireless radio links and are even similar in their appearance with an LCD display, a keypad, and audio accessories. However, a few

Table 1.1: Comparison of wireless positioning and wireless communication

	Positioning	Communication
Goal	Position	Data or Voice
Measurement	Time of arrival (TOA)	Data bits
Required N_{TX}	3	1
Redundancy	$N_{TX} > 3$	Channel coding
Indirect paths	TOA error	Less sensitive

differences make positioning more challenging than communication in urban/indoor areas and these issues are summarized in Table. 1.1.

First, while communication service can be established with one transmitter, positioning requires at least three transmitters, and in fact more than three for redundancy or stable operation. At your home, it may be possible to receive a signal from one or two cellular base stations but it becomes less likely to observe more than three or four transmitters reliably. Thus, the required number of transmitters, N_{TX}, for radio positioning is a critical factor for the expansion of positioning service. Second, positioning uses measurements of time of arrival (TOA) and so a non-line-of-sight signal path introduces a measurement error that communication can tolerate as long as it has sufficient signal power to recover data bits [77]. Multiple signal paths in indoor environments are concerns for both positioning and communication systems. However, the delay on the first arrived signal is more critical to positioning because any departure from a line-of-sight signal adds an error to the position estimation [14]. Due to these differences, positioning service has not achieved great success in transition from outdoor areas to urban/indoor areas where communication service serves well.

Figure 1.2 shows the number of observed GPS channels [3] in various areas including urban canyons and indoor sites. The outdoor locations allow observation of more than five satellites except at the urban sites where only three satellites are in view on average. Evidently, signal blockage is a problem in downtown areas and an average of three satellites does not guarantee sustainable positioning service.

The situation gets worse once we move inside. In residential sites, there are fewer

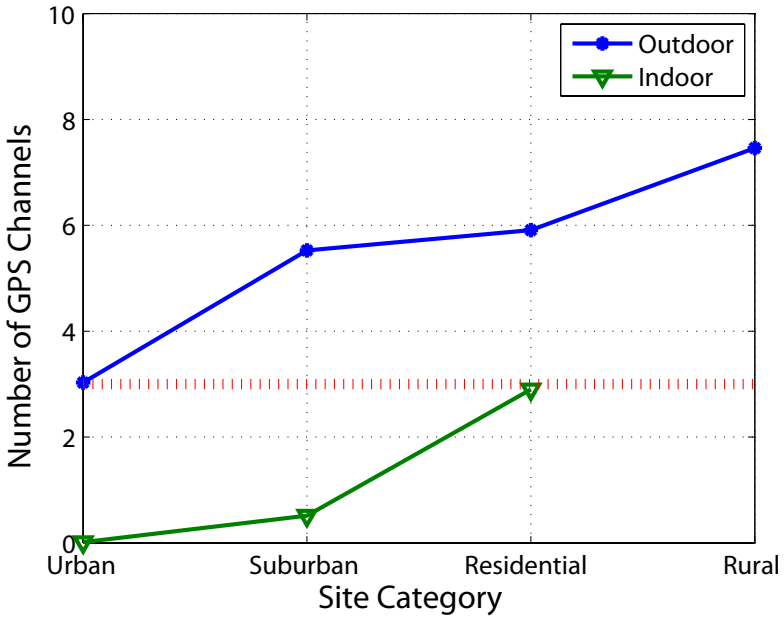

Figure 1.2: Number of observed GPS channels

than three satellites observed. Urban and suburban indoor sites have almost no satellites in view. The red dotted line shows the minimum of three measurements. It clearly sets the limit and displays the challenge for urban and indoor positioning service.

1.2 Candidate Ranging Sources for Urban and Indoor Positioning

The goal of this study is *seamless positioning service* to which urban and indoor positioning is the critical missing piece. Radio signals strong enough to survive in harsh urban and indoor areas are required. In addition, if they are not designed for navigation, these signals must be suitable for ranging.

Let us first search within the existing land-based navigation systems. The land-based positioning systems, with stronger signal power than satellite signals, are deployed and designed to serve large vehicles (airplanes and ships) in limited local space

(airports and coastal areas) [10]. Loran is, exceptionally, available nation-wide in the United States (U.S.) unlike other terrestrial systems. Because of this nation-wide availability, Loran has significance in urban and indoor positioning and its possible role is discussed in Chapter 8. However, with the exception of Loran, the existing terrestrial navigation systems are not within reach of pedestrian users. Therefore, we are going to focus on satellite systems and non-navigational terrestrial systems in this dissertation.

The lack of urban and indoor positioning service has brought about various efforts to utilize existing terrestrial systems for positioning. Among terrestrial broadcasting signals, TV signals are strong and are transmitted in broad spectrum and so are used for the TV positioning system developed by Rabinowitz and Spilker at Rosum Corporation [21]–[26].

The cellular communication community has been keen to adopt positioning technologies for their urban and indoor users. Cellular signals are used for ranging based on signal propagation time [31], [32]. In parallel, many cellular systems support assisted GPS (AGPS), pioneered by Snaptrack Corp., where GPS ephemeris data and satellite Doppler frequency are delivered to GPS receivers for enhanced signal reception [29], [30], [48]–[51]. WiFi (wireless fidelity, a service name for wireless local area networks) signal-based positioning has gained popularity recently because of rapid expansion of WiFi networks into offices and homes. WiFi signal strength measurements [34] or time delay measurements [33] based on modified WiFi transmitters are used for WiFi positioning. Radio frequency identification (RFID) can be found frequently in bookstores or retail stores for asset tracking, however is limited to detection of the existence of an item instead of exact positioning [35].

Figure 1.3 illustrates these possible positioning sources. Various radio signals either from navigation satellites or terrestrial communication transmitters are shown along with their approximate number of transmitters, distance to users, and most importantly, coverage. The space navigation systems (GPS, Glonass, and Galileo) are very well designed in the sense that they provide a global service with tens of transmitters approximately 20,000 km away from Earth. However, due to the significant distance from ground users and limited on-board power resources, satellite

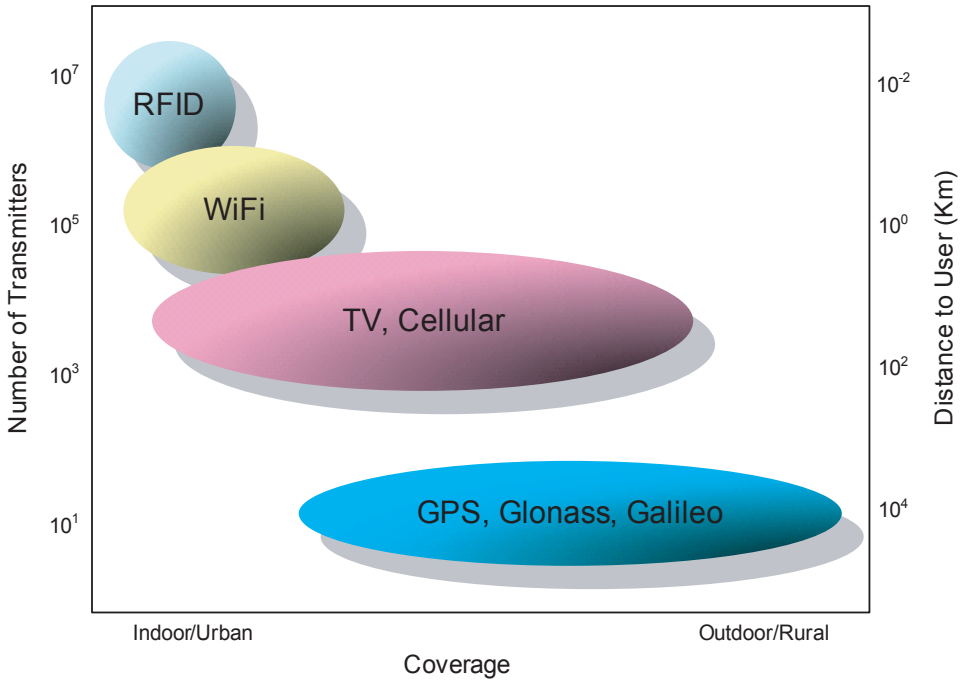

Figure 1.3: Geographic signal space

signal strength is often not strong enough to be reliably received in urban and indoor areas. Furthermore, the number of available satellites are limited due to the high cost of satellite launching and maintenance. Therefore, coverage from the satellite systems is inevitably limited in urban canyons and indoors. To enhance availability, there have been substantial investments made which are expected to become reality in coming decades. These include promising new signals with stronger power and a more diverse spectrum [14], [18]. Although these efforts are certainly welcome news to the GPS user community and the general public, space programs alone cannot solve the whole problem due to the physical limitations outlined above.

To fill this gap of service coverage, it is necessary to move upward in Figure 1.3 to the terrestrial broadcasting and communication signals. Ground transmitters are located near their target audience and there are a substantial number of ground transmitters as compared to satellite systems. Because of these physical advantages, terrestrial systems are in a better position to support users even in challenging environments. When these terrestrial signals are adopted for positioning, the coverage

area of positioning service is expected to be significantly enhanced. Starting from the bottom among the terrestrial positioning sources, television and cellular signals have medium ranges of operation heavily deployed in urban environments; WiFi has a smaller range focusing on indoor office areas; and RFID covers the smallest area but is probably the least expensive in terms of unit cost. Regarding the coverage, it becomes clear that none of the candidate ranging sources is in a position to provide end-to-end coverage from outdoor to indoor and from rural to urban. Thus, a combination of various ranging sources are desired. The combination of TV or cellular signals (medium range sources) with GPS (long range source) comes closest to the goal of universal coverage, while the combination of WiFi or RFID (short range source) with GPS may still have shadow areas where there is no coverage by either system. A comfortable overlap of coverages between medium range sources and a long range source is important to provide reliable service.

Another important viewpoint in the search for a ranging source can be found from the spectrum view in Figures 1.4 and 1.5 depicting two critical signal characteristics: signal strength and frequency bandwidth. The famous Cramer-Rao bound dictates that a stronger signal in a wider bandwidth provides higher accuracy and broader coverage [76], [13]. Each block of the spectrum shows frequency allocations made by the Federal Communications Commission (FCC) for individual systems where one notices that GPS and the cellular communication service—including the personal communication service (PCS, another cellular service at 1.9 GHz)—use relatively small bandwidths compared to their popularity. The industrial, scientific, and medical (ISM) band at 2.4 GHz where WiFi service is provided has a slightly bigger bandwidth than GPS and the cellular service. However, all three of these have far smaller allocations than the frequency allocations for television service. TV bands occupy around 400 MHz spread in very high frequency (VHF) channels (54–88 MHz and 174–216 MHz); and ultra high frequency (UHF) channels (470–806 MHz).

The advantage of a wide bandwidth for TV is amplified by the high transmission power. The received signal power can be approximated from a free space path loss

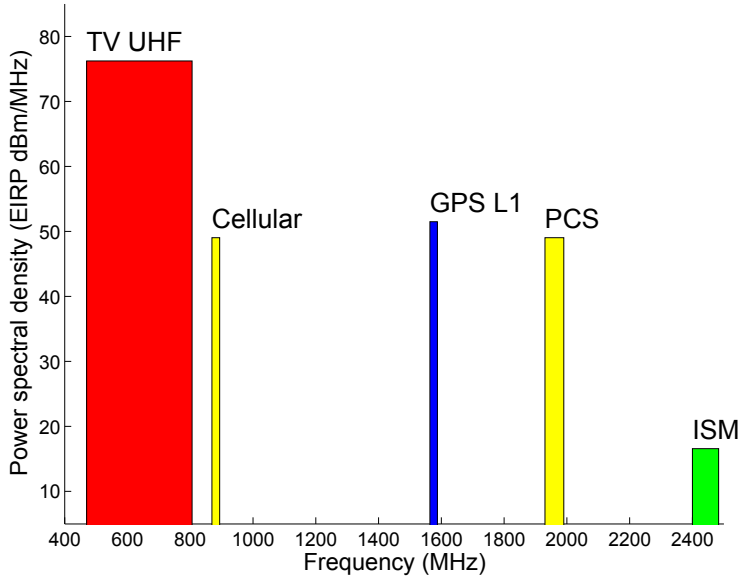

Figure 1.4: Transmission signal spectrum

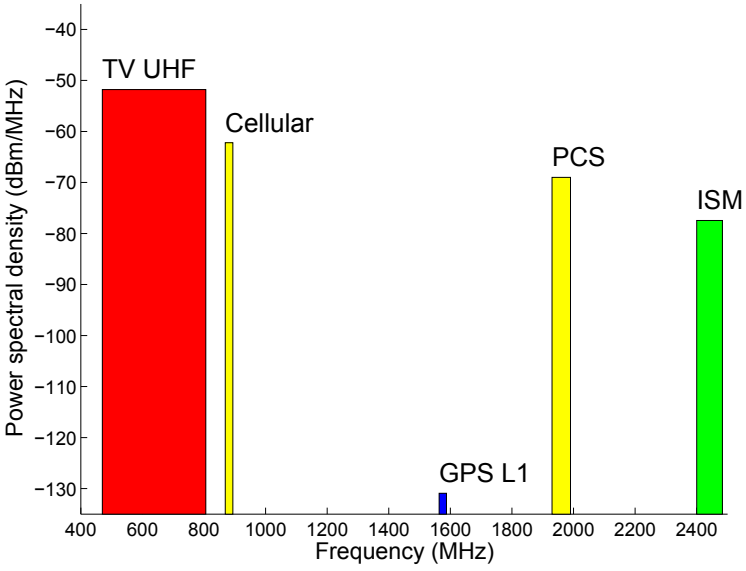

Figure 1.5: Reception signal spectrum

Table 1.2: Comparison of candidate ranging sources

	GPS L1	TV	Cellular	WiFi
Distance (km)	20,000	< 100	< 10	< 0.5
P_{TX} (EIRP, dBm)	55	84	50	30
P_{RX} (dBm)	-128	-44	-61	-64
PSD_{TX} (dBm/MHz)	51	76	49	17
PSD_{RX} (dBm/MHz)	-131	-52	-62	-77
Frequency (MHz)	1563–1587	470–806	869–894	2400–2484
Bandwidth (MHz)	24	336	25	83.5
Channel bandwidth (MHz)	2	6	1.25	22
Coverage	Outdoor	Out/In	Out/In	Indoor
Near-far issue	Mild	None	High	High
Measurement	Range	Range	Range	P_{RX}
Required investment	None	Clock monitoring	None	Periodic surveying

model,

$$P_{RX} = P_{TX} G_{RX} \left(\frac{\lambda}{4\pi d} \right)^2 \tag{1.1}$$

where P_{RX} is a received signal power and G_{RX} is a receiver antenna gain set to unity or 0 dB. The combination of a transmitted signal power and a transmitter antenna gain becomes effective isotropic radiated power (EIRP), P_{TX}. P_{TX} is divided by a channel bandwidth and illustrated in Figure 1.4 in power spectral density (dBm/MHz). The distance between a transmitter and a receiver, d, is assumed to be 20,000 km for GPS, 100 km for TV, 10 km for cellular and 0.5 km for WiFi. The estimated nominal received signal power level (see Figure 1.5) shows the GPS signal power far below those of terrestrial signals due to the substantial travel distance. Among land signals, TV commands the highest power level regardless of the conservative assumption of 100 km travel distance. In most cases this is expected to be 10–50 km.

A comparison of the candidate ranging signals is summarized in Table 1.2 where nominal values for signal power, power spectral density, frequency, and bandwidths are listed as well as three key practical considerations: the near-far issue, measurement

formats, and necessary investments. We describe these now. First, the near-far issue happens when a channel far from a user is blocked by a channel near the user due to spectral channel sharing in cellular and WiFi systems. This phenomenon is rarely an issue with TV because of the generous frequency allocations or with GPS since satellites are all equally far away. This channel competition limits the number of transmitters in view, making an independent cellular positioning system less appealing.

Second, in terms of measurement formats, while range measurements are preferred and widely used in many systems, these cannot operate in conjunction with asynchronous transmitter networks without a clock calibrating scheme or a special protocol for a round trip measurement. Hence, instead of range measurements, WiFi positioning, based on numerous independently operated WiFi transmitters, relies on received signal strength indicator (RSSI) measurements. However, RSSI may not reflect actual range closely when there is severe signal attenuation. Attenuated signal level will be interpreted as a long range from a transmitter to a receiver even though the low RSSI may have been due to attenuation by an object on the signal path.

The last practical consideration is the required investment to convert these broadcasting or communication systems to positioning systems. Since TV stations are not synchronized to one another, we need monitor stations for transmitter clock calibration. However, because TV signals propagate in long ranges, the area served by a monitor station is as large as TV signal ranges. Thus, a few monitor stations in a city could observe and calibrate transmitter clocks and transfer calibration information to users. This solution, however, may not be feasible for WiFi due to the WiFi signals' short range. Therefore, TV positioning uses range measurements while WiFi positioning inevitably selects signal power measurements for positioning. An alternative solution would be to install GPS receivers on each TV station to make them a synchronous network tied to GPS timing. CDMA cellular networks, which are tied to GPS timing, do not need any hardware change, making them economically attractive. GSM cellular networks share the synchronization issue with TV stations. For WiFi positioning, although there are a substantial and ever growing number of WiFi transmitters in metropolitan areas, it is hard to track and locate these due

to the absence of a central entity controlling and monitoring them. Hence, a WiFi positioning system needs periodic surveying of coverage areas to locate transmitters and update any change in their coordinates and corresponding RSSI maps. RFID positioning, not listed in the table, can be implemented only with labor and capital intensive investment since RFID tags or transmitters should be installed every few meters in areas or objects of interest.

Table 1.2 illustrates the advantages and disadvantages of the individual terrestrial signals for positioning. TV has strong signals but requires clock monitoring; CDMA cellular has a synchronized network but must overcome the near-far issue; WiFi is readily available at homes and offices but requires periodic resurveying; RFID works well indoors but requires manual installation of RFID tags or transmitters. The different natures of each system make them suitable for certain applications but not for others. For augmenting GPS in urban and indoor areas, continuous city-wide coverage is necessary. With this requirement, television signals are considered to be one of the best candidates. Therefore, although other terrestrial signals (cellular and WiFi) have their advantages, the combination of TV and GPS is pursued within this dissertation.

1.3 Hybrid GPS and TV Positioning

This dissertation explores the use of GPS and TV for enhanced positioning coverage. There are many other hybrid positioning systems that use GPS with other technologies. An inertial navigation system (INS) is one of GPS' favorite partners. The INS provides dead-reckoning positioning in case of a short GPS outage. Terrestrial signals such as cellular signals [51] or Loran signals [52] are also combined with GPS signals for enhanced availability. In this dissertation, TV signals are combined with GPS signals for the purpose of seamless coverage.

For reliable positioning, observation of a sufficient number of ranging sources must be sustained regardless of location. Figure 1.2 showed that there are not a sufficient number of observed GPS satellites in urban canyons and indoors. Now, let us examine the observed TV channels based on the same field test [3] featuring both GPS and

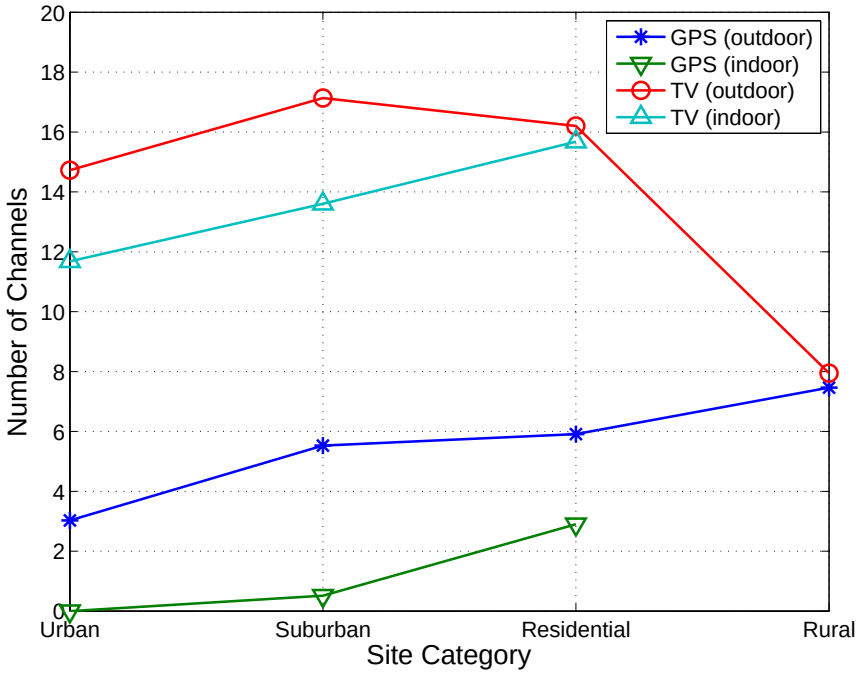

Figure 1.6: Number of observed GPS and TV channels

TV channels (Figure 1.6). Except in rural areas, more than 14 TV channels (on average) are observable outdoors including urban canyons. Even indoors, there are more than 11 TV channels observed. This result is consistent with the expectation illustrated in Figures 1.3 and 1.5. Relative proximity to the users and higher signal power compared to satellites make more TV channels available even in urban canyons and indoors. See Chapter 7 for a detailed discussion of the field test results.

The number of observed channels well illustrates the benefit of hybrid GPS and TV positioning. The substantial number of TV channels can be utilized to provide reliable urban and indoor positioning. In particular, indoor positioning is likely to depend heavily on TV channels. At suburban and residential sites, both systems contain enough channels for positioning. This comfortable overlap of coverage, also illustrated in Figure 1.3, can ensure reliable continuation of positioning. At rural sites, GPS becomes more reliable because of the increased number of available GPS satellites while the number of TV channels drops. This observation highlights the benefit of hybrid GPS and TV positioning. TV coverage is expected to be good

in urban areas and indoors while GPS covers outdoors and rural areas. Suburban and residential areas can benefit from both systems. Therefore, an integrated GPS and TV positioning system is expected to provide wider coverage than the individual systems.

1.4 Contributions

This section describes the dissertation contributions for the development and demonstration of the proposed hybrid GPS and TV positioning system. The contributions include a comparison of pseudorange formats, a hybrid system implementation, a fault detection and exclusion algorithm implementation, and field tests. These are outlined as follows.

First, this dissertation discusses two formats of pseudorange measurements, time of arrival (TOA) and time difference of arrival (TDOA). Pseudoranges (range measurements with a clock bias) can be represented either in a TOA format or in a TDOA format of which TDOA is favored in most terrestrial positioning systems. These two formats were compared before and were proved to be equivalent [53], [54]. However, their relative performance under practical assumptions is described for the first time by the author [1], [4]. Also, the existing proof of equivalence is extended to an integrated system combining signals from heterogeneous networks (for example, GPS and TV signals) in Appendix B.

Second, a hybrid positioning system which combines GPS and TV positioning technology is constructed for the proof of concept and performance assessment. The hybrid system is composed of a GPS receiver, a TV positioning device, and Matlab-based position estimation software (see Figure 1.7). The GPS receiver delivers pseudorange measurements and satellite locations. The TV positioning device measures time of arrival from each TV transmitter while a monitor station estimates time of transmission. These two measurements are combined in a TV pseudorange estimator and become TV pseudorange measurements. Both GPS and TV pseudorange measurements are delivered to the hybrid position estimator which combines these two sets of measurements and estimates user position. The position estimator also includes a

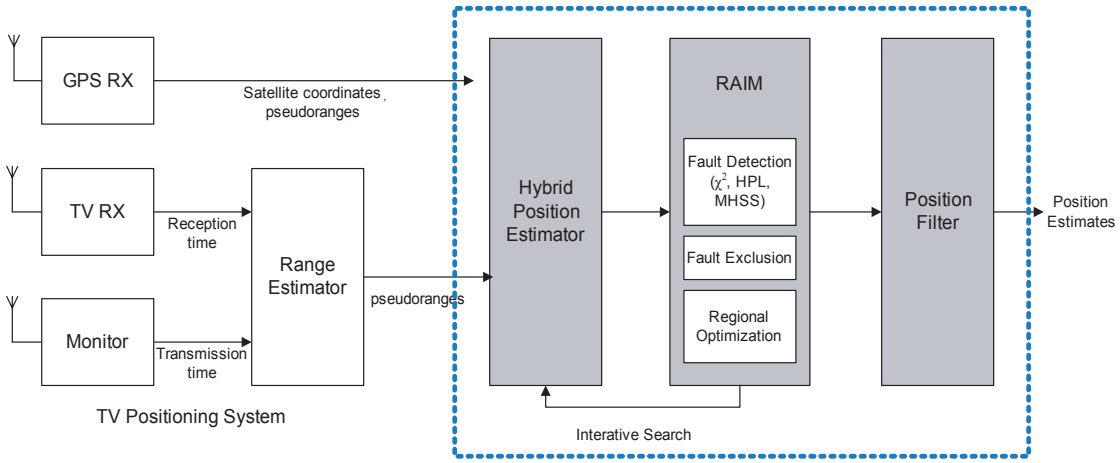

Figure 1.7: Contributions to hybrid GPS and TV positioning

receiver autonomous integrity monitoring (RAIM) algorithm (the third contribution) and a position domain filter for outlier removal and smoother position estimates, respectively.

Third, a multi-fault tolerant iterative RAIM is proposed and implemented. Due to multipath effects in urban canyons and indoors and clock drifts in television transmitters, there exist a large number of outliers with large biases, in particular, in TV pseudoranges. Because a GPS RAIM usually assumes a single outlying measurement [68]–[74], [13], this dissertation introduces a RAIM algorithm that can detect and exclude multiple outliers. The proposed RAIM reconstructs the conventional RAIM algorithms with iterative fault detection and exclusion steps [2]. For fault detection, the following three algorithms are compared: the chi-square test, the horizontal protection level (HPL) test by Brown [68], [69], and the multi-hypothesis solution separation (MHSS) test by Pervan [70], [71]. For fault exclusion, the maximum likelihood test by Sturza is selected [72]. Then, the proposed RAIM combines these fault detection and fault exclusion methods in iterative steps.

Lastly, an extensive field test is conducted and the positioning performance of the hybrid system is analyzed in terms of accuracy and availability [3]. The hybrid positioning system is tested at thirty-nine sites in the San Francisco Bay Area which include outdoors, indoors, urban, suburban, residential, and rural areas. At each

location, one hour of stationary data are collected and post-processed by the hybrid positioning estimator. The positioning performance of the hybrid system is analyzed with respect to locality and also in comparison with the individual positioning systems.

In addition to the contributions described here, the author would like to add a note regarding an interference study conducted during this doctoral study. Since interference is a critical issue to urban and indoor positioning, a spectrum survey was conducted in an effort to assess radio frequency interference levels in the GPS band (L1 band at 1575.42 MHz), the Unified-S band (at 2067.5 MHz, used for satellite communication), and the industrial, scientific, and medical (ISM) band at 2400 MHz. This particular study finds a high level of radio activities in the ISM band and the Unified-S band. In the GPS L1 band, although it is relatively free of interference in most areas, urban areas are shown to be exposed to occasional spill-over from out-of-band interference. The details of this interference study can be found in [6], [7].

1.5 Dissertation Outline

This section provides the outline of this dissertation. There are eight chapters, including this introduction chapter, followed by three appendices, a glossary, and a bibliography. Chapters 1 through 3 provide an introduction to the research and related systems. Chapters 4 through 7 describe the dissertation contributions while the three appendices expand the contributions. A short summary of each chapter is given as follows.

Chapter 1 (this chapter) has given an introduction to this dissertation. It includes motivation and background of the research and explains the proposed solution and dissertation contributions. The goal of this dissertation is the enhancement of coverage of positioning systems, in particular, in urban and indoor areas. For urban and indoor coverage, terrestrial radio signals (TV, cellular, and WiFi signals) are considered as a ranging source. GPS and a TV-based positioning system are proposed to be combined.

Chapter 2 provides an introduction to the existing positioning (navigation) systems and the components of these positioning systems. Navigation systems are classified into two groups, space-based systems and land-based systems. Space-based systems include GPS and land-based systems include Loran. These systems consist of transmitters as ranging sources, receivers as measurement equipment, and monitors for system calibration. We can find these three components in the TV positioning system as well.

Chapter 3 introduces a TV-signal-based positioning system. Television broadcasting systems provide coverage in most populated regions including metropolitan areas. Rabinowitz and Spilker used broadcast TV signals for their TV positioning system for enhanced urban and indoor positioning [21]–[26]. Chapter 3 describes types of broadcast television signals and the TV positioning system and discusses clock stability of TV transmitters.

Chapter 4 describes a hybrid GPS and TV positioning system. The hybrid system can be considered as an overlay of GPS on top of the infrastructure of the TV positioning system. Alternatively, the hybrid GPS and TV system can be considered as a twin of AGPS which relyes on a similar type of infrastructure. In the integration of two positioning systems, there are various possible operational modes depending on positioning dimensions and types of network aiding information. These operational modes and aiding information are discussed. Lastly, the performance of individual GPS and the TV positioning system is analyzed based on signal specifications.

Chapter 5 compares TOA and TDOA formats of pseudorange measurements. The comparison starts under an ideal condition where TOA and TDOA are analytically proven to be equivalent in terms of position accuracy. This proof of equivalence is extended to an integrated system combining signals from heterogeneous networks (for example, GPS and TV signals) in Appendix B. Then, TOA and TDOA are compared under practical assumptions where noise statistics are inaccurately known or weighting schemes do not reflect noise statistics accurately. In this practical case, TOA is preferred.

Chapter 6 proposes a RAIM algorithm which detects and excludes multiple biased range measurements. Three existing fault detection and one fault exclusion algorithm

are introduced. These detection and exclusion methods are incorporated into the proposed RAIM algorithm in an iterative scheme to be tolerant against multiple outliers.

Chapter 7 describes field test results of the hybrid positioning system. Test equipment, methods, and locations are described. Since the field test data contain many outliers, the strictness of the RAIM algorithm determines the results in terms of availability and accuracy. The trade-off between availability and accuracy is investigated by adjusting the parameters for the RAIM implementations. This investigation provides us a trade-off curve in which a trade-off point is searched with a reasonable balance between availability and accuracy. In each categorical region (e.g. urban outdoors, residential indoors), further analysis is provided.

Chapter 8 provides a summary of this dissertation and recommendations for future work. In particular, the recommendations include a proposal of a possible GPS-backup system which combines the TV positioning system and Loran.

Chapter 2

Radio Positioning Systems

This chapter provides a brief introduction to existing positioning systems. Over the years, numerous time and position reference systems have been developed. There are mostly mechanical devices including various types of compasses, sextants, clocks, and "dead reckoning" systems. These mechanical references are slowly being replaced by electrical systems based on radio frequency signaling. Among these the most well-known electrical reference would be satellite-based GPS which provides both time and position information. In this chapter, this revolutionary system, GPS, is introduced along with other radio positioning systems.

2.1 History of Radio Positioning Systems

Radio positioning systems can be classified in two groups according to transmitter types: stationary ground transmitters and moving satellite transmitters. Ground-transmitter-based systems are called terrestrial positioning systems and are usually designed to provide local area service. Satellite-transmitter-based systems are called space positioning systems and are designed to cover wider areas and often the entire Earth. Interestingly, both terrestrial and space systems at their inception were intended to serve governmental purposes, i.e., military or public safety, but were soon taken over by civilian users (one of the few examples of good government initiatives).

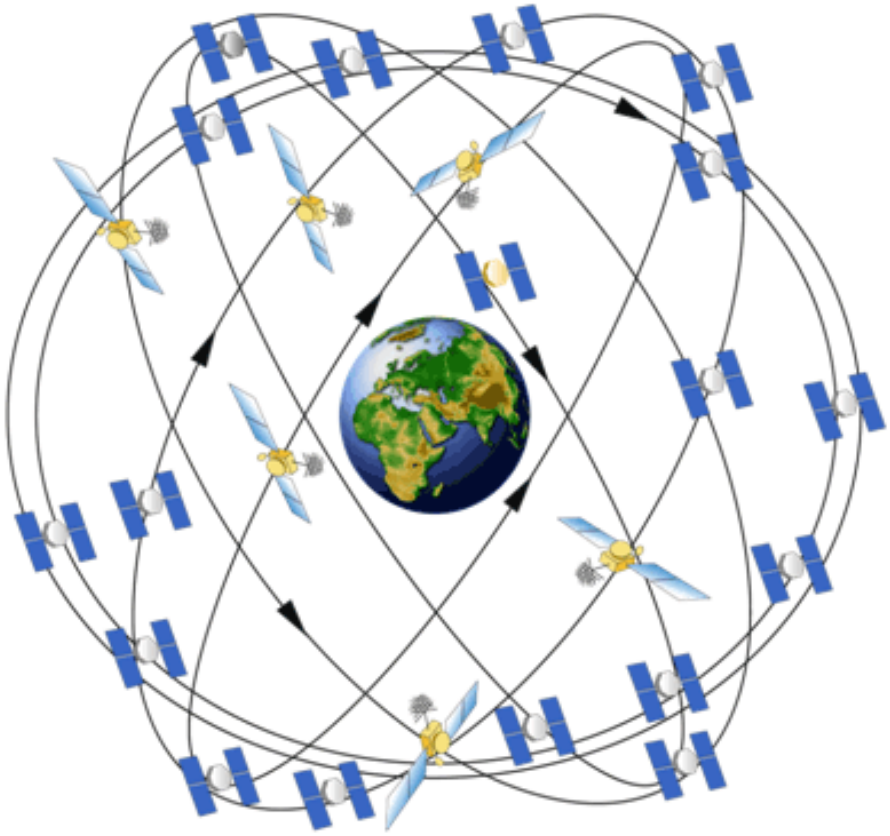

Figure 2.1: GPS constellation (Courtesy: U.S. National Space-Based Positioning, Navigation, and Timing Executive Committee)

2.1.1 Space Positioning Systems

Space positioning systems are tasked with providing a wider and often global service [12]–[19], while most terrestrial positioning systems serve local areas. The first of the space positioning systems was Transit developed by the U.S. Navy in the late 1950s using four to seven satellites. It measured Doppler shifts from satellites and estimated user position based on known satellite position. Transit used low earth orbit (LEO) satellites with an altitude of 1100 km in nearly circular polar orbits, operating at 150 and 400 MHz with 1 W transmission power and providing 25 m in DRMS (RMS

horizontal position error). However, due to the small number of satellites, it served only stationary users which limited the user population. Transit was decommissioned when GPS became operational.

After Transit, the U.S. Air Force and Navy joined together to develop GPS (1970s). GPS is a one-way broadcasting system and has only a downlink from a GPS satellite to a ground user, not an uplink from a user to a satellite. Because GPS is a broadcasting system, there is no limit on the number of users. GPS is one of the first adopters of code division multiple access (CDMA) spread spectrum signals to share a single frequency band among many transmitters. Indeed, spread spectrum signaling enables the very precise range measurements needed for accurate positioning. GPS occupies L bands (L1 band at 1575.42 MHz and L2 band 1227.60 MHz) and uses 24 to 30 (currently) medium earth orbit (MEO) satellites in six near-circular orbits inclined at 55 degrees with radius of 26,560 km and orbit period of 11 hours 58 minutes. GPS satellites are illustrated in Figure 2.1

During the severe competition of the Cold War, the Soviet Union developed an almost identical system called Global'naya Navigatsionnaya Sputnikovaya Sistema (GLONASS) with slightly different specifications. GLONASS uses 24 MEO satellites in three orbits with an inclination angle of 64.8 degrees, an orbital altitude of 19,100 km and orbital period of 11 hours 15 minutes repeating every 8 days. It uses frequency division multiple access (FDMA) instead of CDMA at G1 (1598.0625–1607.0625 MHz) and G2 (1242.9375–1249.9375 MHz) bands but the GLONASS signals are spread spectrum.

Because there have been substantial commercial and infrastructural interests built around GPS, modernization efforts have been ongoing since the 1990s. Modernization efforts include addition of new signals and a new frequency band (see Figure 2.2). In the existing two GPS bands, there is one civilian signal (L1 C/A) and two military signals (L1 P(Y) and L2 P(Y)). In addition to these two bands, GPS users will be able to use a new frequency band at 1176.45 MHz (called "L5") as the GPS modernization efforts progress. The L5 band will host a wide spectrum civilian signal for enhanced positioning accuracy for general GPS users. The L1 and L2 bands are now more crowded with new signals. For civilian users, L2C is added at the L2 band and L1C

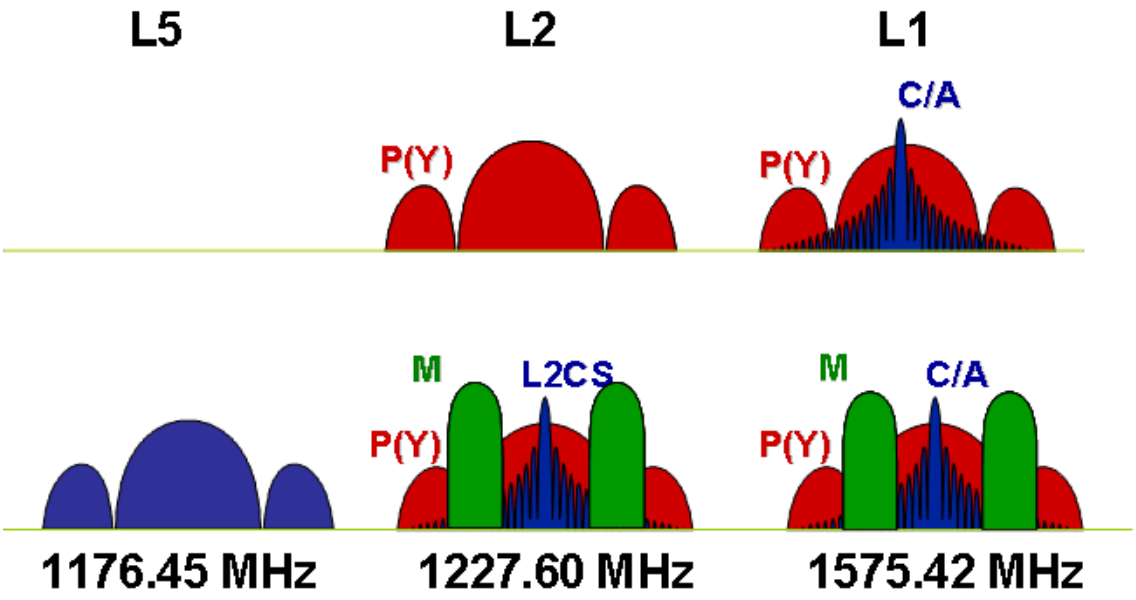

Figure 2.2: GPS modernization (Courtesy: Richard Fontana GPS Deputy Program Manager, U.S. Department of Transportation)

is expected at the L1 band. Both L1C and L2C contain a dataless pilot channel for longer integration without data recovery. This feature is expected to provide higher integration gain and be beneficial to urban or indoor users. For military users, the M code is added both at the L1 and L2 bands which uses a split spectrum (signal power is split into two distinct spectra) called binary offset code (BOC) [14], [17]. This new military signal has better anti-jamming capability and can be demodulated autonomously without a need to lock into the C/A code [14], [16].

The rapid expansion of GPS technologies and GPS markets encouraged many other nations to jump into this new space race. The European Union is in the process of developing a global system called Galileo. Galileo is based on 27 MEO satellites (altitude 23,222 km) in three orbits inclined at 56 degrees with an orbital period of 14 hours 4 minutes repeating every 10 days. It resembles GPS in many ways, including CDMA spread spectrum signals, and shares new features like a dataless pilot channel

Table 2.1: Space positioning systems

System	Meas.	Frequency (MHz)	Intro.	Coverage	N_{TX}	Orbit
Transit	Doppler	150, 400	1958–96	Global	4–7	LEO
GPS	TOA	1575, 1227	1970s–	Global	24+	MEO
GLONASS	TOA	1602, 1245	1970s–	Global	24+	MEO
Galileo	TOA	1575, 1278, 1191	2000s–	Global	27+	MEO
Compass	TOA	1589, 1561, 1268, 1207	2000s–	Global		GEO, MEO
QZSS	TOA	1575	2000s–	Regional		Elliptical

and split spectrum both intended for better signal reception in challenging environments like urban canyons and indoor areas. There are three bands: L1 (1575.42 MHz), E6 (1278.75 MHz), and E5 (1191.795 MHz) [14], [18].

Besides the global systems, there are regional systems to cover a single nation or regional areas. China started to develop Compass (also known as Beidou) with two geostationary earth orbit (GEO) satellites and is developing it into a full-grown global system by adding MEO satellites [19]. Japan is also developing a regional system called Quasi-Zenith Satellite System (QZSS) using geo-synchronous satellites in an elliptical orbit. See Table 2.1 for a list of the space-based positioning systems.

2.1.2 Terrestrial Positioning Systems

During and after World War II, there were various efforts to develop terrestrial positioning systems: Omega and the long range navigation system (Loran) for maritime navigation; the instrument landing system (ILS), the microwave landing system (MLS), the very high frequency omnidirectional range (VOR), the distance measurement equipment (DME), and the tactical air navigation (TACAN) for aircraft landing [10].

Omega was the first worldwide continuously available positioning system. Omega used phase difference of signals at very low frequency (VLF) bands (10–14 kHz) but was decommissioned in 1997 and most of its role has been replaced by GPS. In Loran, the time difference of arrival (TDOA) is measured from amplitude modulated (AM)

Figure 2.3: Loran transmission tower (Courtesy: U.S. Department of Agriculture Forest Service)

Table 2.2: Terrestrial positioning systems

System	Measurement	Frequency (MHz)	Intro.	Coverage	Accuracy
Omega	Phase difference	0.01–0.014	1960s–97	Regional	2-4 km
Loran	TDOA	0.09–0.1	1940s–	Regional	250 m
ILS	Azimuth, elevation	108–112	1940s–	Airport	
MLS	Azimuth, elevation	5031-5091	1960s–	Airport	100 ft
VOR	Azimuth	108–118	1940s–	Airport	4.5 deg.
DME	Round trip time	962–1213	1950s–	Airport	185 m

pulses broadcast from a chain of transmitters, a master station and two to three secondary stations. It operates in the frequency range of 90–100 kHz with a peak transmission power of 1 MW. There are 29 Loran transmitters (see Figure 2.3) in the United States and more worldwide. Loran evolved to Loran-C in the 1950–60s for wider range and better accuracy and a further improvement is expected as it advances into enhanced Loran (e-Loran) [11]. Currently the absolute accuracy in distance root mean squared error (DRMS, two dimensional horizontal position error) is about 250 m while the repeatable accuracy is approximately 50 m. Repeatable accuracy measures the ability to return to a spot previously marked by the same positioning system.

Terrestrial systems supporting aircraft navigation include ILS, MLS, VOR, DME, and TACAN. These systems provide vertical and lateral guidance by azimuth, elevation, and distance measurements. ILS, developed in the 1940s, uses two AM signals at 108.1–111.95 MHz and is composed of three elements: a localizer for lateral guidance, a glidescope for vertical guidance, and marker beacons for discrete distance checks. In the late 1960s, MLS was developed in order to replace ILS, but was not widely accepted due to the advancement of GPS technologies. MLS uses a large number of frequency channels (200) in the range of 5031–5091 MHz to avoid problems with neighboring airports which is one of the main concerns of ILS. VOR, measuring azimuth, usually works with DME which measures distance. VOR uses two 30 Hz sine waves carried at 108–117.95 MHz, whose relative phase is proportional to azimuth. DME measures round trip time of pulses at a carrier frequency of 962–1213 MHz to

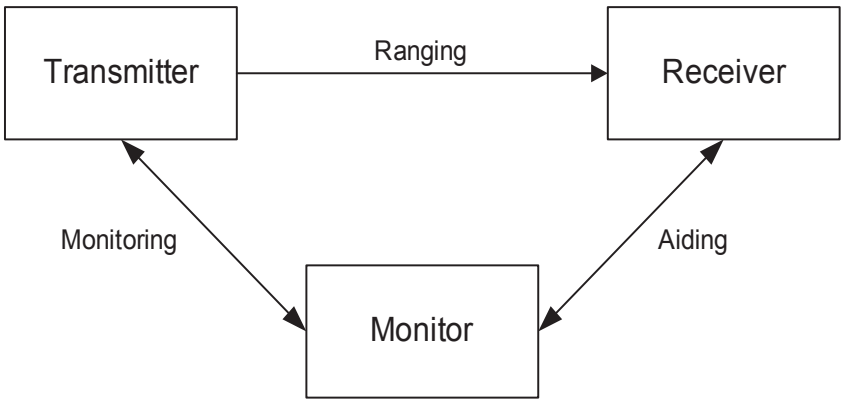

Figure 2.4: Three entities in radio positioning systems

estimate distance. A military version of the VOR/DME system is TACAN, operating in the frequency band of 960-1215 MHz. See Table 2.2 for a comparison of these terrestrial positioning systems.

2.2 Transmitters, Receivers and Monitors

The various radio positioning systems listed previously have three common building blocks which are discussed in this section: transmitters (ranging sources), receivers (user positioning devices), and monitor stations, as illustrated in Figure 2.4. Transmitters broadcast ranging signals, sometimes focusing on a certain coverage area through the use of directional antennas. Since there are four unknown variables associated with a three dimensional space and one dimensional time, at least four transmitters (three transmitters for two dimensional positioning) are required for a receiver to determine its position. Certainly more transmitters are welcome because redundant measurements help to both improve position estimation accuracy and detect and exclude erroneous measurements. This topic is discussed in Chapter 6.

Receivers measure signal travel time (or angle or Doppler shift depending on the system) and estimate their position based on multiple measurements. This is not an easy task since reliable range measurements are often subject to radio frequency environment and geographic environment. In particular, urban canyons and indoor areas

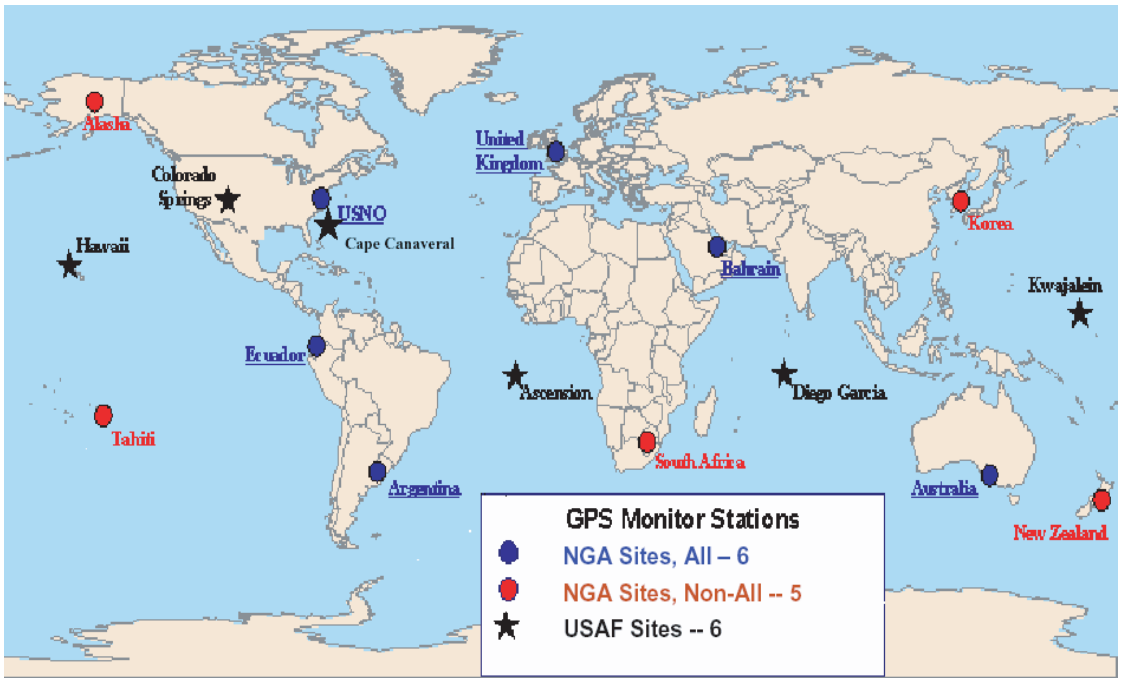

Figure 2.5: Global network of GPS monitor stations (Courtesy: Aerospace Corp.)

are full of multipath effects and signal blockage by buildings. As a remedy, higher receiver sensitivity and better multipath algorithms have been sought in receiver designs as well as stronger signal power and more robust signal structures (pilot only channel and BOC code) from transmitters and more aiding information from monitors.

Monitor stations assist transmitters or receivers. Let us start with transmitter assisting monitors. In the case of GPS, transmitters (GPS satellites) have uncertainty in both time and position. Even though very accurate atomic clocks are on-board, the clocks in each satellite should be monitored and calibrated by a central entity. Furthermore, the satellites are constantly circling around Earth at the speed of approximately 4 km/s, leaving their own position in question. Thus, the U.S. government operates a global network of ground monitor stations for constant monitoring of satellite orbits and timing bases (see Figure 2.5).

Monitors are also needed for a terrestrial positioning system. CDMA cellular networks are synchronized to GPS time. However, most terrestrial communication

transmitters are not synchronized to each other. Synchronization between transmitters is not necessary for their primary purpose of communication but is a required feature for positioning. Therefore, monitor stations need to be installed for time calibration, unless all transmitters are equipped with GPS receivers and synchronized to GPS time. Detailed discussion about transmitter synchronization is given in Section 2.4.

Some monitors are connected directly to the users. The Space Based Augmentation System (SBAS) and the Ground Based Augmentation System (GBAS) are basically a large number of GPS monitor stations more closely located to the user population. Hence, they experience and observe similar types of signal errors from transmitters more closely than the small number of original GPS monitor stations. Consequently, SBAS and GBAS serve user needs by augmenting transmitted signals with locally generated calibration information via independent radio links. The Continuously Operating Reference Stations (CORS) operated by the U.S. National Geodetic Survey (NGS) are a different type of GPS monitor system used in a combined civilian and governmental effort to serve the high accuracy community. After post-processing, CORS provides accurately estimated GPS satellite ephemeris information.

Assisted GPS (AGPS) is an initiative from the cellular communication industry to assist mobile-phone-based GPS receivers by providing aiding information to reduce the burden of these tightly budgeted receivers in terms of cost, size, and power consumption. Since Doppler frequency, satellite orbit, and clock information are provided through cellular networks, user receivers can minimize expensive processing to decode GPS messages and search satellite signals in a large search window of Doppler frequencies and GPS code phases. Moreover, this aiding information helps receivers to integrate signals over a longer time frame for the enhancement of sensitivity in obstructed environments.

2.3 Position Estimation

This section describes how to estimate position based on range measurements.

2.3.1 Range Measurements

The fundamental source of position information comes from range measurements between transmitters and receivers. We are going to focus on range measurements instead of Doppler or angular measurements which are the less common forms of measurement. A range measurement refers to an observed signal travel time between a transmitter and a receiver. If there is a non-zero clock bias, the range measurement is called a pseudorange. A pseudorange, ρ, is a difference between time of reception, $\tilde{t}_{\mathrm{RX}}$, and time of transmission, $\tilde{t}_{\mathrm{TX}}$,

$$\rho_i = \tilde{t}_{\mathrm{RX},i} - \tilde{t}_{\mathrm{TX},i} \tag{2.1}$$

where, for convenience, time measurements are expressed in meters instead of seconds. '$\tilde{t}_{\mathrm{RX}}$' and '$\tilde{t}_{\mathrm{TX}}$' in fact mean '$\tilde{t}_{\mathrm{RX}} \times c$' and '$\tilde{t}_{\mathrm{TX}} \times c$' where '$c$' is the speed of light and $c = 2.99792458 \times 10^8$ m/s. $\tilde{t}_{\mathrm{RX}}$ and $\tilde{t}_{\mathrm{TX}}$ carry errors from clock biases (a receiver clock bias, b, and a transmitter clock bias, B), an atmospheric propagation delay, A, a multipath error, M, and an unmodeled random error, ϵ, in addition to the true t_{RX} and t_{TX}

$$\begin{aligned} \rho_i &= (t_{\mathrm{RX},i} + b + A_i + M_i) - (t_{\mathrm{TX},i} + B_i) + \epsilon_i \\ &= r_i + b - B_i + A_i + M_i + \epsilon_i. \end{aligned} \tag{2.2}$$

Atmospheric propagation delays are concerns for space positioning systems that send signals through the ionosphere and the troposphere. Terrestrial positioning systems are less affected by atmospheric propagation delays because of shorter distances to users. Among these error sources, transmitter clock biases, B, and atmospheric propagation delays, A, have been studied intensively and a reasonable level of compensation is currently provided by GPS and other space positioning systems. The receiver clock bias, b, and multipath errors, M, cannot be estimated or compensated by transmitters and are left as a receiver responsibility. The random error, ϵ, is the accumulated unmodeled error from a transmitter, a receiver, and a channel.

2.3.2 Position Estimation

Position estimation algorithms calculate user position and clock bias based on ranging measurements. If we revisit the definition of a pseudorange given in Equation (2.2), a pseudorange measurement, ρ_i, from the ith transmitter at a location, $\boldsymbol{s}_i = (s_{X,i}, s_{Y,i}, s_{Z,i})$, to a user location, $\boldsymbol{u} = (u_X, u_Y, u_Z)$, consists of a true range, $r_i = ||\boldsymbol{u} - \boldsymbol{s}_i||$, a receiver clock bias, b, and a measurement error, ϵ_i, for n synchronized transmitters (i.e., $B_i = 0$). Here we assume that the unmodeled error term, ϵ_i, includes the remaining error terms (atmospheric errors, A_i and multipath errors, M_i).

$$\begin{aligned} \rho_i &= ||\boldsymbol{u} - \boldsymbol{s}_i|| + b + \epsilon_i \\ &= \sqrt{(u_X - s_{X,i})^2 + (u_Y - s_{Y,i})^2 + (u_Z - s_{Z,i})^2} + b + \epsilon_i \end{aligned} \tag{2.3}$$

Because of the non-linear relationship between $\boldsymbol{\rho}$ and $\boldsymbol{u}$, a first order approximation is taken based on Taylor series [15]. Then, this non-linear estimation problem can be solved incrementally by a series of linear estimation problems.

$$\delta\boldsymbol{\rho} = \boldsymbol{G}\delta\boldsymbol{x} + \boldsymbol{v} \tag{2.4}$$

where $\delta\boldsymbol{\rho} = \boldsymbol{\rho} - \hat{\boldsymbol{\rho}}$ is an $n \times 1$ vector of difference between pseudorange measurements and their estimates, $\delta\boldsymbol{x} = \boldsymbol{x} - \hat{\boldsymbol{x}}$ is a 4×1 vector of difference between user variables and their estimates, and $\boldsymbol{v}$ is an $n \times 1$ residual measurement error vector. n is the number of pseudorange measurements. $\boldsymbol{G}$ is an $n \times 4$ geometry matrix such that

$$\boldsymbol{G} = \begin{bmatrix} \boldsymbol{e}_1^T & 1 \\ \vdots & \vdots \\ \boldsymbol{e}_n^T & 1 \end{bmatrix} = \begin{bmatrix} \boldsymbol{G}_{\mathrm{D}} & \mathbf{1}_{n\times 1} \end{bmatrix}$$

where $\boldsymbol{e}_i = (\hat{\boldsymbol{u}} - \boldsymbol{s}_i)/\left\|\hat{\boldsymbol{u}} - \boldsymbol{s}_i\right\|$ is a directional vector from the ith ranging source to the user, and $\boldsymbol{G}_{\mathrm{D}}$ is an $n \times 3$ geometry matrix used in TDOA (time difference of

arrival) solutions. User variables $\boldsymbol{x}$ are estimated incrementally,

$$\delta\hat{\boldsymbol{x}} = \boldsymbol{G}^{\dagger}\delta\boldsymbol{\rho} \tag{2.5}$$

based on the pseudo-inverse of the geometry matrix, $\boldsymbol{G}^{\dagger}$, and the residual pseudorange measurements, $\delta\boldsymbol{\rho}$, through iterations. The procedure is called the Newton-Raphson method [20].

2.4 Differencing on Range Measurements

From time to time, the range measurements are differenced to remove common errors or simplify processing. Since there are common error sources among range measurements, differencing among measurements removes those common errors.

2.4.1 Removing Transmitter Clock Biases

In this subsection, a method to remove transmitter clock biases is discussed. One such method is differencing range measurements. In Equation (2.3), the transmitter clock biases, B_i, are set to zero because all transmitters are assumed to be synchronized to one another. However, some transmitter networks are not synchronized (for example, TV stations) and so B_i is not zero. Then, each pseudorange measurement, ρ_i, carries one unknown B_i and the total number of unknown variables are $n + 4$ (3 position variables, 1 receiver clock bias, and n transmitter clock biases). Since the number of variables, $n + 4$, are greater than the number of measurements, n, the position estimation becomes an underdetermined problem regardless of n. To avoid this underdetermination, these clock biases must be removed.

Removal of transmitter clock biases in an unsynchronized transmitter network involves another receiver. When two receivers (l and m) observe signals from the same set of transmitters, the transmitter clock biases, B_i, are common error sources

Table 2.3: Number of variables in absolute positioning and relative positioning

Absolute positioning (before differencing)		Relative positioning (after differencing)	
Measurements	Unknowns	Measurements	Unknowns
$2n$	$n+8$	n	4 or 8

among receiver measurements, ρ_i^l and ρ_i^m.

$$\begin{aligned} \rho_i^l &= r_i^l + b^l - B_i + \epsilon_i^l \\ \rho_i^m &= r_i^m + b^m - B_i + \epsilon_i^m \end{aligned} \tag{2.6}$$

Thus, differencing among measurements removes those common errors.

$$\Delta\rho_i^{l,m} = \Delta r_i^{l,m} + \Delta b^{l,m} + \Delta\epsilon_i^{l,m} \tag{2.7}$$

where $\Delta\rho_i^{l,m} = \rho_i^l - \rho_i^m$ and others are defined in a similar way. This is called relative (or differential) positioning because a user location is calculated relative to another receiver location based on the differenced range measurements, $\Delta\rho_i^{l,m}$. In contrast, absolute (or point) positioning estimates absolute position instead of relative position. An example of relative positioning is differential GPS (DGPS).

Table 2.3 describes the change in the number of variables for relative positioning. Since there are two receivers, $2n$ measurements and $n+8$ unknown variables are given. $n+8$ constitutes four variables per each receiver (3 position variables and 1 receiver clock bias) and n transmitter clock biases. After differencing, by losing effectively half of the measurements the unknown variables reduce to four. Hence, as long as more than three transmitters exist $n \geq 4$, the position estimation can provide a solution. In actuality, there are still eight remaining variables since both receivers' location and clock biases are unknown. However, if only relative location between two receivers is of interest, the number of relative terms is four (for three dimensional positioning).

Relative positioning is used in the TV positioning system. A detailed description is given in Chapter 3.

Table 2.4: Number of variables in TOA and TDOA

TOA (before differencing)		TDOA (after differencing)	
Measurements	Unknowns	Measurements	Unknowns
n	4	$n-1$	3

2.4.2 Removing Receiver Clock Bias

The receiver clock bias can be removed using TDOA. TDOA is another type of differencing method for range measurements and removes a common error in measurements observed by a single receiver. In other words, TDOA eliminates receiver-oriented errors while relative positioning tracks transmitter-oriented errors. In contrast, TOA positioning which does not involve differencing. An example of a TDOA positioning system is Loran.

A receiver clock bias is, by definition, an error originating from the receiver itself. Thus, it is a fixed and common error source, b, in all measurements by the receiver.

$$\begin{aligned} \rho_i &= r_i + b - B_i + \epsilon_i \\ \rho_j &= r_j + b - B_j + \epsilon_j \end{aligned} \tag{2.8}$$

Differencing between any two measurements removes the receiver clock bias.

$$\Delta\rho_{i,j} = \Delta r_{i,j} + \Delta B_{i,j} + \Delta\epsilon_{i,j} \tag{2.9}$$

where $\Delta\rho_{i,j} = \rho_i - \rho_j$ and others are defined in a similar way.

TDOA reduces the number unknown variables in the positioning equation by one since only the receiver clock bias has been removed. If all transmitters are assumed to be synchronized (i.e., $\Delta B_i = 0\ \forall i, j$), the total number of unknown variables changes from four to three. Compared to relative positioning (from $n+8$ to 4 or 8), the impact of TDOA is less significant and there is no specific reason to prefer either TOA or TDOA. Table 2.4 lists the number of variables in the TOA and TDOA positioning methods. A deeper comparison between TOA and TDOA is given in Chapter 5.

Chapter 3

Television Positioning System

Television has had a significant role in social, economic, and cultural changes in modern history. It has effected several generations and continues to occupy a central space of our daily lives. Now, it is introduced into a completely different field, *radio positioning*. Within this chapter, we introduce a positioning system based on broadcast television signals.

3.1 Television Signals

This section introduces broadcast television signals and their components used in TV positioning.

3.1.1 Television Standards

Just like many other systems, TV standards vary from country to country. North and South America and East Asia adopted the NTSC standard (National Television Systems Committee) while PAL (Phase Alternating Line) is used in Europe, South Asia, Africa, and South America. SECAM (color sequential with memory) is used in France, Russia, and some countries in Africa. Unfortunately, this division continues to exist and propagates into digital TV standards: ATSC (advanced television systems committee) is used in the U.S. and Korea, DVB (digital video broadcasting) in

Table 3.1: Television standards

Type	Standard	Regions
Analog	NTSC	North/South America, East Asia
	PAL	Europe, South Asia, Africa, South America
	SECAM	France, Russia
Digital	ATSC	United States, Korea
	DVB	Europe
	ISDB	Japan

Europe, and ISDB (integrated services digital broadcasting) in Japan. See Table 3.1 for the list of the TV standards.

The U.S. standard, ATSC, is based on VSB (vestigial sideband modulation) [27] and the other standards, DVB and ISDB, are based on COFDM (coded orthogonal frequency division multiplexing) [28]. The TV positioning system (TPS) to be discussed here is based on either NTSC or ATSC standards but there are no fundamental obstacles in expanding it to other TV standards for positioning.

3.1.2 ATSC Digital TV Signal

There are thousands of TV channels in the U.S., some analog (NTSC) and some digital (ATSC). Since the existing analog stations are expected to be replaced by digital stations in coming years, we are going to focus on the ATSC standard illustrated in Figure 3.1. ATSC signals are composed of fields (with duration 24.2 ms), segments (77.3 μs), and symbols (92.9 ns). Each field contains 312 data segments conveying video and audio information and one field synchronization segment.

Within this field synchronization segment, there are sequences of pseudo-random (PN) symbols (one PN 511 sequence and three PN 63 sequences) designed to provide synchronous reception of data segments. Because of the resemblance of these ATSC PN sequences to GPS PN sequences, it is straightforward to adopt ATSC field segments for positioning by measuring pseudoranges in almost the same manner as we collect GPS range measurements [21]. Compared to GPS C/A (course acquisition)

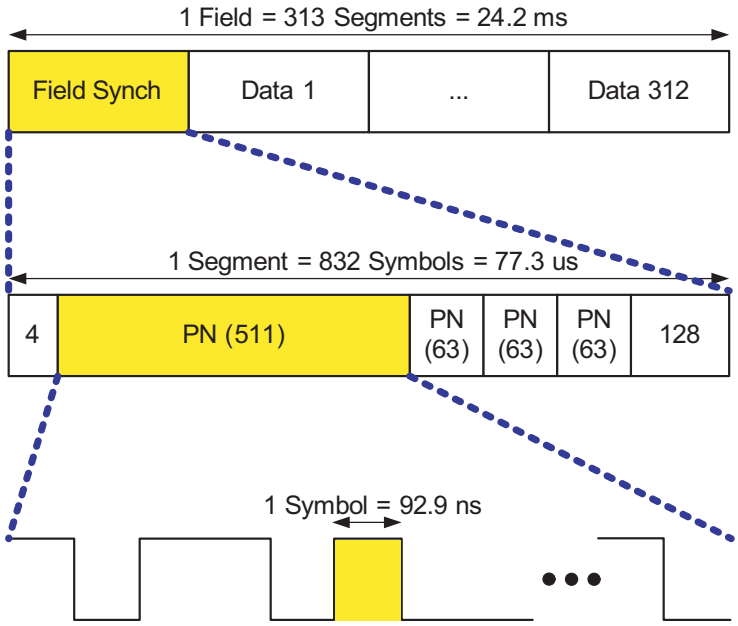

Figure 3.1: ATSC (digital television standard) signal structure

Table 3.2: Pseudo-random sequences

	Symbol rate (10^6 symbol/s)	Symbol duration (ns)	Sequence length	Correlation gain (dB)
ATSC PN511	10.76	92.9	511	27.1
GPS C/A	1.023	978	1023	30.1

code sequence (1023 symbols with each symbol length approximately 1 μs), the number of symbols is about one half of the C/A code but with much shorter duration (92.9 ns, less than one tenth of a GPS symbol duration). Table 3.2 summarizes the comparison of the ATSC PN 511 sequence and the GPS C/A code sequence.

A shorter symbol duration means a narrower correlation peak and so the field synchronization segment potentially outperforms the GPS C/A code in terms of ranging accuracy and multipath mitigation. In particular, it would be useful to resolve multipath—finding a correlation peak out of overlapped multiple correlation functions—in indoor and urban canyons. Figure 3.2 depicts the overall PN sequences (700 symbols $= 511 + 3 \times 63$) and their correlation functions. There are minor correlation peaks besides the primary peak because of the repetitive 63 PN sequences. The

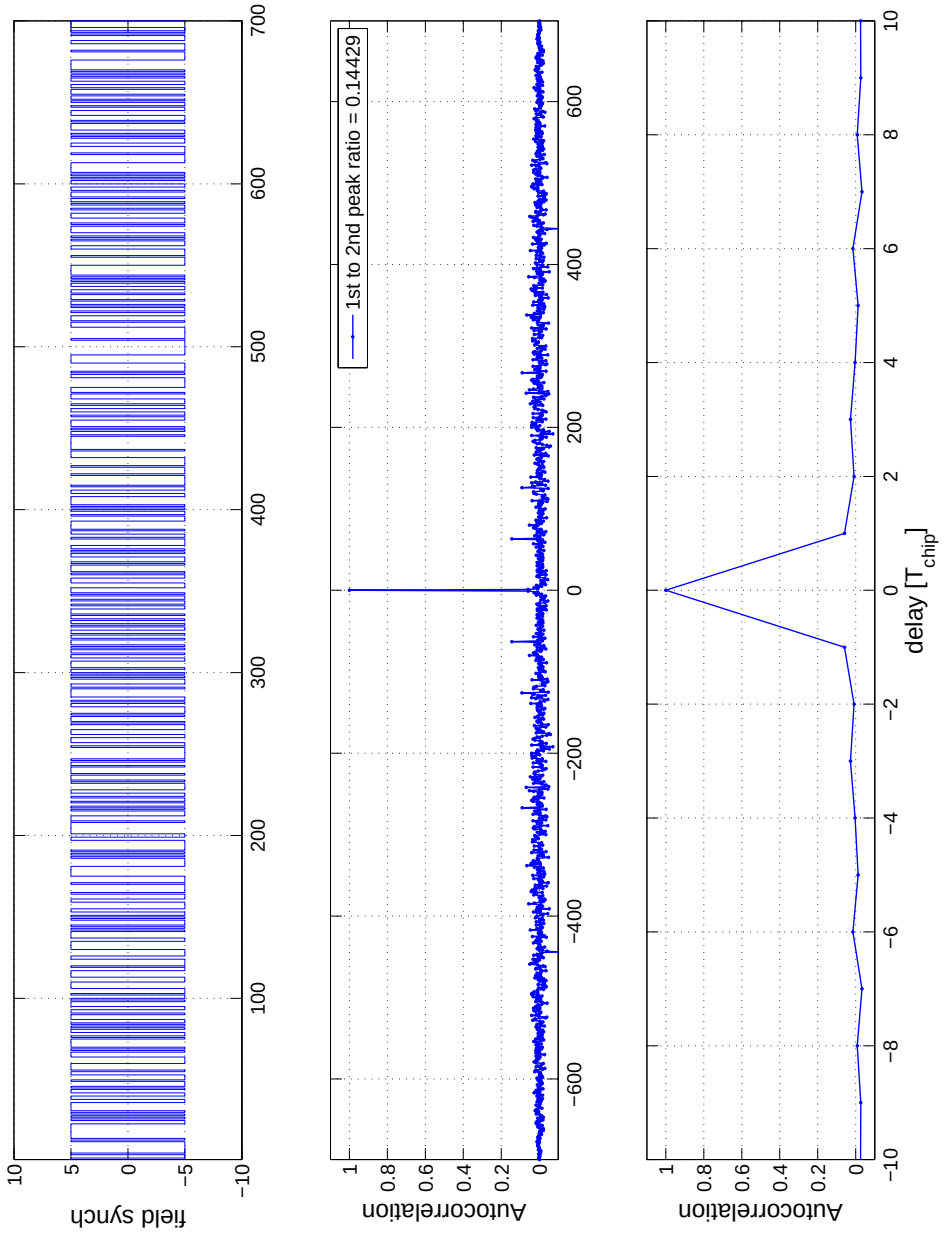

Figure 3.2: Autocorrelation of a field synchronization segment in ATSC signals

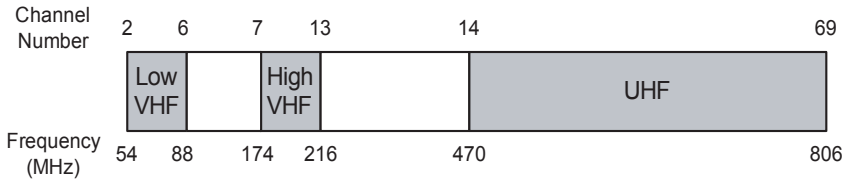

(a) Channel allocation

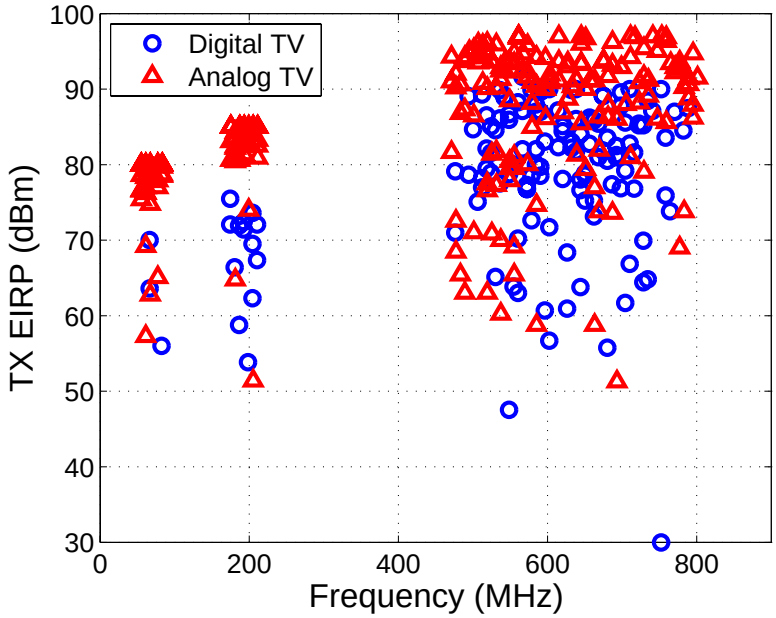

(b) Transmission power

Figure 3.3: TV stations in the United States

secondary peaks are 63 symbols (corresponding to 5.9 μs) apart from the primary peak in time and 8.4 dB below in magnitude. To avoid these additional peaks, only the 511 PN sequence may be used as a local replica.

3.1.3 TV Channels

TV channels are spread in three frequency bands: two VHF bands at 54–88 MHz (Channels 2–6) and 174–216 MHz (Channels 7–13); and a UHF band at 470–806 MHz (Channels 14–69) (see Figure 3.3(a)). Approximately one half GHz of spectrum

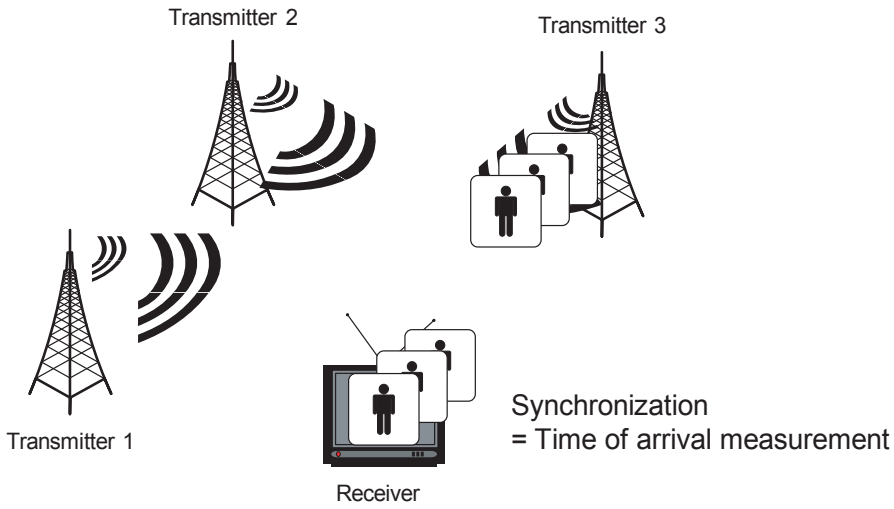

Figure 3.4: Television signal reception

is allocated for TV service with a total of 68 channels having minimal interference with one another. In Figure 3.3(b), a portion of the TV channels (300 channels) is displayed in a spectral signal space with their transmission power (EIRP) and frequency allocations. The transmission power (dBm) can be converted to power spectral density (dBm/MHz) by subtracting 7.8 dB (divided by the 6 MHz bandwidth). The high power level and significant spectral occupancy certainly promote the candidacy of TV signals as a ranging solution in urban and indoor areas as discussed in Chapter 1.

3.2 TV Positioning System (TPS)

This section describes the system structure and operation of the TPS.

3.2.1 System Overview

When we turn on a television at home, it receives a number of TV signals from different channels as illustrated in Figure 3.4. So it first tunes into a channel (a specific frequency) and receives a stream of images transmitted from a TV tower. To receive these images (and audio), the television synchronizes itself with the transmitter based on embedded synchronization segments: field synchronization segments

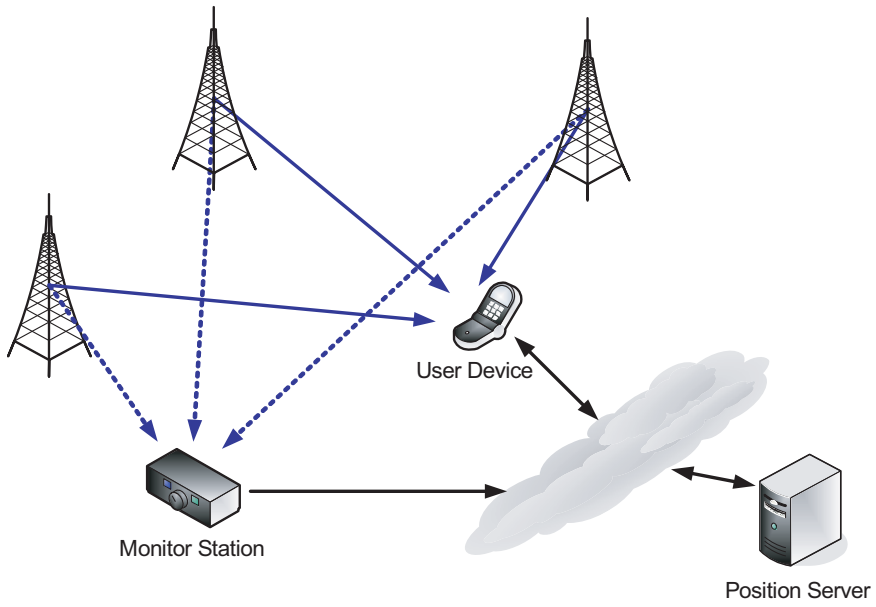

Figure 3.5: Television signals for radio positioning

in ATSC and GCR (ghost canceling reference) in NTSC. "Ghost" refers to images created by multipath signals looking like a ghost on a TV screen.

The synchronization process involves correlation of PN sequences just like a GPS receiver uses C/A code sequences to receive the GPS signals. The time of the correlation peak corresponds to the time of arrival (TOA) of signals. Then, these TOA measurements can be used for positioning after removal of transmitter clock biases. For the clock calibration (removal of clock biases), as discussed in Chapter 2, monitor stations are required to collect independent TOA measurements and generate clock calibration information.

The need for clock calibration makes a TV positioning device depend on supporting monitor stations, while a GPS receiver will work independently. However, the good news is that pedestrian users are the primary target of seamless positioning service. They are likely to carry cell phones through which clock information can be delivered. Considering the current consumer trend toward a "convergence" device combining functions of communication, positioning, and multimedia player, we can imagine a cell phone with a TV tuner on which TV positioning can easily be implemented. These types of devices are already gaining popularity in certain

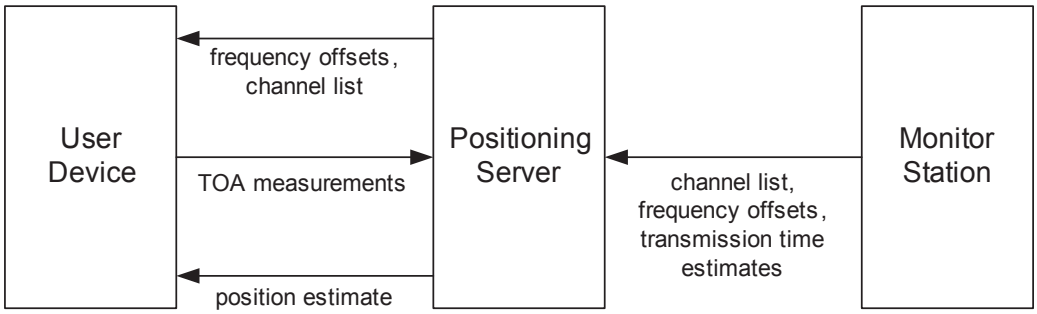

Figure 3.6: TV positioning system diagram

Asian markets like Korea [41]. In short, while GPS delivers time transfer information through its own signals, the TPS does the same job with the help of a cellular network which should be a part of this personal communication and position device.

The information flow between a TV positioning device and a monitor station is illustrated in Figure 3.6. Within the monitor, there is a GPS receiver (generating a time stamp for each measurement) and a TV receiver (monitoring transmitter clocks and maintaining a list of available TV channels). The monitored channel information is sent through a network to the TV positioning device and it collects range measurements. The actual position estimation can be done either at the TV positioning device or at a position server installed as part of the TPS.

3.2.2 TOA Measurements

A TV positioning device ("User Device") is illustrated in Figure 3.7. Based on incoming aiding information (a list of locally available channels and their frequency offsets), a TV tuner tunes to channels, one at a time. After sampling at an analog to digital converter (ADC), the captured TV signal, $y_i(t)$, is correlated with a local replica of the field synch segment, $r(t)$, for the duration of a field synch, T. For longer integration, T is increased beyond a single segment length. The correlation output, $R_i(\tau)$, is given as follows

$$R_i(\tau) = \int_0^T y_i(t) r(t-\tau) dt \tag{3.1}$$

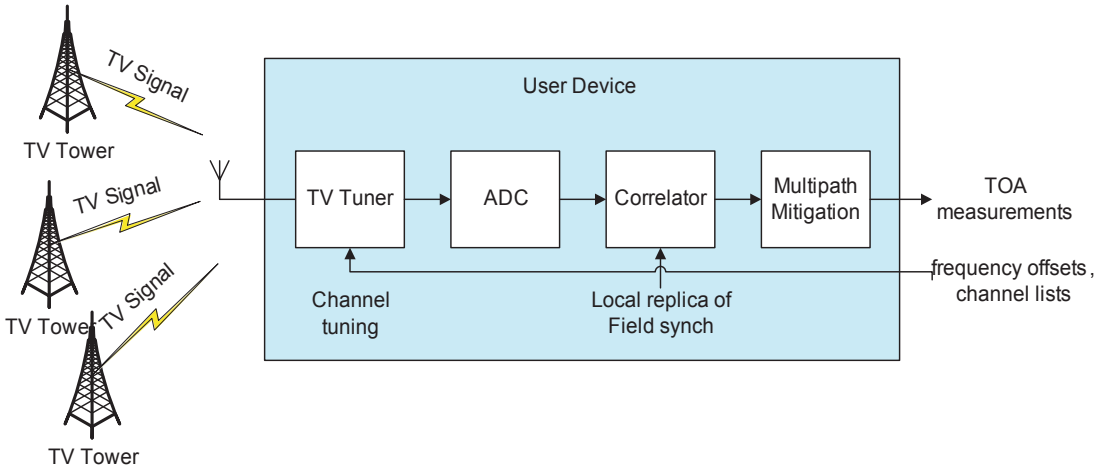

Figure 3.7: TV positioning device

where $r(t)$ is common to all channels. When the correlation is maximized, the time instance, τ, becomes the time of arrival

$$\tilde{t}^u_{RX,i} = T_i + \arg\max_{\tau} R_i(\tau) \tag{3.2}$$

relative to the receiver time stamp, T_i, corresponding to the starting point of $y_i(t)$. The determination of the TOA is complicated in the presence of multipath signals. To avoid locking into a secondary peak caused by a strong multipath signal, a multipath mitigation algorithm is applied to the correlation output [5], [42]–[45]. Multipath mitigation remains outside of the scope of this dissertation.

Since TV channels are spread in various frequency bands, a TV tuner is set to sweep through channels in order to collect TOA measurements, $\tilde{t}^u_{RX,i}$, from each channel. Then, the TOA measurements are converted to range measurements, ρ_i, from TV towers:

$$\rho_i \quad = \quad \tilde{t}^u_{RX,i} - \tilde{t}^u_{TX,i} \tag{3.3}$$

However, there is a difference from GPS which is the lack of a time tag, i.e., embedded time of transmission information. The time of transmission of TV signals, $\tilde{t}^u_{TX,i}$, is

unknown to the receiver. Thus, the TOA measurement itself is considered to be the pseudorange, $\tilde{\rho}_i$.

$$\begin{aligned} \tilde{\rho}_i &= \tilde{t}^u_{RX,i} \\ &= t^u_{RX,i} + b + \epsilon_i \\ &= r_i + t^u_{TX,i} + b + \epsilon_i \end{aligned} \tag{3.4}$$

since $r_i = t^u_{RX,i} - t^u_{TX,i}$. If TV towers are synchronized to each other and transmit signals at the same time instances, time of transmission is the same for all channels, $t^u_{TX} = t^u_{TX,i}\ \forall i$. Then, after combining two time variables, $t^u_{TX}+b$, as a single unknown, the range measurement becomes equivalent to the GPS range measurement. Single frequency TV standards such as digital video broadcasting-handheld (DVB-H) are based on synchronized transmitters.

However, ATSC TV networks are based on unsynchronized independent transmitters. In order to build a positioning system from a unsynchronized network, monitor stations at fixed locations are used. A monitor station monitors TV signals and estimates the time of transmission of each transmitter, $\hat{t}^{\text{mon}}_{TX,i}$:

$$\begin{aligned} \hat{t}^{\text{mon}}_{TX,i} &= t^{\text{mon}}_{RX,i} - r^{\text{mon}}_i \\ &= t^{\text{mon}}_{TX,i} + b^{\text{mon}} + \epsilon^{\text{mon}}_i \end{aligned} \tag{3.5}$$

where $t^{\text{mon}}_{RX,i}$ is a monitor TOA measurement and r^{mon}_i is the known range between the monitor and the transmitter. For now, the true time of transmission at the monitor and at the receiver are assumed to be equal, $t^{\text{mon}}_{TX,i} = t^u_{TX,i}$. Combining the reception time measured by the receiver, $\tilde{t}^u_{RX,i}$, and the transmission time estimated by the monitor, a pseudorange can be obtained without the transmitter clock biases.

$$\begin{aligned} \hat{\rho}_i &= t^u_{RX,i} - \hat{t}^{\text{mon}}_{TX,i} \\ &= (t^u_{RX,i} - t^u_{TX,i}) + (b - b^{\text{mon}}) + (\epsilon_i - \epsilon^{\text{mon}}_i) \\ &= r_i + \Delta b + \Delta\epsilon_i \end{aligned} \tag{3.6}$$

$\hat{\rho}_i$ is the form of pseudoranges used in the TPS. $\hat{\rho}_i$ is based on measurements from the receiver and the monitor and is equivalent to GPS pseudoranges. For a monitor with a stable clock under unobstructed signal paths, $\Delta b \approx b$ and $\Delta\epsilon_i \approx \epsilon_i$ since $|b| \gg |b^{\text{mon}}|$ and $|\epsilon| \gg |\epsilon^{\text{mon}}|$.

Equation (3.6) is a variation of relative positioning discussed in Chapter 2. Here, relative positioning is slightly modified to take advantage of the known and fixed locations of monitor stations. Instead of differencing range measurements between two receivers to remove clock biases, the transmission time is estimated from a receiver (in this case, the monitor station) and delivered to the user receiver. This is done for ease of implementation but generates the same type of range measurements. Let us revisit the formulation of relative positioning.

$$\Delta\rho_i = \Delta r_i + \Delta b + \Delta\epsilon_i \tag{3.7}$$

where $\Delta\rho_i = \rho_i - \rho_i^{\text{mon}}$ and others are defined in a similar way. If the true range from the monitor, r_i^{mon}, is added to both sides, the equation becomes equal to Equation (3.6).

$$\begin{aligned} \Delta\rho_i + r_i^{\text{mon}} &= \Delta r_i + r_i^{\text{mon}} + \Delta b + \Delta\epsilon_i \\ &= r_i + \Delta b + \Delta\epsilon_i \end{aligned} \tag{3.8}$$

Relative positioning or more specifically a monitor station enables an unsynchronized TV network to act as ranging sources for radio positioning.

3.2.3 Integer Ambiguity

One thing we should be careful to interpret is the time of transmission which is the estimated value at a monitor station. Since ATSC TV channels are separated by frequency, a monitor station does not necessarily monitor all channels at the same time. In our implementation, only one channel is monitored in a single time instance and the monitor station sequentially visits channels. Although a user receiver also sweeps through channels, the list and order of channels may not be same with those

the monitor is visiting. Thus, it is less likely for the monitor station and the user receiver to observe the same field from a channel.

This difference causes an integer number of field differences between the time of transmission at the user receiver, $t^u_{TX,i}$ and the time of transmission at the reference receiver, $t^{\text{mon}}_{TX,i}$. In terms of range measurements, this ambiguous integer number, N_i, is multiplied by the wavelength of a TV signal field, λ.

$$\begin{aligned} t^u_{TX,i} - t^{\text{mon}}_{TX,i} &= N_i\lambda + B(t^u_{TX,i}) - B(t^{\text{mon}}_{TX,i}) \\ &\approx N_i\lambda + a_{B,i}(t^u_{TX,i} - t^{\text{mon}}_{TX,i}) \\ &\approx N_i\lambda + a_{B,i}N_i\lambda \end{aligned} \tag{3.9}$$

In addition to field ambiguity, there is clock instability effect represented by the clock drift parameter of a transmitter clock, $a_{B,i}$. Transmitter clock biases, B_i, drift between two fields observed by the receiver and by the monitor, and this drift is approximated by a first order model. A detailed discussion is given in Subsection 3.3.

The estimated time of transmission, $\hat{t}^{\text{mon}}_{TX,i}$, now includes the field ambiguity and the clock drift parameter,

$$\hat{t}^{\text{mon}}_{TX,i} = t^u_{TX,i} - N_i\lambda(1 + a_{B,i}) + b^{\text{mon}} + \epsilon^{\text{mon}}_i \tag{3.10}$$

and so does the estimated pseudorange, $\hat{\rho}_i$:

$$\hat{\rho}_i = r_i + N_i\lambda(1 + a_{B,i}) + \Delta b + \Delta\epsilon_i \tag{3.11}$$

The addition of $N_i\lambda(1 + a_{B,i})$ compared to Equation (3.6) is because the true time of transmission at the monitor and at the receiver are not assumed to be equal any more, i.e., $t^{\text{mon}}_{TX,i} \neq t^u_{TX,i}$.

The wavelength of TV fields are significantly large in terms of distance. The duration of a field is approximately 24.2 ms for ATSC which corresponds to 7254 km in distance. Because the TV field wavelength is significantly larger than a range between a transmitter and the receiver, r_i, and a measurement error, $\Delta\epsilon_i$, the integer

ambiguity, N_i, can be estimated by taking the integer value of $\hat{\rho}_i/\lambda(1+a_{B,i})$,

$$\hat{N}_i = round\left(\frac{\rho_i}{\lambda(1+a_{B,i})}\right). \tag{3.12}$$

Then, we can go back to $\hat{\rho}_i$ and remove the integer ambiguity,

$$\begin{aligned}\hat{\hat{\rho}}_i &= \hat{\rho}_i - \hat{N}_i\lambda(1+a_{B,i}) \\ &= r_i + (N_i - \hat{N}_i)\lambda(1+a_{B,i}) + \Delta b + \Delta\epsilon_i. \end{aligned} \tag{3.13}$$

However, there is a hidden source of error in this integer estimation which is the receiver clock bias, Δb. The receiver clock bias can be as large as tens or hundreds of seconds and is usually much larger than a TV field wavelength, unless there is some form of time synchronization at the initialization of the user receiver. If the magnitude of the clock bias is bigger than one half of the wavelength, $|\Delta b| \geq 1/2\lambda(1+a_{B,i})$, there will be an error in the estimated integer, $\hat{N}_i$.

$$\begin{aligned}\hat{N}_i &= round\left(\frac{r_i + N_i\lambda(1+a_{B,i}) + \Delta b + \Delta\epsilon_i}{\lambda(1+a_{B,i})}\right) \\ &= N_i + round\left(\frac{\Delta b}{\lambda}\right) + \{-1,0,1\} \\ &= N_i + N^b + \{-1,0,1\} \end{aligned} \tag{3.14}$$

where λ is the nominal wavelength of a TV field and $N^b = round\left(\frac{\Delta b}{\lambda}\right)$. N^b is the integer estimation error due to the clock bias, Δb. See Appendix A for the detailed discussion of integer ambiguity resolution. $\hat{N}_i$ may have a difference of ± 1 from $N_i + N^b$ due to r_i and $\Delta\epsilon_i$. However, this difference is easily resolvable when the estimated pseudoranges are aligned together. In other words, the difference between pseudoranges should be much smaller than a single field wavelength.

The corrected pseudorange, $\hat{\hat{\rho}}_i$, in Equation (3.13) now can be expressed in terms

of N^b and $a_{B,i}$,

$$\begin{aligned}\hat{\hat{\rho}}_i &= r_i - N^b\lambda(1 + a_{B,i}) + \Delta b + \Delta\epsilon_i \\ &= r_i - a_{B,i}N^b\lambda + (\Delta b - N^b\lambda) + \Delta\epsilon_i. \end{aligned} \tag{3.15}$$

$a_{B,i}N^b\lambda$ is a new type of error introduced in the pseudoranges. This error is caused by the integer ambiguity and depends on the magnitude of clock bias, N^b, and the stability of the transmitter clocks, $a_{B,i}$. This error is called a frequency instability-induced range error. $N^b\lambda$ is also an additional unknown variable but has a constant value. Thus, it does not affect position estimation.

3.3 Clock Stability

This section continues the discussion of the frequency instability-induced error described in Equation (3.15). A clock is the source of frequency from which timing is derived. Timing is converted to range measurements, which are the basis of radio positioning. Thus, a clock is the core of positioning and its stability determines the overall positioning performance.

3.3.1 Clock Errors

Inside a clock (see Figure 3.8), there is an oscillator generating periodic events and a counter adding up those events. The clock error comes from internal clock deviation (oscillator), measurement error (counter), and external environmental perturbations, such as temperature change [38]. In particular, frequency offsets due to these errors are the main concern for the TPS. Oscillation is based on physical movement of the oscillator (crystal) and the frequency of free running crystal cannot be guaranteed to be free from a frequency offset. This frequency offset is represented by the clock drift parameter, a_B, in Equation (3.15).

In GPS, great effort has been made to put atomic clocks on satellites and to monitor them with a world-wide network of ground stations (see Chapter 2) to support high positioning accuracy. In the case of TV positioning, transmitter clocks (installed

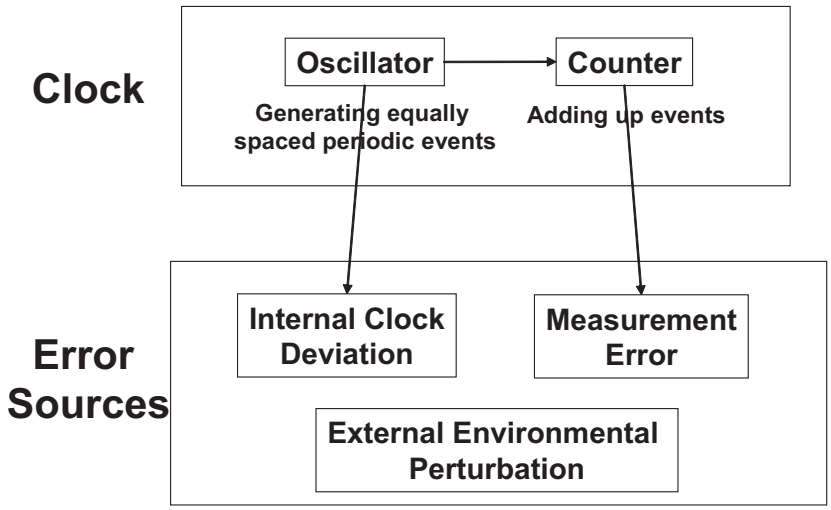

Figure 3.8: Source of clock errors

in TV stations) are not expected to be as good as GPS atomic clocks in terms of stability because the required stability for high accuracy positioning is certainly greater than that for broadcasting audio and video information. However, dedicated monitor stations for TV signals can generate high accuracy clock calibration information (a_B) and provide it to receivers to enable high accuracy positioning.

3.3.2 TV Range Error Caused by Clock Instability

Figure 3.9 and Figure 3.10 illustrate the relationship of a clock error with a range error and a position error, respectively. Three ranging sources are used for two dimensional positioning and a user is at the center of the three towers. Assuming all three transmitters start to send video fields at exactly the same time, the user device is expected to receive fields after an equal amount of time delay from all three transmitters. If the three transmitter clocks are very stable, the time delays will remain the same regardless of which field synchronization segments are used for ranging. In this case, it does not matter which field we capture and there is no need to resolve field (integer) ambiguity as long as all three measurements are projected properly to the same time reference.

However, if there are unstable transmitter clocks, the field resolution is critical

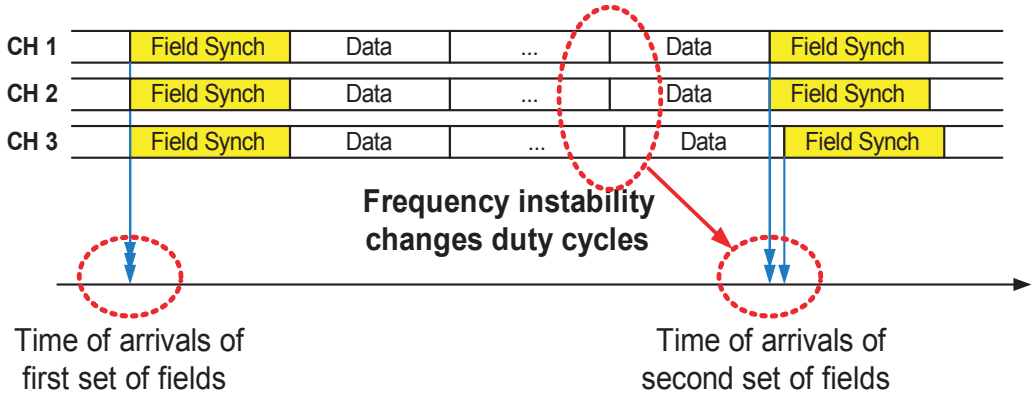

Figure 3.9: Frequency instability-induced range errors

because a choice of incorrect integers generates range errors and corresponding position errors. For example, Channel 3 in Figure 3.9 has a slower clock rate than other channels. In this case, even if all three channels are set to transmit signals at the same time, only the first set of fields will align and the later fields from Channel 3 will be delayed due to the slow clock rate. If the user receiver happens to observe the first set of fields, $(N_1, N_2, N_3) = (1, 1, 1)$, and the integers are estimated correctly (see Figure 3.10(a)), there will be no position error due to the unstable clock of Channel 3. However, if the integers (field numbers) are incorrectly estimated, there will be proportional range errors. Failed integer estimation, $(\hat{N}_1, \hat{N}_2, \hat{N}_3) = (2, 2, 2)$, in Figure 3.10(b) generates a range error in the Channel 3 measurement and the estimated position is no longer at the true location.

3.3.3 Clock Stability Measurements

In Figure 3.11, an example of four ATSC TV channels is given and their clock drifts are illustrated by changes in time of transmission. If the clocks are stable, transmission time relative to the nominal field length (i.e., modulo 24.2 ms) will stay constant over time. The green curve represents a very accurate transmitter clock which maintains constant time of transmission over a 10 minute period. In contrast, the blue curve corresponds to a clock with a significant frequency offset and its transmission time

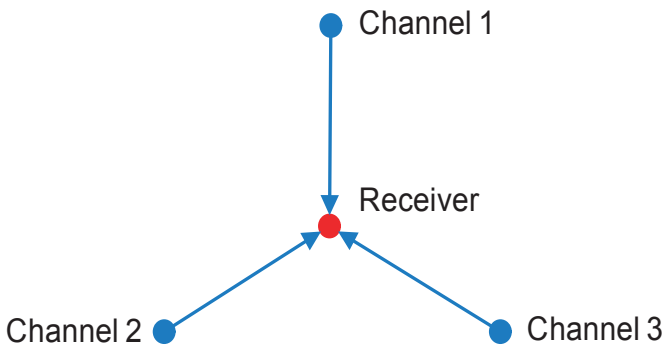

(a) Successful integer estimation , $(\hat{N}_1, \hat{N}_2, \hat{N}_3) = (1, 1, 1)$

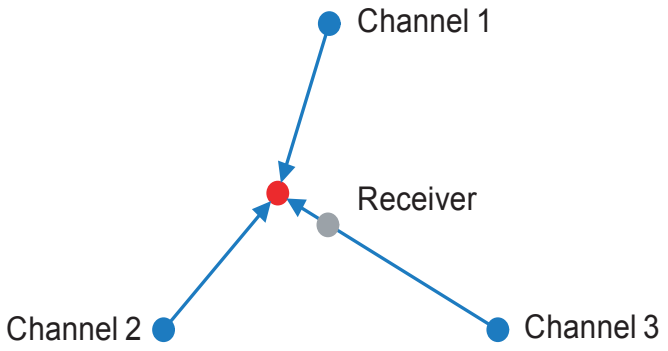

(b) Integer estimation error, $(\hat{N}_1, \hat{N}_2, \hat{N}_3) = (2, 2, 2)$

Figure 3.10: Frequency instability-induced position errors

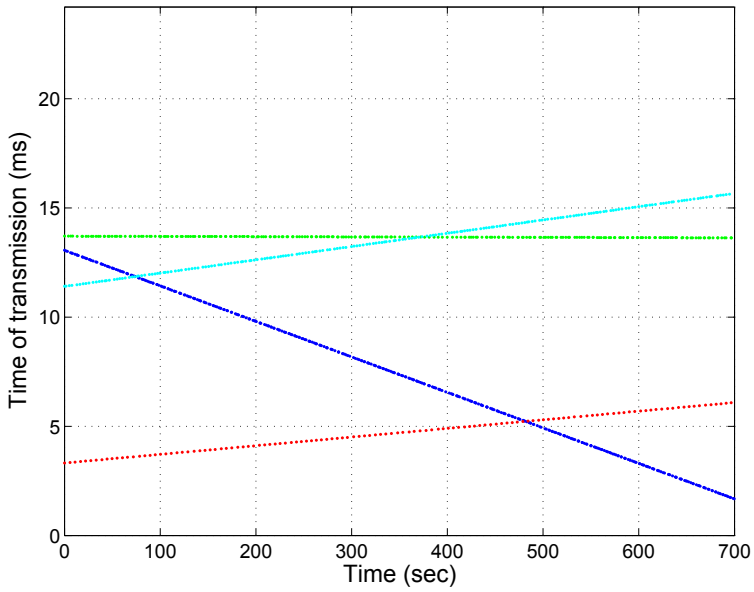

Figure 3.11: Drift of time of transmission

continuously changes over time. Since these clocks contain large but fixed frequency offsets, the clock drift of these clocks can be modeled by a first order liner model in Equation (3.15). In the linear approximation model, the temporal behavior of these clocks can be estimated accurately based on the clock drift parameter, a_B. For the green curve, $a_B \approx 0$ ppm (part per million) and for the rest of channels, a_B is -16.3, 4.1 and 6.3 ppm respectively.

Let us examine possible range errors in this example of four channels. For an integer error of one, $\hat{N} - N = N^b = 1$, the resulting range errors,

$$\text{range error} = -a_B N^b \lambda \tag{3.16}$$

are 118 m for $a_B = -16.3$ ppm and -30 m and -46 m for $a_B = 4.1$ and 6.3 ppm. If the clock bias is as large as 1 second (corresponds to $N^b = 41$), the range errors become 4.9 km, -1.2 km and -1.9 km.

A broader survey result is described in Figure 3.12. 159 ATSC channels are

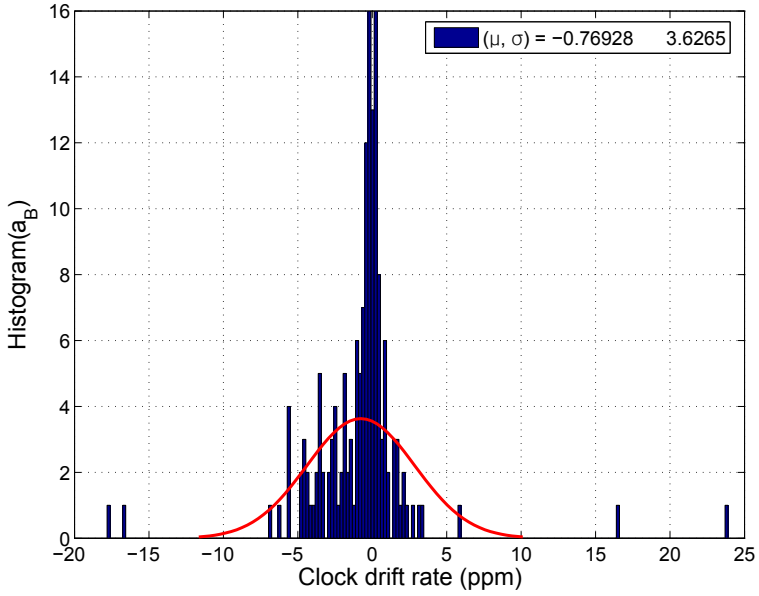

Figure 3.12: Histogram of clock drift parameter

Table 3.3: Frequency instability-induced range error

a_B (ppm)		Range error (m)	
		for $N^b = 1$	for $N^b = 41$
$\mu_{a_B} + \sigma_{a_B}$	2.9	−21	−851
$\mu_{a_B} - \sigma_{a_B}$	−4.4	32	1309

surveyed and the histogram of the clock drift rates is illustrated. The mean clock drift rate, μ_{a_B}, is −0.8 ppm and the standard deviation, σ_{a_B}, is 3.6 ppm. A few worst cases include −17.8 and 23.9 ppm clock drifts. Table 3.3 lists the possible range errors for $a_B = \mu_{a_B} + \sigma_{a_B} = 2.9$ ppm and $a_B = \mu_{a_B} - \sigma_{a_B} = 4.4$ ppm. Again for an integer error of one, $N^b = 1$, the expected range errors are −21 m and 32 m. For $N^b = 41$ (1 second clock bias), the range errors become −851 m and 1309 m.

These substantial range errors are again due to transmitter clock instability. To avoid this type of range errors, the clock drift parameters are constantly updated by

the monitor stations. Also, in the case of favorable geometry and redundant measurements, these range errors are more easily detectable by receivers because there will be large disagreement among range errors. However, in a challenging environment, it becomes difficult to detect these errors which are observed during the field test results discussed in Chapter 7.

Chapter 4

Integration of GPS and TPS

As discussed in the preceding chapters, both GPS and TPS have their advantages and disadvantages. GPS provides a global service but lacks availability in dense urban areas and indoor areas; TPS penetrates well into urban and indoor areas but has weak coverage in less populated regions since there are lower commercial needs. Because their coverage areas are complementary, the combination of GPS and TPS is expected to provide significantly enhanced coverage as compared to individual coverages. In this chapter, we discuss the integration of GPS and TPS, describing the integrated system structure and analyzing its performance.

4.1 Hybrid GPS and TV Positioning System

This section provides a description of the system architecture of a hybrid GPS and TV positioning system.

4.1.1 System Overview

A hybrid GPS and TPS system is introduced in Figure 4.1 where both a user receiver and a monitor station are equipped with GPS and TV receivers. A position server routes monitor aiding information and estimates user location based on user and monitor measurements. If GPS satellites are removed from Figure 4.1, we are left with

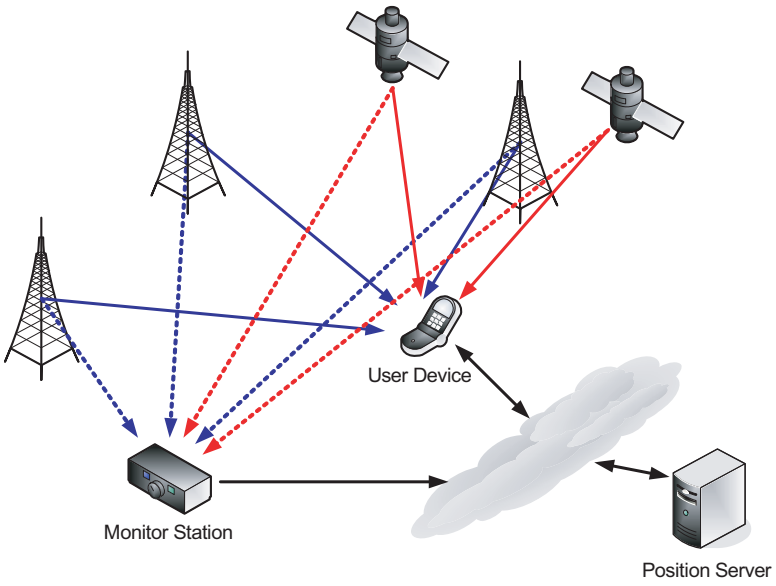

Figure 4.1: Combined GPS and TV positioning system

only TPS as described in Chapter 3. On the other hand, without TV transmitters, the system is able to function as an AGPS where aiding information (satellite locations and Doppler frequency) is fed forward to a GPS receiver for quicker and more stable acquisition and tracking of GPS signals. However, within this dissertation, only stand-alone GPS operation is assumed and all data are based on autonomous GPS measurements without network aiding.

There are two outstanding benefits of integration. First, ranging sources are increased by the marriage of GPS and TPS. In low visibility areas like indoor or urban canyons, it is difficult to maintain enough satellites to produce position estimates, and so the addition of TV towers is critically important to higher availability. The increased number of range measurements are helpful in high visibility regions, too, improving accuracy and providing redundancy. In particular, redundancy is important in detection and exclusion of erroneous measurements which is discussed in Chapter 6. Second, geometric diversity is enhanced. Vertically, there are GPS satellites (in urban environments, only high elevation satellites are likely visible); and horizontally there are TV towers. This combination of vertical and horizontal diversity provides a better geometry with a smaller DOP (dilution of precision) and consequently a better

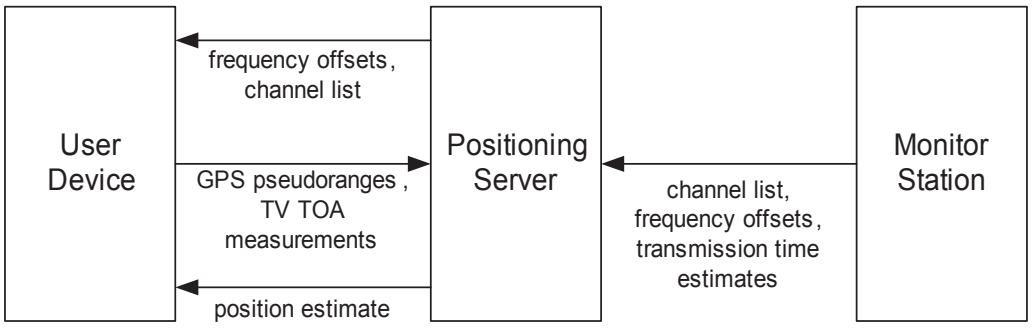

Figure 4.2: Hybrid GPS and TV positioning system diagram

position accuracy for a given range accuracy.

The aiding information from monitor stations is collected at a position server connected to a communication network. Then, the position server sorts out relevant information and delivers it to a receiver through a communication link such as simple SMS (short message service) messaging on a cell phone network (see Figure 4.2). Although the amount of data flow between a receiver and a position server should be minimized to avoid unnecessary data traffic, there is still room for improvement of the hybrid GPS/TV system since both a monitor and a user receiver are equipped with a GPS receiver and a TV receiver. We can envision that AGPS or DGPS can be easily implemented within this hybrid GPS/TV positioning system, an untapped potential improvement to be exploited in future studies.

4.1.2 Range Measurements

A hybrid positioning device consists of a TV positioning device and a GPS receiver (see Figure 4.3). Unlike TV channels, GPS channels are not separated by frequency but are distinguished by a correlator which uses multiple PN sequences specific to each channel. Thus, the RF front end of a GPS receiver is tuned to a fixed frequency, 1575.42 MHz, while the TV tuner adjusts its frequency in 54–804 MHz.

When a GPS signal, $y_{GPS}(t)$, is captured, it contains all observed GPS channels. $y_{GPS}(t)$ is correlated with PN sequences, $r_{GPS,i}(t)$, one at a time. The correlation

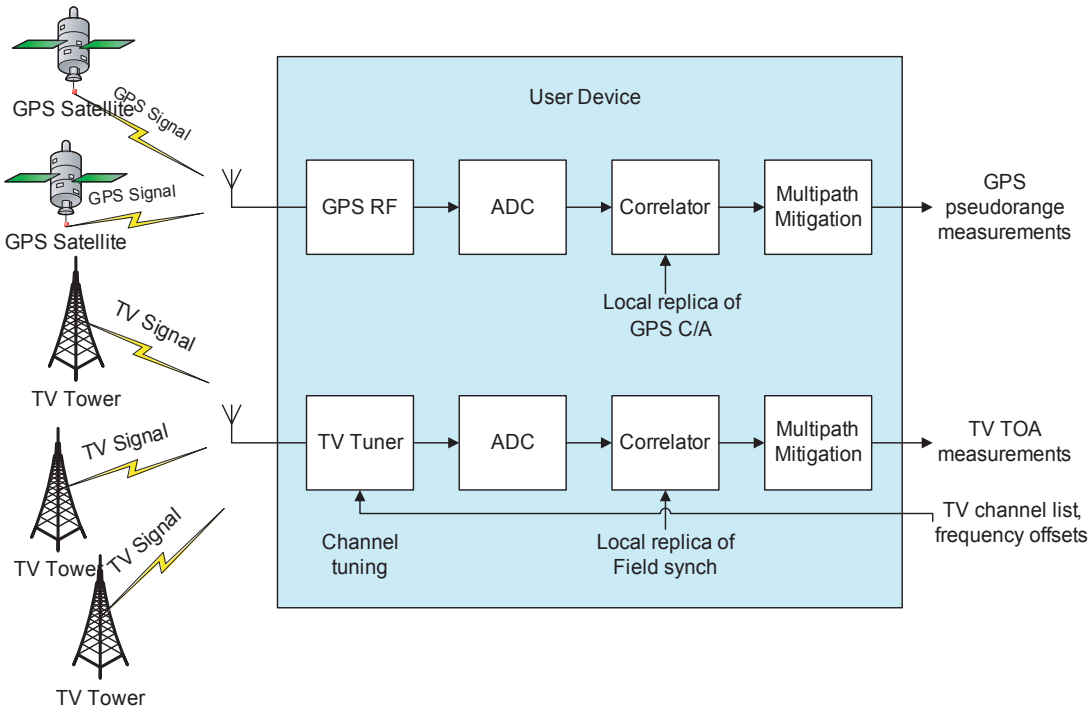

Figure 4.3: Hybrid GPS and TV positioning device

output, $R_{GPS,i}(\tau)$, is given as follows

$$R_{GPS,i}(\tau) = \int_0^T y_{GPS}(t) r_{GPS,i}(t-\tau) dt. \tag{4.1}$$

The time of arrival, $\tilde{t}_{RX,i}^{GPS}$, is calculated relative to a receiver time stamp, T_0, corresponding to the starting point of $y_{GPS}(t)$.

$$\tilde{t}_{RX,i}^{GPS} = T_0 + \arg\max_{\tau} R_i(\tau) \tag{4.2}$$

$$\rho_{GPS,i} = \tilde{t}_{RX,i}^{GPS} - t_{TX,i}^{GPS} \tag{4.3}$$

A GPS pseudorange, $\rho_{GPS,i}$, is obtained by subtracting the time of transmission, $t_{TX,i}^{GPS}$, from $\tilde{t}_{RX,i}^{GPS}$. $t_{TX,i}^{GPS}$ is calculated from the time stamp in the GPS signal and adjusted by clock calibration parameters which are also embedded in the GPS signal (see Appendix A for details).

The GPS pseudoranges in Equation (4.3) are combined with TPS pseudorange measurements for the integration of GPS and TPS. Since both pseudoranges are in the same format and contain an individual receiver's clock bias and an unmodeled random error, the integration is implemented straightforward.

$$\text{GPS: } \rho_{GPS,i} = r_i + b_{GPS} + \epsilon_{GPS,i} \tag{4.4}$$

$$\text{TV: } \rho_{TV,j} = r_j + b_{TV} + \epsilon_{TV,j} \tag{4.5}$$

Following the same linear approximation based on Taylor series in Chapter 2, the combined positioning equation becomes

$$\text{Hybrid: } \delta\boldsymbol{\rho} = \boldsymbol{G}\delta\boldsymbol{x} + \boldsymbol{v} \tag{4.6}$$

where $\delta\boldsymbol{\rho}$, $\delta\boldsymbol{x}$, $\boldsymbol{G}$, and $\boldsymbol{v}$ are

$$\delta\boldsymbol{\rho} = \begin{bmatrix} \delta\boldsymbol{\rho}_{GPS} \\ \delta\boldsymbol{\rho}_{TV} \end{bmatrix},\ \delta\boldsymbol{x} = \begin{bmatrix} \delta x \\ \delta y \\ \delta z \\ \delta b_{GPS} \\ \delta b_{TV} \end{bmatrix},\ \boldsymbol{G} = \begin{bmatrix} \boldsymbol{e}_1^T & 1 & 0 \\ \vdots & \vdots & \vdots \\ \boldsymbol{e}_{n_{GPS}}^T & 1 & 0 \\ \boldsymbol{e}_{n_{GPS}+1}^T & 0 & 1 \\ \vdots & \vdots & \vdots \\ \boldsymbol{e}_{n_{GPS}+n_{TV}}^T & 0 & 1 \end{bmatrix},\ \boldsymbol{v} = \begin{bmatrix} \boldsymbol{v}_{GPS} \\ \boldsymbol{v}_{TV} \end{bmatrix}$$

and $\boldsymbol{e}_i = (\boldsymbol{u} - \boldsymbol{s}_i)/\left\|\boldsymbol{u} - \boldsymbol{s}_i\right\|$. The only difference from the ordinary GPS positioning equation or the TV positioning equation is the inclusion of two receiver clock biases , b_{GPS} and b_{TV}. However, in exchange for two unknown variables, there are usually more TV and GPS range measurements offsetting the increase in the number of unknowns. In a fully integrated GPS and TV positioning device with an internal synchronization scheme across GPS and TV receivers, the two clock bias terms, b_{GPS} and b_{TV}, can be combined.

4.2 Hybrid Operational Modes

This section describes the operational modes of hybrid GPS and TV positioning, focusing on external network aiding and positioning dimensions.

4.2.1 Network Aiding

A user positioning device and a monitor station (described in Chapter 2) both receive signals from common ranging sources. However, a user receiver suffers from signal obstruction and multipath while a monitor station is placed in clear view of transmitters, enjoying unobstructed signal reception. To help the hindered user receiver, the high quality measurements at a monitor can be used to enhance the sensitivity of the user receiver by providing aiding information such as the list of transmitters in view and their signal characteristics.

The aiding information given in Table 4.1 allows a TV receiver to quickly acquire

Table 4.1: Aiding information to TV receiver

Aiding information	Description
TV channel list	List of available TV channels in a region
Frequency offset	Pilot and symbol clock offsets of TV channels
Time offset	Transmitter clock biases of TV channels

TV channels with enhanced sensitivity. Exact knowledge of pilot (carrier) frequencies for a given list of channels speeds up the signal acquisition, while known code rate offset is used to compensate code offsets enabling longer integration of signals. The fast signal acquisition has significance since a TV receiver needs to scan for channels in a wide spectrum range and the overall process is done in an accumulation of time spent on each channel. Thus, knowing which channel to scan for and what its pilot frequency offset is minimizes the scan time per channel and eventually the overall acquisition time as well. The code rate offset is important for sensitivity enhancement. In a harsh indoor environment, even strong TV signals can be substantially attenuated where a single field measurement (repeating every 24.2 ms) may not be sufficient enough to provide a reliable range measurement—remember that only one field synch segment (77.3 μs long) out of a field (24.2 ms) is usable for range measurements. Then, integration over multiple fields becomes critical for which the knowledge of code rate offset is used for alignment of field synch segments occurring every 24.2 ms.

Much similarity exists between TPS and GPS regarding aiding information. The list of available channels and their frequency offsets are helpful, but not required, aiding information because these can be estimated at receivers without network aiding. However, the baseline information regarding transmitter position and time bias should be provided and cannot be estimated at receivers independently. For GPS, these data are the essence of GPS messages delivered by GPS signals: satellite orbit correction and clock calibration data. Unfortunately, in the case of TV, this information is not contained in the signals and should be provided as aiding information by a positioning server. Since TV signals come from stationary TV towers, there is no need for a constant update of transmitter position information and a table of

Table 4.2: Hybrid operational modes

Mode	N_{SV}	N_{TV}	Variables	Network Aid
3D GPS	≥ 4		(e, n, u, b_{GPS})	N/A
2D TV		≥ 3	(e, n, b_{TV})	Δf_{TV}, Δt_{TV}, TV TX list
3D Hybrid	$N_{total} \geq 5$		$(e, n, u, b_{GPS}, b_{TV})$	Δf_{TV}, Δt_{TV}, TV TX list

Note: For the 2D position fix, only east and north directions (e,n) are considered, excluding altitude ("up" direction). For the 3D position fix, east, north and up directions (e,n,u) are considered.

transmitter location stored in receiver memory can be sufficient. The critical and time-varying information, requiring constant updates for TV positioning, is the time offsets of TV transmitters, since TV positioning is based on an unsynchronized transmitter network. This information is provided by monitor stations to either a receiver or a positioning server depending on where the actual position estimation happens. Due to the necessity of aiding information regarding transmitter time offsets, a TV positioning device relies on network aiding regardless of signal quality while a GPS receiver can operate autonomously as long as received signal quality supports successful data recovery.

4.2.2 Positioning Modes

With combined GPS and TV positioning, there are three possible scenarios of operation depending on availability of GPS satellites and TV stations in a specific region as well as network aiding (see Table 4.2). On a remote mountain, without a communication link, only GPS would be available for which three dimensional positioning is preferred because of the vertical diversity of GPS satellites. On the other hand, in an office area without access to GPS signals, TV positioning is the only possibility. In this case, two dimensional positioning is recommended due to the lack of vertical diversity. At least three transmitters must be available for this operation.

The last scenario falls between these two cases when a mixture of TV and GPS signals are in view and is supported by hybrid GPS and TV positioning. Taking advantage of the high altitude of GPS satellites, we can perform three dimensional

positioning in these inbetween cases if at least five transmitters (including both GPS and TV transmitters) can be observed. If the number of transmitters in any of the ranging sources becomes fewer than two, then the hybrid system falls back into either of the single modes. In the presence of accurate signal statistics, we can expect the hybrid mode to outperform the GPS mode and the TV mode both in accuracy and availability.

4.3 Performance Analysis

In this section, the positioning accuracy of GPS and TPS is analyzed based on signal specifications and the Cramer-Rao Bound.

4.3.1 Signal Power and Bandwidth

The noise-only performance limits of GPS and TPS can be derived from their physical conditions: transmission power, path loss, and bandwidth. While GPS satellites have strictly limited on-board energy sources which are neither replaceable nor expandable due to space and weight constraints, TV towers have access to relatively unlimited energy resources, sending stronger signals than GPS signals. Furthermore, path losses are also not in favor of GPS. While GPS satellites are in medium earth orbits (MEO) more than 20,000 km away from ground users, TV towers are normally less than 100 km away from urban users. Consequently, the path loss of TPS is significantly lower than that of GPS. In addition to the power factors, the broader per-channel frequency bandwidth—5.38 MHz for TV (ATSC signal) and 2 MHz for GPS (C/A code)—is another advantage of TV signals. These physical advantages of TV signals help TPS to penetrate into urban canyons and indoors.

Detailed signal power budgets in urban areas are given in Table 4.4 where we assume line-of-sight GPS signals and obstructed TV signals, assumptions favorable to GPS but conservative to TPS. The major differences come from transmission power (EIRP)(Δ = about 29.5 dB) and path loss (Δ = 14.4 dB) where the nominal TV transmission power (EIRP) is given by the average of the surveyed ATSC transmission

Table 4.3: Path loss exponents for different environments [78]

Environment	Path loss exponent
Free space	2
Urban area cellular radio	2.7–3.5
Shadowed urban cellular radio	3–5
In building line-of-sight	1.6–1.8
Obstructed in building	4–6
Obstructed in factories	2–3

power levels in the U.S. EIRP combines the transmitter power and the transmitter antenna gain in Table 4.4.

Path loss is approximated from the log distance path loss model with the path loss exponents of two for GPS and four for TPS (see Table 4.3). Note that the path loss exponent of two was used in Chapter 1 but now a more conservative approach is taken for TV signals. The log distance path loss model dictates

$$P_{RX} = P_{TX} \frac{G_{TX} G_{RX}}{L_{air}} \left(\frac{\lambda}{4\pi d_0} \right)^2 \left(\frac{d_0}{d} \right)^n \tag{4.7}$$

where P_{RX} is a received signal power, P_{TX} is a transmitted signal power, G_{TX} is a transmitter antenna gain, G_{RX} is a receiver antenna gain, and L_{air} is an atmospheric loss. The GPS carrier wavelength, λ_{GPS}, is 0.19 m and a nominal TV carrier wavelength, λ_{TV}, is set to be 0.5 m from the range of 0.37–0.64 m corresponding to 470–806 MHz. d_0 represents the reference distance for a far field assumption and 1 km is a typical value for large scale systems like TV broadcasting. The distance between a transmitter and a receiver, d, is assumed to be 20,000 km for GPS and 100 km for TPS. The path loss exponent, n, represents the harshness of environments, determining signal degradations over distance. n is known to be 2.7–3.5 in urban areas and 3–5 in shadowed urban areas [78]. The path loss exponent of 4 for TV signals represents a severe urban environment; that of 2 for GPS signals assumes free space propagation without any obstruction in the signal path.

From Equation (4.7), the received signal powers show a difference of 40 dB between

Table 4.4: Signal power budget in urban areas

Power		GPS	TPS	Δ
TX Power (dBm)		44.3	70.0	25.7
Loss & gain	TX antenna gain (dB)	10.2	14.0	3.8
	Path loss (dB)	182.4	168.0	-14.4
	Atmospheric loss (dB)	0.5	0.0	-0.5
	RX antenna gain (dB)	4.0	0.0	-4.0
RX Power (dBm)		-124.4	-84.0	40.4
Noise power	Thermal noise floor (dBm)	-111.1	-106.7	4.4
	System noise figure (dB)	3.0	5.0	2.0
RX SNR (dBm)		-16.3	17.7	34.0
Post-processing	De-spreading gain (dB)	30.1	27.1	-3.0
	Integration gain (dB)	20.0	6.0	-14.0
Post-processing SNR (dB)		33.8	50.8	17.0

GPS and TPS. This results from the accumulation of gaps in transmission power and path loss. Given noise powers and spreading gains, the resulting signal to noise ratio (SNR) shows a slightly reduced gap due to the higher noise floor, 4 dB higher than that of GPS, because of a wider RF bandwidth. A wider bandwidth appears damaging but it becomes irrelevant after de-spreading.

The post-processing gain is composed of a de-spreading gain and an integration gain by the coherent integration of consecutive signal frames. GPS receivers de-spread the C/A code of 1023 chips, while TV receivers de-spread the field synchronization code of 511 chips. Here it is assumed that the signals integrate coherently in multiple code periods within 100 ms (corresponding to 100 code periods for GPS and four fields for TPS). Since the infrequent existence of field synch segments in the TV signal—0.3% of a frame repeating every 24.2 ms—provides a lower integration gain than GPS integration gain, the gap reduces to 17 dB in the overall post-processing SNR but is still quite a wide margin if interpreted in range error limits.

Table 4.5: Cramer-Rao bound on pseudoranges

Cramer-Rao bound	GPS	TPS
SNR (γ) (dB)	33.8	50.8
Bandwidth (β) (MHz)	2	5.38
σ_ρ in time (ns)	10.2	0.5
σ_ρ in distance (m)	3.1	0.2

4.3.2 Cramer-Rao Bound

The final step to the noise-only performance limits is the Cramer-Rao Lower Bound (CRLB) [13], [61]. The CRLB is a well known bound for an unbiased estimator and is often used in the positioning community for calculation of a limit on range accuracy. The CRLB combines the estimated SNR (see Table 4.4) and signal bandwidth and converts these into the range domain and provides a noise-only performance limit.

The bound for the standard deviation of range errors, σ_ρ, is derived from the CRLB [13], [61] and is given as follows,

$$\sigma_\rho \geq \sqrt{\frac{1}{\gamma\beta^2}} \tag{4.8}$$

where γ is an SNR, and β is a signal bandwidth. The combined gain of the power and bandwidth is equivalent to 26 dB gain of TPS (see Table 4.5). The CRLB for GPS is 3.1 m (10.2 ns in time) and that for TPS is 0.2 m (0.5 ns in time). The low CRLB for TPS is because of its advantage in power, path loss, and bandwidth. These limits are based on the nominal values assumed here and are subject to changes in the underlying assumptions such as integration time.

The readers also should note that this noise-only limit may not be achievable in reality. Often other types of error sources such as clock offsets, receiver implementation losses, and atmospheric and environmental effects could be the dominant source of range errors in practice. For example, the frequency instability-induced range error, discussed in Chapter 3, can be tens of meters even for mis-estimation of a single field. Hence, the CRLB can be understood as the best case performance that the actual range accuracy can approach as other types of error sources are mitigated.

Chapter 5

TOA and TDOA Positioning

This chapter explains why TOA is adopted for both GPS and TPS in this dissertation by comparing TOA and TDOA. While TOA is used in GPS systems, TDOA is adopted in many terrestrial positioning systems and TPS can be implemented to use either TOA or TDOA. However, it is preferable to have a single format of pseudoranges for simplification of the integrated GPS and TPS system. In particular, TOA reduces the complexity of the fault detection and exclusion algorithm in Chapter 6. Thus, this chapter develops a unified TOA approach for both GPS and TPS.

5.1 Equivalence of TOA and TDOA under Ideal Conditions

Assuming perfect knowledge of noise statistics and ideal implementation of the position estimation algorithm, TOA and TDOA are known to have equivalent positioning performance because TOA and TDOA measurements contain essentially the same position information. This equivalence is proven [53], [54] and has been known within the geodetic society but not to many positioning engineers including the author. Thus, without knowledge of the existing proofs by the geodetic community, an independent study is conducted and a proof of equivalence is developed based on Shin's work [55]. The presented proof is in a generalized form and supports the case of

non-homogeneous (containing different variances) and correlated ranging sources.

5.1.1 Contradicting Intuitions

The comparison starts with two arguments, for and against the equivalence of TOA and TDOA. This contradiction is explained in terms of weightings applied to measurements and leads us to the proof of the equivalence of TOA and TDOA.

The first argument states that TOA and TDOA are equivalent in terms of their performance because TOA and TDOA measurements can be transformed into the other without loss of information regarding user positions. The preservation of the information can be observed in the conversions between TOA and TDOA. A TOA measurement, ρ_i, can be transformed into a TDOA measurement, $\Delta\rho_{i,n}$, after differencing according to the definition of TDOA.

$$\rho_i = r_i + b + \epsilon_i \tag{5.1}$$

$$\Delta\rho_{i,n} = \rho_i - \rho_n = (r_i - r_n) + (\epsilon_i - \epsilon_n) \tag{5.2}$$

The conversion from TDOA to TOA does not require any modification. After the rearrangement of the elements in Equation (5.2) and the introduction of a new clock bias term, $\tilde{b} = b - \rho_n$, a TDOA measurement, $\Delta\rho_{i,n}$, becomes a TOA measurement, $\tilde{\rho}_i$.

$$\Delta\rho_{i,n} = r_i + b + \epsilon_i - \rho_n = r_i + \tilde{b} + \epsilon_i = \tilde{\rho}_i \tag{5.3}$$

$\tilde{\rho}_i$ derived from $\Delta\rho_{i,n}$ is different from ρ_i but the only difference is the clock bias, $b \neq \tilde{b}$. Besides the clock bias, $\tilde{b}$, there is no loss of information , in particular, regarding the user position. Therefore, it can be claimed that the position estimations based on TOA and TDOA measurements should be equivalent.

In contrast to the first argument, the second argument claims the inequivalence of TOA and TDOA because the error variances of TDOA measurements are usually higher than those of TOA measurements. For the example of homogeneous and uncorrelated ($\sigma_i = \sigma_j$ and $\sigma_{i,j} = 0\ \forall i, j$) sources, $\Delta\rho_{i,n}$ has a variance that is twice as

large as that for ρ_i and has artificially created correlations with other range measurements. For $n = 4$, the range error covariance matrices for ρ_i and $\Delta\rho_{i,n}$ are given as an example.

$$\begin{bmatrix} \sigma^2 & 0 & 0 & 0 \\ 0 & \sigma^2 & 0 & 0 \\ 0 & 0 & \sigma^2 & 0 \\ 0 & 0 & 0 & \sigma^2 \end{bmatrix} \Longrightarrow \begin{bmatrix} 2\sigma^2 & \sigma^2 & \sigma^2 \\ \sigma^2 & 2\sigma^2 & \sigma^2 \\ \sigma^2 & \sigma^2 & 2\sigma^2 \end{bmatrix}$$

This deterioration demonstrates the error propagation between measurements due to the differencing process in TDOA. Since data with larger error variances could not generate better estimation results than cleaner data, TOA can be claimed to be a better format of measurements than TDOA.

The answer to these contradicting arguments can be found in weighting schemes. Because, in the first argument, TOA and TDOA measurements are shown to have the same information, position estimates should be the same as long as the best effort processing—optimal weighting—is applied. This optimal weighting can decorrelate the artificial correlations in TDOA measurements and restore their variances to the level of those in TOA measurements in the example of the second argument. However, if sub-optimal weightings are applied, the deterioration in TDOA data cannot be removed. Thus, the relative performance between TOA and TDOA relies upon the type of weightings. Here "optimality" refers to any value or condition that is required to minimize position error variance.

5.1.2 Proof of Equivalence

Pseudoranges in the TOA format and in the TDOA format are given in Equation (5.4) and (5.5) with weighting matrices, $\boldsymbol{W}$ and $\boldsymbol{W}_{\mathrm{D}}$. The weighting matrices are multiplied for implementation of the weighted least square (WLS) method.

$$\boldsymbol{W}\delta\boldsymbol{\rho} = \boldsymbol{W}\boldsymbol{G}\delta\boldsymbol{x} + \boldsymbol{W}\boldsymbol{v} \tag{5.4}$$

$$\boldsymbol{W}_{\mathrm{D}}\boldsymbol{D}\delta\boldsymbol{\rho} = \boldsymbol{W}_{\mathrm{D}}\boldsymbol{D}\boldsymbol{G}_{\mathrm{D}}\delta\boldsymbol{u} + \boldsymbol{W}_{\mathrm{D}}\boldsymbol{D}\boldsymbol{v} \tag{5.5}$$

where $\boldsymbol{D} = [\boldsymbol{I}_{(n-1)\times(n-1)}, -\boldsymbol{1}_{(n-1)\times 1}]$ is a differencing matrix for TDOA.

With the given weightings, the position—and the clock bias for TOA—estimates can be calculated using WLS,

$$\hat{\boldsymbol{\theta}}_{\mathrm{TOA}} = (\boldsymbol{W}\boldsymbol{G})^{\dagger}\boldsymbol{W}\delta\boldsymbol{\rho} \tag{5.6}$$

$$\hat{\boldsymbol{\theta}}_{\mathrm{D,TDOA}} = (\boldsymbol{W}_{\mathrm{D}}\boldsymbol{D}\boldsymbol{G}_{\mathrm{D}})^{\dagger}\boldsymbol{W}_{\mathrm{D}}\boldsymbol{D}\delta\boldsymbol{\rho} \tag{5.7}$$

as well as their variances,

$$\boldsymbol{\Sigma}_{\hat{\boldsymbol{\theta}},\mathrm{TOA}} = (\boldsymbol{W}\boldsymbol{G})^{\dagger}\boldsymbol{W}\boldsymbol{\Sigma}_{\boldsymbol{v}}\boldsymbol{W}^{T}[(\boldsymbol{W}\boldsymbol{G})^{\dagger})]^{T} \tag{5.8}$$

$$\begin{aligned}\boldsymbol{\Sigma}_{\hat{\boldsymbol{\theta}}_{\mathrm{D}},\mathrm{TDOA}} &= (\boldsymbol{W}_{\mathrm{D}}\boldsymbol{D}\boldsymbol{G}_{\mathrm{D}})^{\dagger} \\ &\quad \times \boldsymbol{W}_{\mathrm{D}}\boldsymbol{D}\boldsymbol{\Sigma}_{\boldsymbol{v}}\boldsymbol{D}^{T}\boldsymbol{W}_{\mathrm{D}}^{T}[(\boldsymbol{W}_{\mathrm{D}}\boldsymbol{D}\boldsymbol{G}_{\mathrm{D}})^{\dagger}]^{T}\end{aligned} \tag{5.9}$$

where $\boldsymbol{\theta} = \delta\boldsymbol{x} = [\delta\boldsymbol{u}^{T}, \delta b]^{T}$ and $\boldsymbol{\theta}_{\mathrm{D}} = \delta\boldsymbol{u}$. $\boldsymbol{\Sigma}_{\boldsymbol{v}}$, $\boldsymbol{G}$, and $\boldsymbol{G}_{\mathrm{D}}$ are assumed to be of full rank. $(\cdot)^{\dagger}$ is the Moore-Penrose pseudo-inverse of a matrix. The residual measurement noises, $\boldsymbol{v}$, are assumed to have zero mean. Based on the knowledge of a noise covariance matrix, $\boldsymbol{\Sigma}_{\boldsymbol{v}}$, optimal weightings can be obtained.

$$\boldsymbol{W}^{*} = \boldsymbol{\Sigma}_{\boldsymbol{v}}^{-1/2} \tag{5.10}$$

$$\boldsymbol{W}_{\mathrm{D}}^{*} = (\boldsymbol{D}\boldsymbol{\Sigma}_{\boldsymbol{v}}\boldsymbol{D}^{T})^{-1/2} \tag{5.11}$$

where $(\cdot)^{*}$ represents optimality. The position estimates and their variances are recalculated based on the optimal weightings, tagged with TOA/WLS and TDOA/WLS.

$$\hat{\boldsymbol{\theta}}_{\mathrm{TOA/WLS}} = (\boldsymbol{G}^{T}\boldsymbol{\Sigma}_{\boldsymbol{v}}^{-1}\boldsymbol{G})^{-1}\boldsymbol{G}^{T}\boldsymbol{\Sigma}_{\boldsymbol{v}}^{-1}\delta\boldsymbol{\rho} \tag{5.12}$$

$$\begin{aligned}\hat{\boldsymbol{\theta}}_{\mathrm{D,TDOA/WLS}} &= [\boldsymbol{G}_{\mathrm{D}}^{T}\boldsymbol{D}^{T}(\boldsymbol{D}\boldsymbol{\Sigma}_{\boldsymbol{v}}\boldsymbol{D}^{T})^{-1}\boldsymbol{D}\boldsymbol{G}_{\mathrm{D}}]^{-1} \\ &\quad \times \boldsymbol{G}_{\mathrm{D}}^{T}\boldsymbol{D}^{T}(\boldsymbol{D}\boldsymbol{\Sigma}_{\boldsymbol{v}}\boldsymbol{D}^{T})^{-1}\boldsymbol{D}\delta\boldsymbol{\rho}\end{aligned} \tag{5.13}$$

$$\boldsymbol{\Sigma}_{\hat{\boldsymbol{\theta}},\mathrm{TOA/WLS}} = (\boldsymbol{G}^{T}\boldsymbol{\Sigma}_{\boldsymbol{v}}^{-1}\boldsymbol{G})^{-1} \tag{5.14}$$

$$\boldsymbol{\Sigma}_{\hat{\boldsymbol{\theta}}_{\mathrm{D}},\mathrm{TDOA/WLS}} = [\boldsymbol{G}_{\mathrm{D}}^{T}\boldsymbol{D}^{T}(\boldsymbol{D}\boldsymbol{\Sigma}_{\boldsymbol{v}}\boldsymbol{D}^{T})^{-1}\boldsymbol{D}\boldsymbol{G}_{\mathrm{D}}]^{-1} \tag{5.15}$$

Despite the different expressions in Equation (5.12) and (5.13), TOA and TDOA

actually generate the same position estimate. The difference in the equations occurs because the position and the clock bias are calculated in TOA, while only the position is pursued in TDOA. Thus, if the clock bias related terms are removed from the TOA estimates, the equivalence can be shown between the TOA solutions and the TDOA solutions,

$$\boxed{\hat{\boldsymbol{\theta}}_{\mathrm{D,TOA/WLS}} \equiv \hat{\boldsymbol{\theta}}_{\mathrm{D,TDOA/WLS}}}$$

as well as between their position variances,

$$\boxed{\boldsymbol{\Sigma}_{\hat{\boldsymbol{\theta}}_{\mathrm{D}},\mathrm{TOA/WLS}} \equiv \boldsymbol{\Sigma}_{\hat{\boldsymbol{\theta}}_{\mathrm{D}},\mathrm{TDOA/WLS}}}$$

The existing proof of the equivalence has been limited to the special case of a noise covariance, $\boldsymbol{\Sigma}_{\boldsymbol{v}} = \sigma^2 \boldsymbol{I}$ [55]. To remove such a limitation, we now prove that this equivalence holds for any noise distribution, $\boldsymbol{\Sigma}_{\boldsymbol{v}}$, including non-homogeneous or correlated terrestrial transmitter networks.

After the removal of the clock bias related terms, the position variance matrix for TOA, $\boldsymbol{\Sigma}_{\hat{\boldsymbol{\theta}}_{\mathrm{D}},\mathrm{TOA/WLS}}$, can be extracted from the covariance matrix for TOA in Equation (5.14). Then, $\boldsymbol{\Sigma}_{\hat{\boldsymbol{\theta}}_{\mathrm{D}},\mathrm{TOA/WLS}}$ is shown to be equal to the position variance for TDOA, $\boldsymbol{\Sigma}_{\hat{\boldsymbol{\theta}}_{\mathrm{D}},\mathrm{TDOA/WLS}}$. First, let the TOA covariance matrix be divided into submatrices.

$$\begin{aligned}
\boldsymbol{\Sigma}_{\hat{\boldsymbol{\theta}},\mathrm{TOA/WLS}} &= (\boldsymbol{G}^T \boldsymbol{\Sigma}_{\boldsymbol{v}}^{-1} \boldsymbol{G})^{-1} \\
&= \begin{bmatrix} \boldsymbol{G}_{\mathrm{D}}^T \boldsymbol{\Sigma}_{\boldsymbol{v}}^{-1} \boldsymbol{G}_{\mathrm{D}} & \boldsymbol{G}_{\mathrm{D}}^T \boldsymbol{\Sigma}_{\boldsymbol{v}}^{-1} \mathbf{1} \\ \mathbf{1}^T \boldsymbol{\Sigma}_{\boldsymbol{v}}^{-1} \boldsymbol{G}_{\mathrm{D}} & \mathbf{1}^T \boldsymbol{\Sigma}_{\boldsymbol{v}}^{-1} \mathbf{1} \end{bmatrix}^{-1} \\
&= \begin{bmatrix} \boldsymbol{\Sigma}_{11} & \boldsymbol{\Sigma}_{12} \\ \boldsymbol{\Sigma}_{21} & \boldsymbol{\Sigma}_{22} \end{bmatrix}
\end{aligned} \tag{5.16}$$

where $\mathbf{1}$ is the $n \times 1$ vector of ones. The submatrices of $\boldsymbol{\Sigma}_{\hat{\boldsymbol{\theta}},\mathrm{TOA/WLS}}$ are derived as the functions of

$$\boldsymbol{P} = \boldsymbol{\Sigma}_{\boldsymbol{v}}^{-1} - \boldsymbol{\Sigma}_{\boldsymbol{v}}^{-1} \mathbf{1}\mathbf{1}^T \boldsymbol{\Sigma}_{\boldsymbol{v}}^{-1} / (\mathbf{1}^T \boldsymbol{\Sigma}_{\boldsymbol{v}}^{-1} \mathbf{1})$$

which represent the part of the noise that affects the position estimates. For TOA, a clear symmetry is found between $\boldsymbol{P}$ and $\boldsymbol{\Sigma}_{\boldsymbol{v}}^{-1}$. $\boldsymbol{P}$ in the position estimation plays

the same role as $\boldsymbol{\Sigma}_{\boldsymbol{v}}^{-1}$ in the estimation of the position and the clock bias, as shown in Equation (5.17) and (5.14).

$$\begin{aligned}
\boldsymbol{\Sigma}_{11} =& \left(\boldsymbol{G}_{\mathrm{D}}^T \boldsymbol{\Sigma}_{\boldsymbol{v}}^{-1} \boldsymbol{G}_{\mathrm{D}} - \frac{\boldsymbol{G}_{\mathrm{D}}^T \boldsymbol{\Sigma}_{\boldsymbol{v}}^{-1} \mathbf{1}\mathbf{1}^T \boldsymbol{\Sigma}_{\boldsymbol{v}}^{-1} \boldsymbol{G}_{\mathrm{D}}}{\mathbf{1}^T \boldsymbol{\Sigma}_{\boldsymbol{v}}^{-1} \mathbf{1}} \right)^{-1} \\
=& \left[\boldsymbol{G}_{\mathrm{D}}^T \left(\boldsymbol{\Sigma}_{\boldsymbol{v}}^{-1} - \frac{\boldsymbol{\Sigma}_{\boldsymbol{v}}^{-1} \mathbf{1}\mathbf{1}^T \boldsymbol{\Sigma}_{\boldsymbol{v}}^{-1}}{\mathbf{1}^T \boldsymbol{\Sigma}_{\boldsymbol{v}}^{-1} \mathbf{1}} \right) \boldsymbol{G}_{\mathrm{D}} \right]^{-1} \\
=& (\boldsymbol{G}_{\mathrm{D}}^T \boldsymbol{P} \boldsymbol{G}_{\mathrm{D}})^{-1} \qquad (5.17) \\
\boldsymbol{\Sigma}_{12} =& -\frac{(\boldsymbol{G}_{\mathrm{D}}^T \boldsymbol{P} \boldsymbol{G}_{\mathrm{D}})^{-1} \boldsymbol{G}_{\mathrm{D}}^T \boldsymbol{\Sigma}_{\boldsymbol{v}}^{-1} \mathbf{1}}{\mathbf{1}^T \boldsymbol{\Sigma}_{\boldsymbol{v}}^{-1} \mathbf{1}} = \boldsymbol{\Sigma}_{21}^T \qquad (5.18) \\
\boldsymbol{\Sigma}_{22} =& \frac{1}{\mathbf{1}^T \boldsymbol{\Sigma}_{\boldsymbol{v}}^{-1} \mathbf{1}} \\
& + \frac{\mathbf{1}^T \boldsymbol{\Sigma}_{\boldsymbol{v}}^{-1} \boldsymbol{G}_{\mathrm{D}} (\boldsymbol{G}_{\mathrm{D}}^T \boldsymbol{P} \boldsymbol{G}_{\mathrm{D}})^{-1} \boldsymbol{G}_{\mathrm{D}}^T \boldsymbol{\Sigma}_{\boldsymbol{v}}^{-1} \mathbf{1}}{(\mathbf{1}^T \boldsymbol{\Sigma}_{\boldsymbol{v}}^{-1} \mathbf{1})^2} \qquad (5.19)
\end{aligned}$$

Among these submatrices, $\boldsymbol{\Sigma}_{11}$ is the position variance matrix, corresponding to $\boldsymbol{\theta}_{\mathrm{D}}$. Thus $\boldsymbol{\Sigma}_{11} = \boldsymbol{\Sigma}_{\hat{\boldsymbol{\theta}}_{\mathrm{D}},\mathrm{TOA/WLS}}$.

$\boldsymbol{\Sigma}_{\hat{\boldsymbol{\theta}}_{\mathrm{D}},\mathrm{TDOA/WLS}}$ can be shown to be equal to $\boldsymbol{\Sigma}_{\hat{\boldsymbol{\theta}}_{\mathrm{D}},\mathrm{TOA/WLS}}$, after steps of derivation leading into an expression with $\boldsymbol{P}$. Such steps need the modified definitions of matrices, $\tilde{\boldsymbol{G}}_{\mathrm{D}} = \boldsymbol{\Sigma}_{\boldsymbol{v}}^{-1/2} \boldsymbol{G}_{\mathrm{D}}$, $\tilde{\boldsymbol{D}} = \boldsymbol{D} \boldsymbol{\Sigma}_{\boldsymbol{v}}^{1/2}$, and $\tilde{\mathbf{1}} = \boldsymbol{\Sigma}_{\boldsymbol{v}}^{-1/2} \mathbf{1}$, where $\tilde{\mathbf{1}}$ is orthogonal to $\tilde{\boldsymbol{D}}$ as $\mathbf{1}$ is orthogonal to $\boldsymbol{D}$. Because of this orthogonality, the projection matrix to the range of $\tilde{\boldsymbol{D}}^T$, $\tilde{\boldsymbol{D}}^T (\tilde{\boldsymbol{D}} \tilde{\boldsymbol{D}}^T)^{-1} \tilde{\boldsymbol{D}}$, is equal to $\boldsymbol{I} - \tilde{\mathbf{1}} \tilde{\mathbf{1}}^T / (\tilde{\mathbf{1}}^T \tilde{\mathbf{1}})$. Then, after replacing the modified matrices with the original ones, we can finally see the familiar matrix $\boldsymbol{P}$ again.

$$\boldsymbol{P} = \boldsymbol{D}^T (\boldsymbol{D} \boldsymbol{\Sigma}_{\boldsymbol{v}} \boldsymbol{D}^T)^{-1} \boldsymbol{D}$$

Applying these steps of a transformation, the equivalence of the position variances of

TOA/WLS and TDOA/WLS is shown in the following equations.

$$\begin{aligned}
\boldsymbol{\Sigma}_{\hat{\boldsymbol{\theta}}_{\mathrm{D,TDOA/WLS}}} &= \left[\boldsymbol{G}_{\mathrm{D}}^{T}\boldsymbol{D}^{T}(\boldsymbol{D}\boldsymbol{\Sigma}_{\boldsymbol{v}}\boldsymbol{D}^{T})^{-1}\boldsymbol{D}\boldsymbol{G}_{\mathrm{D}}\right]^{-1} \\
&= \left[\tilde{\boldsymbol{G}}_{\mathrm{D}}^{T}\tilde{\boldsymbol{D}}^{T}(\tilde{\boldsymbol{D}}\tilde{\boldsymbol{D}}^{T})^{-1}\tilde{\boldsymbol{D}}\tilde{\boldsymbol{G}}_{\mathrm{D}}\right]^{-1} \\
&= \left[\tilde{\boldsymbol{G}}_{\mathrm{D}}^{T}\left(\boldsymbol{I}-\frac{\tilde{\mathbf{1}}\tilde{\mathbf{1}}^{T}}{\tilde{\mathbf{1}}^{T}\tilde{\mathbf{1}}}\right)\tilde{\boldsymbol{G}}_{\mathrm{D}}\right]^{-1} \\
&= \left[\boldsymbol{G}_{\mathrm{D}}^{T}\left(\boldsymbol{\Sigma}_{\boldsymbol{v}}^{-1}-\frac{\boldsymbol{\Sigma}_{\boldsymbol{v}}^{-1}\mathbf{1}\mathbf{1}^{T}\boldsymbol{\Sigma}_{\boldsymbol{v}}^{-1}}{\mathbf{1}^{T}\boldsymbol{\Sigma}_{\boldsymbol{v}}^{-1}\mathbf{1}}\right)\boldsymbol{G}_{\mathrm{D}}\right]^{-1} \\
&= (\boldsymbol{G}_{\mathrm{D}}^{T}\boldsymbol{P}\boldsymbol{G}_{\mathrm{D}})^{-1} \\
&= \boldsymbol{\Sigma}_{\hat{\boldsymbol{\theta}}_{\mathrm{D,TOA/WLS}}}
\end{aligned} \tag{5.20}$$

This proves the equivalence of the position variances of TOA/WLS and TDOA/WLS.

Now, the position solutions of TOA/WLS and TDOA/WLS in Equation (5.12) and (5.13) are compared.

$$\begin{aligned}
\hat{\boldsymbol{\theta}}_{\mathrm{TOA/WLS}} &= (\boldsymbol{G}^{T}\boldsymbol{\Sigma}_{\boldsymbol{v}}^{-1}\boldsymbol{G})^{-1}\boldsymbol{G}^{T}\boldsymbol{\Sigma}_{\boldsymbol{v}}^{-1}\delta\boldsymbol{\rho} \\
&= \begin{bmatrix}\boldsymbol{\Sigma}_{11} & \boldsymbol{\Sigma}_{12}\\ \boldsymbol{\Sigma}_{21} & \boldsymbol{\Sigma}_{22}\end{bmatrix}\begin{bmatrix}\boldsymbol{G}_{\mathrm{D}}^{T}\\ \mathbf{1}^{T}\end{bmatrix}\boldsymbol{\Sigma}_{\boldsymbol{v}}^{-1}\delta\boldsymbol{\rho}
\end{aligned} \tag{5.21}$$

Again, only the position related part of the TOA/WLS solution needs to be obtained, using $\boldsymbol{\Sigma}_{11}$ and $\boldsymbol{\Sigma}_{12}$ in Equation (5.17) and (5.18).

$$\begin{aligned}
&\hat{\boldsymbol{\theta}}_{\mathrm{D,TOA/WLS}} \\
&= (\boldsymbol{\Sigma}_{11}\boldsymbol{G}_{\mathrm{D}}^{T}+\boldsymbol{\Sigma}_{12}\mathbf{1}^{T})\boldsymbol{\Sigma}_{\boldsymbol{v}}^{-1}\delta\boldsymbol{\rho} \\
&= (\boldsymbol{G}_{\mathrm{D}}^{T}\boldsymbol{P}\boldsymbol{G}_{\mathrm{D}})^{-1}\boldsymbol{G}_{\mathrm{D}}^{T}\left(\boldsymbol{\Sigma}_{\boldsymbol{v}}^{-1}-\frac{\boldsymbol{\Sigma}_{\boldsymbol{v}}^{-1}\mathbf{1}\mathbf{1}^{T}\boldsymbol{\Sigma}_{\boldsymbol{v}}^{-1}}{\mathbf{1}^{T}\boldsymbol{\Sigma}_{\boldsymbol{v}}^{-1}\mathbf{1}}\right)\delta\boldsymbol{\rho} \\
&= (\boldsymbol{G}_{\mathrm{D}}^{T}\boldsymbol{P}\boldsymbol{G}_{\mathrm{D}})^{-1}\boldsymbol{G}_{\mathrm{D}}^{T}\boldsymbol{P}\delta\boldsymbol{\rho} \\
&= \hat{\boldsymbol{\theta}}_{\mathrm{D,TDOA/WLS}}
\end{aligned} \tag{5.22}$$

This proves the equivalence of the position solutions of TOA/WLS and TDOA/WLS.

In this section, the equivalence of TOA and TDOA is proven for systems with

a single clock bias, $\delta\boldsymbol{x} = [\delta\boldsymbol{u}^T, \delta b]^T$, a case that describes a GPS only receiver or synchronously integrated receivers using multiple types of ranging sources. For the multiple sources from different transmitter networks, it is certainly desirable to have hardware synchronization between receivers for integrated positioning. However, even in the case of asynchronously integrated systems, with multiple clock bias terms, $\delta\boldsymbol{x} = [\delta\boldsymbol{u}^T, \delta b_A, \delta b_B, \ldots]^T$, the equivalence between TOA/WLS and TDOA/WLS holds. It is proven for the case of two clock biases in Appendix B. To summarize, regardless of the noise types and the number of integrated receivers, TOA and TDOA generate the same position estimate and the same position variance, as long as the corresponding optimal weightings are employed.

5.2 Robustness of TOA and TDOA

In this section, TOA and TDOA are compared under practical assumptions since their performance depends on how one implements these systems and how well known the noise distributions are [1], [4]. In our forthcoming Monte Carlo simulations, we assume that the noise statistics are not perfectly known or that a sub-optimal estimator is used.

5.2.1 Sub-Optimal Weightings

Let us revisit the weighting matrices in the weighted least square (WLS) solutions,

$$\boldsymbol{W}_{\text{TOA/WLS}} = {\boldsymbol{\Sigma}_{\boldsymbol{v}}}^{-1/2}, \tag{5.23}$$

$$\boldsymbol{W}_{\text{TDOA/WLS}} = (\boldsymbol{D}\boldsymbol{\Sigma}_{\boldsymbol{v}}\boldsymbol{D}^T)^{-1/2}. \tag{5.24}$$

Here TDOA pseudoranges are assumed to be generated by subtracting a TOA pseudorange with a lowest variance (called a reference channel) from the rest of the TOA pseudoranges. The consequence of this differencing is the creation of artificial cross-correlation between TDOA pseudoranges represented by the off-diagonal terms in $\boldsymbol{D}\boldsymbol{\Sigma}_{\boldsymbol{v}}\boldsymbol{D}^T$. This artificial cross-correlation is distinguished from any intrinsic cross-correlation between TOA measurements and is due to the differencing process.

Table 5.1: Performance loss by covariance inaccuracy

Covariance Inaccuracy		3 dB	5 dB	7 dB	10 dB
healthy	TOA/WLS	0%	0%	0%	0%
($\boldsymbol{\Sigma_v}$)	TDOA/WLS	0%	0%	0%	0%
	TDOA/DWLS	2%	2%	2%	2%
faulty	TOA/WLS	4%	10%	20%	40%
($\hat{\boldsymbol{\Sigma}}_{\boldsymbol{v}}$)	TDOA/WLS	4%	10%	20%	40%
	TDOA/DWLS	5%	11%	21%	40%

For simpler implementations, the off-diagonal elements in $\boldsymbol{D\Sigma_v D}^T$ could be ignored and weights can be approximated based only on the diagonal terms of $\boldsymbol{\Sigma_v}$. This is a sub-optimal but often used solution for TDOA, named the diagonal weighted least square (DWLS) method with a diagonal weighting matrix.

$$\boldsymbol{W}_{\text{TDOA/DWLS}} = diag\left((\sigma_1^2 + \sigma_n^2)^{-1/2}, \ldots, (\sigma_{n-1}^2 + \sigma_n^2)^{-1/2}\right) \tag{5.25}$$

where σ_i^2 is the error variance of the ith measurement in decreasing order such that $\sigma_1^2 = \sigma_{\max}^2$ and $\sigma_n^2 = \sigma_{\min}^2$. Because TDOA/DWLS does not account for the cross-correlation terms (which are dominated by σ_n^2 from the reference channel), its performance critically relies on the quality of the reference measurement, while TDOA/WLS is not affected by the choice of a reference channel since the artificial cross-correlation is treated in the structure of the weighting matrix for TDOA/WLS.

5.2.2 Loss by Inaccurate Noise Covariance

All weighting matrices in Equation (5.23)–(5.25) depend on the knowledge of the covariance matrix, $\boldsymbol{\Sigma_v}$. If an incorrect covariance matrix, $\hat{\boldsymbol{\Sigma}}_{\boldsymbol{v}}$, is used, there will be a resulting increase in position errors. We now describe Monte Carlo simulations used to explore these issues. This unintentional sub-optimality may happen due to the inaccuracy or perturbation in the covariance matrix and is measured in Monte Carlo simulations as an assessment of the robustness of TOA and TDOA position solutions. In the simulations, the generated error covariance matrices are delivered

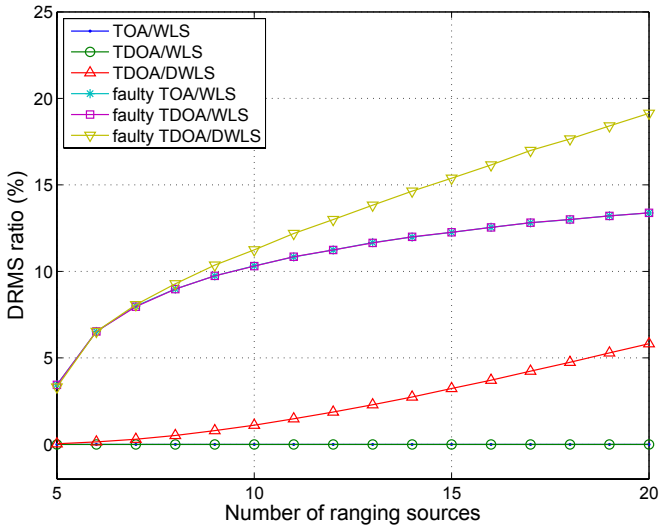

(a) Performance losses for fixed covariance inaccuracy (n = 5–20, $\sigma^2_{\max}/\sigma^2_{\min} = 20$ dB, and $\hat{\sigma}^2_i/\sigma^2_i < 5$ dB)

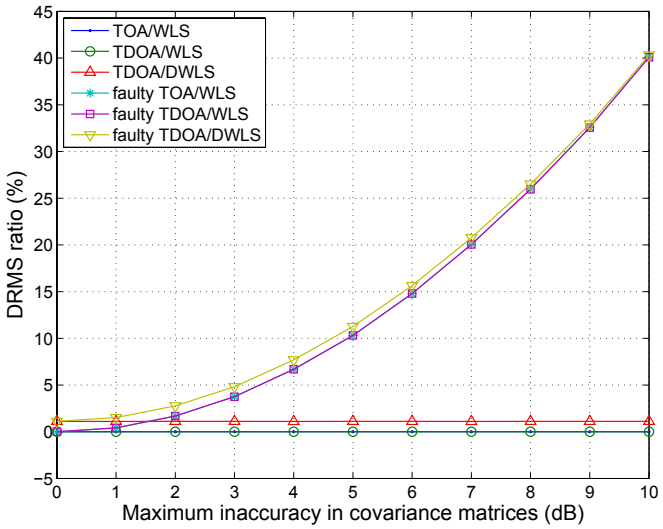

(b) Inaccuracy on known covariance matrices versus performance losses for fixed number of ranging sources (n = 10, $\sigma^2_{\max}/\sigma^2_{\min}$ =20 dB, and $\hat{\sigma}^2_i/\sigma^2_i < 0$–10 dB)

Figure 5.1: Performance losses due to inaccurate knowledge of error covariance matrices compared to TOA/WLS based on accurate covariance matrices

to the user with the inserted inaccuracy up to 10 dB. Ranging sources (n = 5–20) are randomly located on the surface of a hemisphere centered on a user and their range error variances, σ_i^2, are randomly generated in the log scale between 0–20 dB. The ratio of $\sigma^2_{\max}/\sigma^2_{\min}$ is held at 20 dB and no intrinsic cross-correlation is assumed, $\sigma_{ij} = 0$ for $i \neq j$. Then, horizontal position errors are evaluated in 10^5 trials.

The first simulation is conducted for a fixed limit (5 dB) on the covariance inaccuracy and uses 5–20 channels (see Figure 5.1(a)). Each point represents the increase of horizontal position error variance. Positioning errors are measured in DRMS (distance root mean squared) and are compared to the optimal solution, TOA/WLS, based on $\mathbf{\Sigma}_{\boldsymbol{v}}$. There are six results in the comparison: TOA/WLS, TDOA/WLS, and TDOA/DWLS based on the true covariance $\mathbf{\Sigma}_{\boldsymbol{v}}$, noted as the 'healthy' cases; and their corresponding cases based on the estimated covariance, $\hat{\mathbf{\Sigma}}_{\boldsymbol{v}}$, noted as the 'faulty' cases. Here, the notion of 'healthy' and 'faulty' only refers to the reliability of a given covariance matrix per case. As expected, the faulty cases based on $\hat{\mathbf{\Sigma}}_{\boldsymbol{v}}$ show performance losses compared to their healthy counterparts. The losses are in the range of 4% to 13% and proportionally increase as the number of ranging sources increases. In the healthy group, TOA/DWLS maintains a low level of performance losses (less than 6%). Among these variations, TOA/WLS and TDOA/WLS are shown to be equivalent as predicted by the theoretical proofs. Interestingly, even in the faulty cases, the equivalence still holds between TOA/WLS and TDOA/WLS.

As the covariance inaccuracy increases, performance loss increases significantly. To assess this proportionality, n is fixed to 10 and the limit on the covariance inaccuracy is swept from 0 to 10 dB. With the hike in the covariance inaccuracy, the robustness of the positioning methods disappears in Figure 5.1(b). Neither of the faulty WLS and DWLS methods remain reliable. Their performance losses reach 40% at 10 dB inaccuracy from 4–5% at 3 dB inaccuracy. For the example of applications with 20% loss tolerance, the positioning methods can be considered to be robust only to covarinace inaccuracy lower than approximately 7 dB, on which 20–21% losses are observed. Under the same condition, the healthy TDOA/DWLS shows only a constant 2% loss. See details in Table 5.1.

Table 5.2: Performance loss by sub-optimal implementation (weighting)

n	5	10	15	20
TOA/LS	16%	70%	90%	99%
TDOA/LS	17%	59%	76%	84%
TDOA/DWLS	0%	2%	4%	6%

5.2.3 Loss by Sub-Optimal Implementation

Figures 5.1(a) and 5.1(b) illustrate that the sub-optimality of the DWLS implementation is dwarfed by the sub-optimality due to the inaccurate knowledge of covariance matrices. As a further investigation into this sub-optimality due to simplified implementations, the diagonal weighting method is tested along with the least square methods (LS) where $\boldsymbol{W}_{\text{LS}} = \boldsymbol{I}$.

As n increases, TOA/LS and TDOA/LS suffer substantial losses (70% and 59% for $n = 10$, and 99% and 84% for $n = 20$, respectively). This level of performance loss is certainly unacceptable to most applications. In contrast, TDOA/DWLS is very close to optimal with less than 6% loss (see Figure 5.2(a)). But this low loss is subject to changes in the max-to-min variance ratio, $\sigma^2_{\text{max}}/\sigma^2_{\text{min}}$. In Figure 5.2(b), where the variance ratio changes from 0 to 25 dB for $n = 10$, the loss of TDOA/DWLS varies from 1% to 17%, worst at 0 dB deviation among measurements where the reference channel is no better than the others (i.e., a large σ_n^2). However, for 10–20 dB nomimal deviations (meaning a small σ_n^2), the average loss by TDOA/DWLS can be restricted to 5% in close proximity to the optimal solutions, while the LS methods remain unreliable.

5.3 Conclusion

This chapter starts with the question of which pseudorange format (TOA and TDOA) is more suitable for the hybrid GPS and TPS system. To solve this issue, TOA and TDOA have been compared analytically and via Monte Carlo simulations. In the analytical analysis, the existing proof of the equivalence of TOA and TDOA by Shin

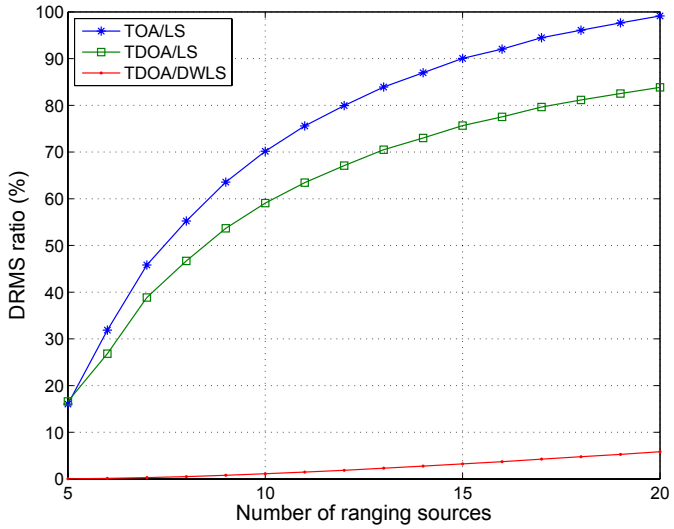

(a) Performance losses for fixed deviation in pseudorange variances (n = 5–20 and $\sigma^2_{\max}/\sigma^2_{\min}$ = 20 dB)

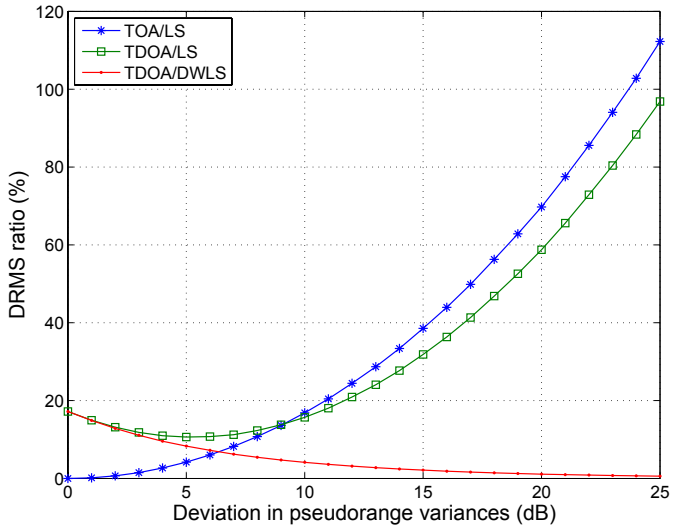

(b) Deviation in pseudorange variances versus performance losses for fixed number of ranging sources (n = 10 and $\sigma^2_{\max}/\sigma^2_{\min}$ = 0–25 dB)

Figure 5.2: Performance losses due to sub-optimal implementation compared to TOA/WLS

was extended to more general cases including an integrated positioning system which combines multiple types of sources such as GPS satellites and terrestrial sources (see Appendix B). This proof confirms that neither a stand-alone receiver nor a group of integrated receivers should experience differences between TOA and TDOA under ideal conditions.

In the Monte Carlo simulations, the robustness of TOA and TDOA positioning methods in practical situations was examined. First, it was shown that both TOA and TDOA become less reliable when the inaccuracy in the knowledge of measurement covariances exceeds approximately 7 dB, showing rapidly increasing performance losses. Second, TDOA was shown to be less robust than TOA to inaccurate error statistics or system sub-optimality. However, the performance gap between TOA and TDOA is relatively small and is less than 17% across all tested cases. In other words, TOA is better but the margin is not substantial.

The last remaining question is which of these methods is more computationally efficient for implementation of a positioning system. The position estimation process itself is approximately the same for both methods. However, a fault exclusion process makes a difference. Exclusion of an outlier is straightforward among TOA range measurements. This is not the case for TDOA measurements since TDOA is basically a difference between two measurements and often it is less clear which combination of TDOA measurements does, in fact, contain an outlier. This becomes more problematic if there are more than one outliers, to be discussed in detail in Chapter 6. Thus, the implementation of fault exclusion for TDOA is more complex and requires more computation than its counterpart TOA, making TDOA less favorable.

This chapter has taught us that TOA is more robust than TDOA in practice although not by a large margin. However, since a fault exclusion process can be simpler with TOA, TOA is adopted for our hybrid GPS and TPS system and assumed within this dissertation as a baseline positioning method.

Chapter 6

Fault Detection and Exclusion

The strength of television signals as ranging sources is the capability of deeper penetration into urban and indoor areas. However, because TV signals are not designed for positioning and travel in more severe multipath environments, there tend to be more outlying pseudorange measurements in TPS than in GPS. The resulting multiplicity of outliers makes it more challenging for receiver autonomous integrity monitoring (RAIM) algorithm to provide reliable position estimates because conventional RAIM algorithm for satellite systems usually assumes a single satellite failure. To handle this multi-fault case, existing RAIM algorithms are revisited and a modified RAIM algorithm is proposed.

6.1 Fault Detection

After a short introduction to hypothesis testing, this section introduces the three existing RAIM algorithms used for fault detection from the rich literature covering this topic [13], [15], [68]–[74]. The three RAIM algorithms are the chi-square test [15], the horizontal protection level (HPL) test by Brown [68], [69], and the multi-hypothesis solution separation (MHSS) test by Pervan [70], [71].

6.1.1 Introduction to Fault Detection

The fault detection RAIM algorithms are based on the theory of hypothesis testing. In hypothesis testing, two important probability values should be considered: the probability of false alarm, P_{FA}, and the probability of missed detection, P_{MD}. These two key parameters represent two different types of errors. Let us assume two hypotheses: a null hypothesis, H_0, where no anomaly happens and an alternative hypothesis, H_1, where an anomaly event happens. Then, provided a data set, it can be detected whether there is an anomaly or not. When we choose H_1, although H_0 is the correct hypothesis, "false positive" decision error (or more formally "Type I error") occurs. In our terms, this failed decision is a false alarm and corresponds to P_{FA}. On the other hand, if we declare H_0, although H_1 is true, a "false negative" decision error (or more formally "Type II error") occurs. A false negative error means a missed detection of an anomaly and is represented by P_{MD}. Both false alarm and missed detection are not desirable but in many cases trade-offs between these two types of decision errors need to be made. An attempt to reduce P_{MD} will increase P_{FA} and vice versa.

Hypothesis testing requires test statistics to determine the validity of certain hypotheses. In positioning systems, the parity vector is usually used as a test statistic. In the positioning equation,

$$\delta\boldsymbol{\rho} = \boldsymbol{G}\delta\boldsymbol{x} + \boldsymbol{v} \tag{6.1}$$

the error vector, $\boldsymbol{v}$, is assumed to be normally distributed, $\boldsymbol{v} \sim \mathcal{N}(\boldsymbol{\mu_v}, \boldsymbol{\Sigma_v})$. After applying a weighting matrix, $\boldsymbol{W} = \boldsymbol{\Sigma_v}^{-1/2}$, the error covariance becomes an identity matrix, $\boldsymbol{Wv} \sim \mathcal{N}(\boldsymbol{W\mu_v}, \boldsymbol{I}_n)$. For convenience, it is assumed that $\boldsymbol{\Sigma_v} = \boldsymbol{I}_n$ within this chapter. The parity vector, $\boldsymbol{p}$, can be derived from the parity matrix, $\boldsymbol{P}$, and $\delta\boldsymbol{\rho}$. $\boldsymbol{P}$ spans the null space of $\boldsymbol{G}$ so that $\boldsymbol{PG} = \boldsymbol{0}$ and $\boldsymbol{PP}^T = \boldsymbol{I}_k$. k is the degree of freedom or in other words the number of redundant measurements in the positioning equation. k is equal to the number of measurements, n, less the number of variables and is summarized in Table 6.1.

The parity vector can be considered as measurements transformed by the parity

Table 6.1: Degree of freedom in measurements (k)

Operation Mode	Hybrid	GPS	TV
three dimensional	$n-5$	$n-4$	N/A
two dimensional	$n-4$	$n-3$	$n-3$

matrix. $\boldsymbol{p}$ is given as follows

$$\boldsymbol{p} = \boldsymbol{P}\delta\boldsymbol{\rho} = \boldsymbol{P}(\boldsymbol{G}\delta\boldsymbol{x} + \boldsymbol{v}) = \boldsymbol{P}\boldsymbol{v} \tag{6.2}$$

since $\boldsymbol{PG} = \boldsymbol{0}$ by definition. $\boldsymbol{p}$ follows a Gaussian distribution, $\boldsymbol{p} \sim \mathcal{N}(\boldsymbol{P\mu_v}, \boldsymbol{I}_k)$, and the mean of the parity vector, $\boldsymbol{P\mu_v}$, is an indicator of the existence of biases in range measurements. In the absence of an anomaly (represented by H_0), the range errors are supposed to have a zero mean. $\boldsymbol{P\mu_v} \neq \boldsymbol{0}$ indicates that there are persistent biases in the measurements and this case is represented by H_1.

6.1.2 Chi-Square (χ^2) Test

Now, let us start to look into our three candidate RAIM algorithms. The first RAIM algorithm is the χ^2 test [15]. The χ^2 test is a hypothesis test used to verify whether a null hypothesis, H_0, is true by examining whether or not given test statistics follow a χ^2 distribution. Because the elements of the parity vector are independently and normally distributed, $p_i \sim \mathcal{N}((\boldsymbol{P\mu_v})_i, 1)$, the squared sum of these components follows a χ^2 distribution,

$$\sum_{i=1}^{k} p_i^2 = \|p\|^2 \sim \chi^2(k, \lambda) \tag{6.3}$$

where λ is a non-centrality parameter in a χ^2 distribution. When $\lambda = 0$, H_0 is true and the distribution is called the central χ^2 distribution. Otherwise, H_1 is true and the distribution is called the non-central χ^2 distribution. λ is given as follows

$$\lambda = \sum_{i=1}^{k} \mu_{p_i}^2 = \sum_{i=1}^{k} (\boldsymbol{P\mu_v})_i^2 \tag{6.4}$$

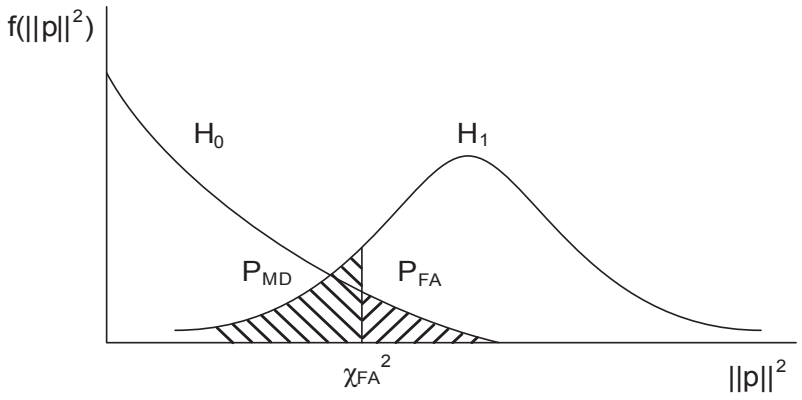

Figure 6.1: Chi-square (χ^2) test

The reader should distinguish between λ as a non-centrality parameter in this chapter and λ as a wavelength in the rest of the dissertation.

The probability distribution function (PDF) of a χ^2 distribution for $X \sim \chi^2(k, \lambda)$ is given as follows

$$f(x; k, \lambda) = \begin{cases} \dfrac{e^{-(x+\lambda)/2}}{2^{k/2}} \displaystyle\sum_{i=0}^{\infty} \frac{\lambda^i x^{k/2+i-1}}{\Gamma(k/2+i)2^{2i}i!} & \text{for } x > 0, \\ 0 & \text{for } x \leq 0, \end{cases} \tag{6.5}$$

where $\Gamma(\cdot)$ is the gamma function. This PDF represents the non-central χ^2 distribution with $\lambda \neq 0$. If $\lambda = 0$, the PDF becomes simplified

$$f(x; k, \lambda = 0) = \begin{cases} \dfrac{1}{2^{k/2}\Gamma(k/2)} x^{(k/2)-1} e^{-x/2} & \text{for } x > 0, \\ 0 & \text{for } x \leq 0, \end{cases} \tag{6.6}$$

which is known as the central χ^2 distribution.

An illustration of these PDFs are given in Figure 6.1. These PDFs represent two hypotheses, H_0 for $\lambda = 0$ and H_1 for $\lambda \neq 0$. The determination between H_0 and H_1 is feasible by comparing the test statistics, $\|p\|^2$, with a threshold value, χ^2_{FA}. P_{FA}

reaches a given upper limit, $P_{\text{FA, th}}$, for

$$\chi^2_{\text{FA}} = \{x | P_{\text{FA, th}} = 1 - F(x; k, \lambda = 0)\} \tag{6.7}$$

where $F(x; k, \lambda)$ is the cumulative distribution function (CDF) of a χ^2 distribution. The decision rule of the χ^2 test is given as follows

$$H = \begin{cases} H_0 & \text{for } \|p\|^2 < \chi^2_{\text{FA}}, \\ H_1 & \text{for } \|p\|^2 \geq \chi^2_{\text{FA}}. \end{cases} \tag{6.8}$$

Under this decision rule, let us examine the probabilities of false alarm and missed detection. Regarding P_{FA}, the probability of false alarm is fixed to its limit ($P_{\text{FA}} = P_{\text{FA, th}}$) because χ^2_{FA} is derived from $P_{\text{FA, th}}$. On the other hand, the probability of missed detection is undecided and depends on the size of λ, $P_{\text{MD}} = F(\chi^2_{\text{FA}}; k, \lambda)$. Then, for a given limit on P_{MD}, a corresponding λ_{MD} can be found

$$\lambda_{\text{MD}} = \{\lambda | P_{\text{MD, th}} = F(\chi^2_{\text{FA}}; k, \lambda)\} \tag{6.9}$$

and used as an upper limit on the sum of squared range biases ($\lambda < \lambda_{\text{MD}}$). If $\lambda \geq \lambda_{\text{MD}}$, this large bias can be detected with $P_{\text{MD}} < P_{\text{MD, th}}$ so that a positioning solution is protected against large range errors.

6.1.3 Horizontal Protection Level (HPL) Test

The χ^2 test detects range measurements with large biases. However, the critical weakness of the χ^2 test as a fault detection algorithm is the lack of consideration of a position error. Fortunately, we can translate range errors to position errors by considering the transmitter geometry. A small range error with bad geometry will be magnified, while a large range error with good geometry will have minimal impact in the position domain.

The second RAIM algorithm in this section, the horizontal protection level (HPL) test [68], [69], overcomes this shortfall by projecting the worst case horizontal position

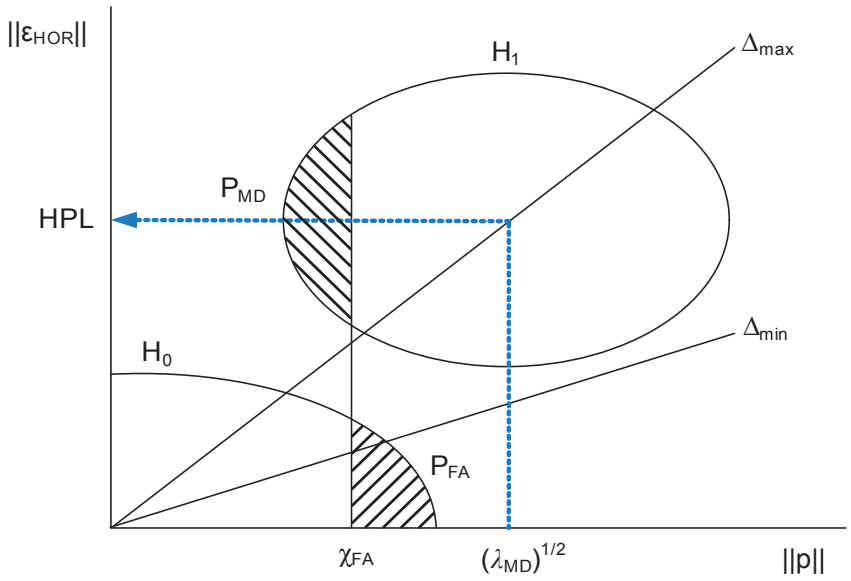

Figure 6.2: HPL test

error. The worst case horizontal position error, HPL, is derived from the worst case geometry, $\Delta_{\max}$, and the worst case bias on a measurement error, λ_{MD}. In other words, a range error, λ_{MD}, is translated to a position error, HPL, based on a transmitter geometry, $\Delta_{\max}$.

$$\mathrm{HPL} = \Delta_{\max} \cdot \sqrt{\lambda_{\mathrm{MD}}} \tag{6.10}$$

where λ_{MD} is the non-centrality parameter given in Equation (6.9). In order to provide protection against outlying position errors, the HPL test compares HPL with a horizontal alert limit (HAL) in the position domain in addition to the χ^2 test in the range domain. HAL is a maximum tolerable horizontal position error (only horizontal position errors are monitored because of our focus on pedestrian applications).

$\Delta_{\max}$ in Equation (6.10) is a metric that represents the worst case error propagation from a range bias to a position error and is given as follows [15]

$$\Delta_{\max} = \max_i \Delta_i = \max_i \sqrt{\frac{\sum_{j=1}^{2} (\boldsymbol{G}_{ji}^{\dagger})}{(\boldsymbol{P}^T \boldsymbol{P})_{ii}}} \tag{6.11}$$

where $\boldsymbol{G}^{\dagger}$ is the pseudo-inverse of a geometry matrix, $\boldsymbol{G}$. Δ_i is a ratio between the magnitudes of the expected horizontal position error, $\|E(\boldsymbol{\epsilon}_{\mathrm{HOR}})\|$, and the expected parity vector, $\|E(\boldsymbol{p})\|$, due to a bias on the ith range measurement. First, let us determine $\boldsymbol{\epsilon}_{\mathrm{HOR}}$. In Equation (6.1), after iterative estimation, a position and clock bias estimate, $\hat{\boldsymbol{x}}$, is given as a sum of true position, $\boldsymbol{x}$, and a position error, $\boldsymbol{\epsilon}_{\boldsymbol{x}}$,

$$\hat{\boldsymbol{x}} = \boldsymbol{x} + \boldsymbol{\epsilon}_{\boldsymbol{x}} = \boldsymbol{x} + \boldsymbol{G}^{\dagger}\boldsymbol{v} \tag{6.12}$$

where $\boldsymbol{\epsilon}_{\boldsymbol{x}} = \boldsymbol{G}^{\dagger}\boldsymbol{v}$. Then, the corresponding horizontal position error is $\boldsymbol{\epsilon}_{\mathrm{HOR}} = \big((\boldsymbol{G}^{\dagger}\boldsymbol{v})_1, (\boldsymbol{G}^{\dagger}\boldsymbol{v})_2\big)$. Second, let us calculate $\|E(\boldsymbol{\epsilon}_{\mathrm{HOR}})\|$ and $\|E(\boldsymbol{p})\|$. To determine the most geometrically critical channel, only the ith measurement is supposed to contain a non-zero bias.

$$\|E(\boldsymbol{\epsilon}_{\mathrm{HOR}})\|^2 = \sum_{j=1}^{2} \left[(\boldsymbol{G}^{\dagger}\boldsymbol{\mu}_{\boldsymbol{v}})_j\right]^2 = \sum_{j=1}^{2} (\boldsymbol{G}^{\dagger}_{ji})^2 \left[(\boldsymbol{\mu}_{\boldsymbol{v}})_i\right]^2 \tag{6.13}$$

$$\|E(\boldsymbol{p})\|^2 = \|\boldsymbol{P}\boldsymbol{\mu}_{\boldsymbol{v}}\| = (\boldsymbol{P}^T\boldsymbol{P})_{ii} \left[(\boldsymbol{\mu}_{\boldsymbol{v}})_i\right]^2 \tag{6.14}$$

Finally, Δ_i is given as the ratio of Equation (6.13) and (6.14),

$$\Delta_i = \frac{\|E(\boldsymbol{\epsilon}_{\mathrm{HOR}})\|}{\|E(\boldsymbol{p})\|} = \frac{\sqrt{\sum_{j=1}^{2} (\boldsymbol{G}^{\dagger}_{ji}) \left[(\boldsymbol{\mu}_{\boldsymbol{v}})_i\right]^2}}{\sqrt{(\boldsymbol{P}^T\boldsymbol{P})_{ii} \left[(\boldsymbol{\mu}_{\boldsymbol{v}})_i\right]^2}} = \sqrt{\frac{\sum_{j=1}^{2} (\boldsymbol{G}^{\dagger}_{ji})}{(\boldsymbol{P}^T\boldsymbol{P})_{ii}}}. \tag{6.15}$$

In the illustration given in Figure 6.2, Δ_i is a slope connecting a range bias to a position error. For the same range bias, the channel with $\Delta_{\max}$ is expected to generate the largest position error and is the most geometrically critical channel.

Based on $\Delta_{\max}$ and λ_{MD}, HPL is calculated and used in the following decision rule for the HPL test,

$$H = \begin{cases} H_0 & \text{for } \|p\|^2 < \chi^2_{\mathrm{FA}} \text{ and HPL} < \mathrm{HAL}, \\ H_1 & \text{otherwise.} \end{cases} \tag{6.16}$$

This decision rule includes the position domain test (HPL<HAL) in addition to the

range domain test ($\|p\|^2 < \chi^2_{\mathrm{FA}}$) so that a positioning solution is protected against large position and range errors.

6.1.4 Multi-Hypothesis Solution Separation (MHSS) Test

Our last approach, the multi-hypothesis solution separation (MHSS) test [70], [71], is an attempt to directly assess P_{MD} in the position domain. The MHSS test uses multiple hypotheses, each of which assumes a different set of outlying measurements. In a hypothesis, H_i, all measurements are assumed to be without a bias except the ith measurement, ρ_i.

$$H_i : (\boldsymbol{\mu_v})_i \neq 0 \text{ and } (\boldsymbol{\mu_v})_j = 0 \ \forall j \neq i$$

For H_i, a position estimate, $\hat{x}_i$, is calculated after excluding ρ_i. Although hypotheses can be constructed to incorporate more than one outlier, a single outlier ($L = 1$) is assumed per hypothesis. Multiple outliers are intended to be excluded through the iterations of fault detection and exclusion processes, since the number of hypotheses, $1 + \sum_{l=1}^{l=L} \frac{n!}{(n-l)!\,l!}$, increases significantly as more outliers ($L > 1$) are supposed. Under the single outlier assumption, there are $n + 1$ hypotheses and corresponding position estimates, $(\hat{x}_0, \ldots, \hat{x}_n)$, of which $\hat{x}_0$ is based on H_0. Now P_{MD} is calculated per the given hypothesis

$$P_{\mathrm{MD},i} = \Pr\{||X - \hat{x}_0|| > \mathrm{HAL}|H_i\} \tag{6.17}$$

where X is a random variable representing a true user position and $X|H_i$ follows a Gaussian distribution with mean at $\hat{x}_i$. The overall P_{MD} is the accumulation of the individual $P_{\mathrm{MD},i}$ weighted by the probabilities of the corresponding hypotheses, $(\mathrm{P}(H_0), \ldots, \mathrm{P}(H_n))$,

$$P_{\mathrm{MD}} = \sum_{i=0}^{n} P_{\mathrm{MD},i} \cdot \mathrm{P}(H_i) \tag{6.18}$$

which is compared with the threshold of missed detection probability, $P_{\mathrm{MD,th}}$, as shown in Figure 6.3. $\mathrm{P}(H_i)$ is based on prior knowledge of the probability of a channel failure. In this dissertation, these *a priori* probabilities are set to be relatively high, 10^{-3} for

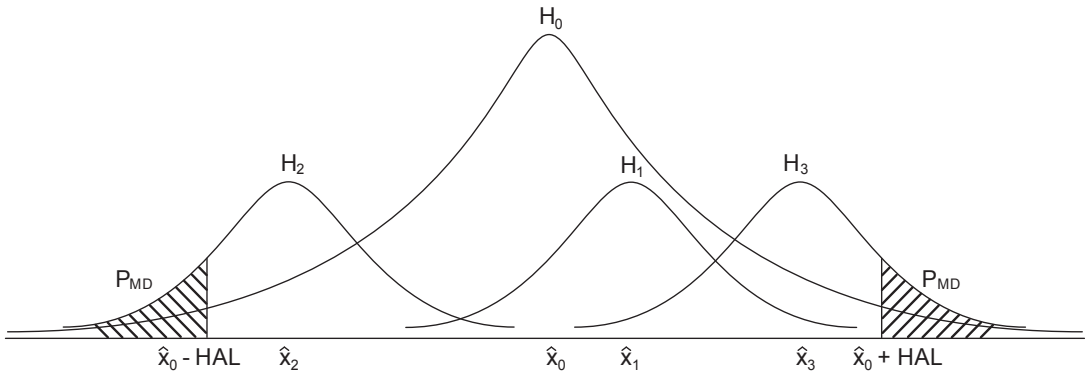

Figure 6.3: MHSS test

GPS channels and 10^{-1} for TV channels, because of the challenging environments of the data collection to be shown later. Apart from the original MHSS algorithm, the χ^2 test on the range domain is added to ensure protection against outliers.

The decision rule of the MHSS test is based on P_{MD} and is given as follows:

$$H = \begin{cases} H_0 & \text{for } \|p\|^2 < \chi^2_{\mathrm{FA}} \text{ and } P_{\mathrm{MD}} < P_{\mathrm{MD,\,th}}, \\ H_1 & \text{otherwise.} \end{cases} \tag{6.19}$$

This decision rule includes the position domain test ($P_{\mathrm{MD}} < P_{\mathrm{MD,\,th}}$) in addition to the range domain test ($\|p\|^2 < \chi^2_{\mathrm{FA}}$) so that a positioning solution is protected against large position and range errors.

6.2 Fault Exclusion

Upon the detection of a fault, the next step will be the exclusion of the fault. In addition to the three fault detection RAIM tests, a fault identification and exclusion method by Sturza is introduced [72], [74]. The maximum likelihood test by Sturza searches for an outlying measurement by minimizing the distance between the parity

vector, $\boldsymbol{p}$, and its reconstruction, $\hat{\boldsymbol{p}}_i = \boldsymbol{P}_{\cdot i}(\boldsymbol{P}_{\cdot i})^{\dagger}\boldsymbol{p}$, based on H_i,

$$i^* = \arg\min_i ||\boldsymbol{p} - \hat{\boldsymbol{p}}_i|| = \arg\max_i \frac{||(\boldsymbol{P}_{\cdot i})^T\boldsymbol{p}||^2}{(\boldsymbol{P}^T\boldsymbol{P})_{ii}} \tag{6.20}$$

where $\boldsymbol{P}_{\cdot i}$ is the ith column vector in $\boldsymbol{P}$.

For a multi-outlier hypothesis ($L > 1$), we propose an extension of the maximum likelihood test by Sturza. Equation (6.20) can be extended to

$$(i_1^*, \ldots, i_k^*) = \arg\min_{(i_1,\ldots,i_k)} ||\boldsymbol{p} - \hat{\boldsymbol{p}}_{(i_1,\ldots,i_k)}|| \tag{6.21}$$

where $\hat{\boldsymbol{p}}_{(i_1,\ldots,i_k)} = \tilde{\boldsymbol{P}}\tilde{\boldsymbol{P}}^{\dagger}\boldsymbol{p}$ and $\tilde{\boldsymbol{P}}$ is a matrix composed of the $(i_1, \ldots, i_k)$th columns of the parity matrix, $\boldsymbol{P}$. If the number of outliers, L, is known, Equation (6.21) can be used to search for those multiple outliers at the same time. However, since L is usually unknown, Equation (6.20) is used for our RAIM implementation for iterative removal of outliers.

6.3 Multi-Fault Tolerant RAIM Algorithm

To address the multiplicity of outlying measurements in the hybrid GPS and TV positioning system, a multi-fault tolerant RAIM algorithm is proposed. This algorithm is designed to handle more than one erroneous pseudorange measurement efficiently and is based on the χ^2 test, the HPL test, the MHSS test, and the maximum likelihood test discussed in the preceding sections. The three fault detection algorithms (χ^2, HPL, and MHSS) may be sufficient when outliers rarely occur but are not suitable for a large number of outliers. Thus, fault exclusion by the maximum likelihood test is combined with fault detection.

The proposed RAIM algorithm combining these fault detection and fault exclusion algorithms is illustrated in Figure 6.4. The combined scheme is run iteratively in order to detect and exclude multiple outliers. Starting with a set of measurements in an epoch, channels are continuously removed until a subset of channels is found with test statistics below the given thresholds. Then, the epoch is declared to be a success

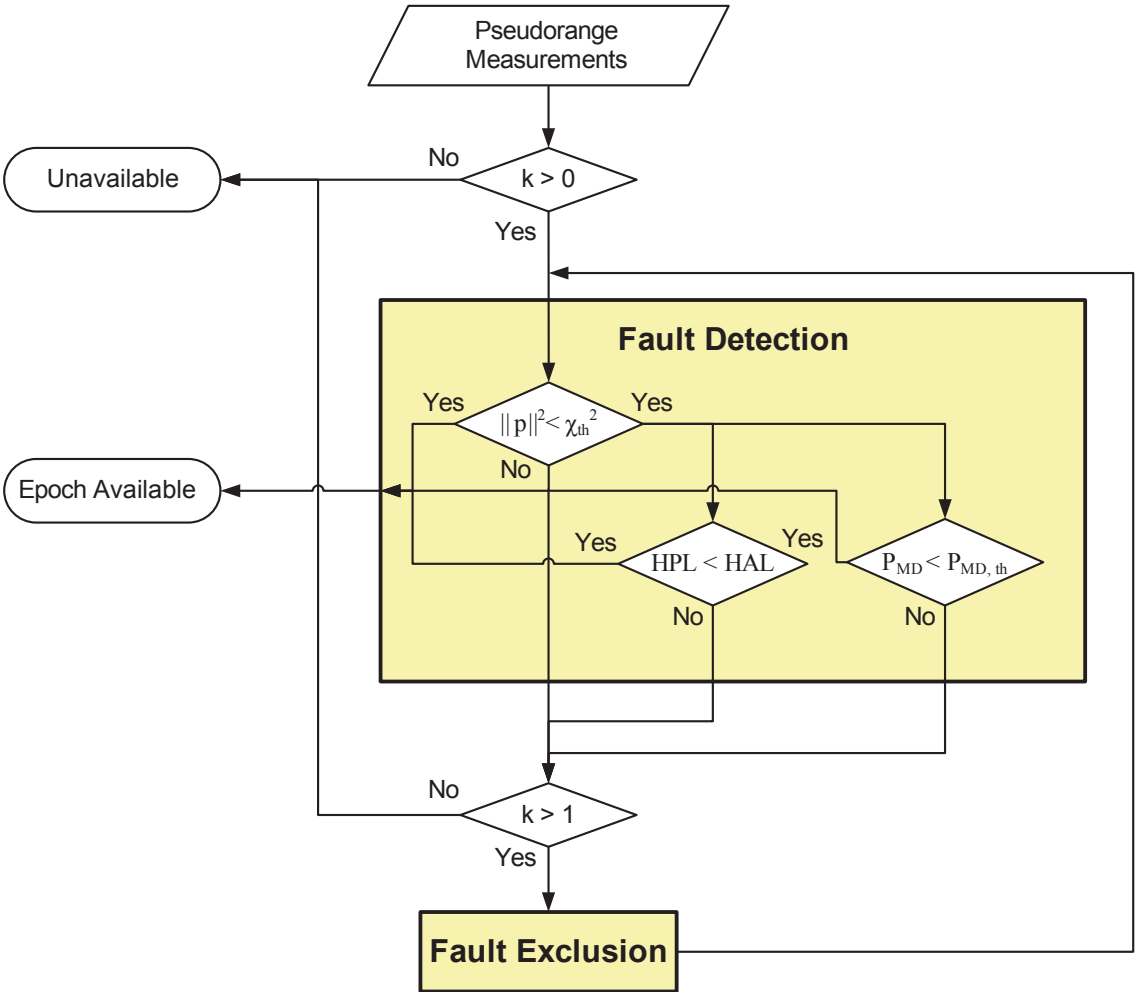

Figure 6.4: RAIM implementation with iterative fault detection and exclusion steps

(or available). Otherwise, the epoch is called a failure (or unavailable).

The fault detection and exclusion steps proceed as follows. First, the fault detection is applied if there is one or more redundant measurements ($k > 0$). If there is no redundancy, it is not possible to detect outliers and consequently the epoch is declared to be unavailable. For measurements with redundancy there are three paths which lead to the χ^2 test, the HPL test, and the MHSS test, respectively. Among these tests, the χ^2 test serves as a pre-test for the remaining two tests. If no fault is detected, the epoch is declared to be available. Second, if a fault is detected and if there are two or more redundant measurements ($k > 1$), measurements are directed to the fault exclusion step. If there is only one redundant measurement ($k = 1$), it is not possible to verify its integrity because the subsequent fault detection step cannot be performed after the last redundant measurement is removed in the fault exclusion step. Thus, at least two redundant measurements are required for the fault exclusion step. After a channel is determined to be biased and excluded, the remaining measurement set is redirected to the fault detection step.

The proposed multi-fault tolerant RAIM algorithm is used to remove outliers in GPS and TV pseudorange measurements in Chapter 7 where the three fault detection algorithms are compared to one another.

Chapter 7

Field Test of Integrated System

To assess the performance of the hybrid GPS and TV positioning system, a TPS receiver and a GPS receiver were used for the positioning field tests in the San Francisco Bay Area, where the measurement sites were selected from indoors and outdoors in urban, suburban, residential, and rural areas. The performance of the hybrid system is presented across the categorized areas, showing the promising aspects of the combination of space signals and terrestrial signals [2], [3].

7.1 Test Methods and Locations

The system performance of TPS and GPS was examined in the field test campaign during the summer of 2005 at 39 selected sites in the San Francisco Bay Area. The GPS L1 signal, ATSC (digital), and NTSC (analog) television signals were used as ranging sources. This section describes the measurement system, sites, and data collection method.

7.1.1 Hybrid Measurement System

Figure 7.1(a) illustrates the configuration of the hybrid measurement system used for field tests in the San Francisco Bay Area. The measurement system consists of two positioning sensors (a SiRF StarII GPS receiver and a Rosum TV receiver), a

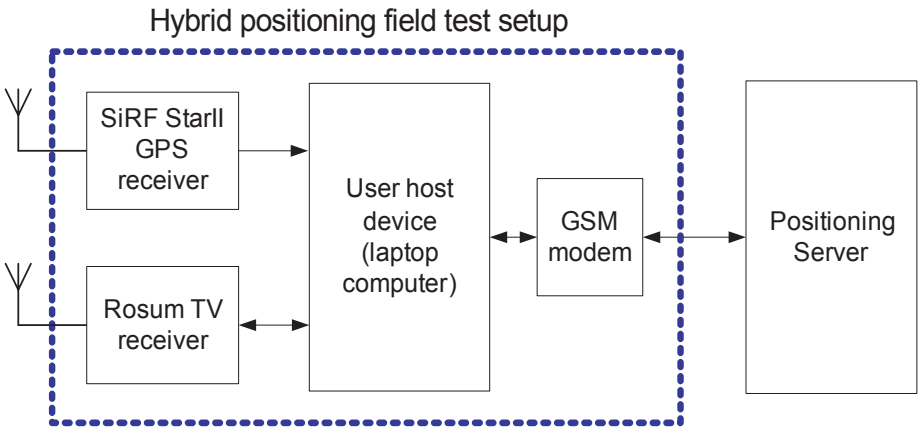

(a) Configuration of hybrid positioning unit

(b) Typical placement of hybrid positioning unit

Figure 7.1: Hybrid GPS and TPS positioning field test unit

notebook computer, and a GSM (global system for mobile communications) modem. The GPS receiver works independently from the rest of the system, generating GPS pseudorange measurements without external aiding information. In contrast, the TV receiver depends on external aiding information from a positioning server.

The internal communication among the TV and GPS receivers, a host computer, and a network modem is established through serial connections. The external network connection is supported through GPRS (general packet radio service). The notebook computer delivers pseudorange measurements from both GPS and TV receivers to a position server and requests aiding information for the TV receiver. In general, the need to send aiding information to the TV receiver can limit its operational range. However, the GSM GPRS connection was proven to be robust and consistently available within our test region. The communication link is not limited to GSM; any form of communication can be used depending upon its availability since the required data rate is very low.

At each measurement site, the hybrid measurement system was placed at a fixed location for one hour period. The two receivers were located side by side or on top of each other in order to minimize the physical distance between them. In both cases, the external GPS antenna was placed so that the skyview was not blocked by the rest of the measurement system. Figure 7.1(b) shows the typical placement of the measurement system during the field tests.

7.1.2 Measurement Sites

Positioning tests are highly sensitive to environment due to variation of local signal availability and severity of multipath effects. This section provides a description and pictures of the measurement sites.

Because of the variety of highly developed populated areas and pristine natural areas, the San Francisco Bay Area is suitable for testing a positioning system in various types of environments. In this measurement campaign, we selected the measurement sites to address seven different categories: outdoor sites in urban, suburban, residential, and rural areas; and indoor sites in urban, suburban, and residential areas.

Table 7.1: Measurement sites in San Francisco Bay Area

Category	Location	Outdoor	Indoor
Urban	San Francisco downtown	6	4 (+2)
Suburban	Palo Alto downtown	4	5
Residential	Stanford graduate housing	8	5
Rural	Half Moon Bay and Highway 280	5	N/A

Urban areas are the most challenging environment for any type of positioning system due to multipath and blockage by buildings but these areas enjoy extensive coverage by TV signals. Suburban and residential areas are relatively mild environments for both GPS and TV receivers with less obstruction from buildings and robust coverage of TV signals. Rural areas provide an unblocked open sky, best for GPS receivers but challenging for TV signals which may not reach every corner of the area due to lower commercial needs. Table 7.1 displays the number of sites in each category.

Urban sites were selected from the San Francisco downtown where buildings create urban canyons, as shown in Figure 7.2(a). Because only a small portion of sky is visible, the number of observable GPS satellites were often fewer than three while there were a substantial number of measured TV channels in spite of the obstruction by neighboring building structures. The urban indoor measurements (see Figure 7.2(b)) were taken at the lower levels of 4–8 story buildings located in the same downtown area. There were six urban indoor sites but two of those sites were excluded due to the absence of any meaningful measurements. The two excluded sites are depicted in Figure 7.6.

The Palo Alto downtown provided suburban sites, an area with a combination of business buildings and dining places, as shown in Figure 7.3(a). There are many 2–5 story buildings, a few 10–15 story buildings, and densely placed street trees. The residential sites were chosen from the Stanford graduate housing, an area with two story wooden town houses, 10–15 story concrete highrise apartment buildings, and open yards, as shown in Figure 7.4(a). The wooden structures were shown to be less obstructive than concrete buildings, allowing GPS reception outside and inside (see Figure 7.4(b)) those dwellings. The residential sites were located in combinations of

(a) Outdoor site

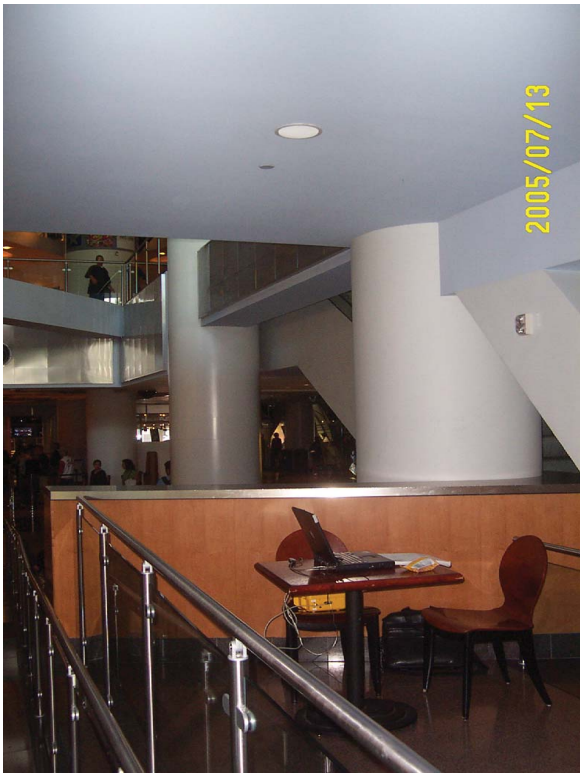

(b) Indoor site

Figure 7.2: Urban sites at San Francisco downtown

(a) Outdoor site

(b) Indoor site

Figure 7.3: Suburban sites at Palo Alto downtown

(a) Outdoor site

(b) Indoor site

Figure 7.4: Residential sites at Stanford campus

Figure 7.5: A rural site in Half Moon Bay

these two types of buildings. Five outdoor and two indoor sites were near or inside of wooden structures and three outdoor and three indoor sites were near or inside of concrete buildings.

The western region of the San Francisco Bay Area is well preserved land with low population density and few buildings. Within this region, five rural sites were selected from Half Moon Bay and the roadside of Highway 280, remote from residential and commercial areas as shown in Figure 7.5. Due to their remoteness, a smaller number of television channels were observed.

Again, the reader should note that two outlying urban indoor sites are removed from the data set due to lack of sufficient range measurements for positioning. One site is a basement cafe at an eight story building and the other site is a seven story parking structure in downtown San Francisco (see Figure 7.6).

(a) A basement cafe at a 8 story building

(b) 3rd floor at a 7 story parking structure

Figure 7.6: Outlying urban indoor sites removed from the data set

7.2 Preliminary Results without RAIM

This section describes the characteristics of the field test results before any optimization effort. After examining these raw results, a further improvement is sought through RAIM (described in Chapter 6) and additional optimization efforts (described in Section 7.3).

7.2.1 Urban Example

Let us first visit the urban outdoor site illustrated in Figure 7.2(a) where only a narrow strip of the sky in the north-west direction is visible from the ground. In this type of environment, radio waves are exposed to signal blockage and attenuation by surrounding building structures. For the GPS receiver, the marginal skyview limits the number of observable GPS satellites on the ground while multiple TV signals were observed by the TV receiver.

Two performance metrics are used to assess the quality of positioning results: availability and accuracy. Availability is defined to be the percentage of successful epochs among all epochs and accuracy is measured in DRMS (distance root mean squared) of horizontal position errors.

$$\text{Availability} = \frac{\text{number of succeeded epochs}}{\text{number of total epochs}} \tag{7.1}$$

$$\text{Accuracy} = \text{DRMS (distance root mean squared)} \tag{7.2}$$

Along with DRMS, there is another accuracy metric used in this chapter circular error probable (CEP). CEP comes with a percentile number and, for example, 50% CEP indicates a median error. 67% CEP and 95% CEP are also used as accuracy measures.

First, GPS position estimation succeeded in only 62% of the trials due to the limited number of observable satellites and the accuracy was 206 m (see Table 7.2). In contrast, TPS generated position fixes in 100% of the position fix attempts and the accuracy was 1,473 m. The significantly higher availability of TPS demonstrates the physical advantage of terrestrial ranging sources in urban positioning. However, the

Table 7.2: Availability and accuracy in an urban canyon site

	GPS Fixes	TPS Fixes	Hybrid Fixes
Availability	62 %	100 %	100 %
Accuracy	206 m	1473 m	1173 m

corresponding low accuracy reveals the challenge due to large outlying TV pseudorange measurements. The hybrid solution combined the individual strengths of GPS and TPS and managed to have high availability with improved accuracy from TPS.

7.2.2 Accuracy and Availability Results

Now let us examine the statistics of positioning results at all test sites, again without RAIM processing. The results are presented in three modes of positioning: GPS, TPS, and Hybrid. Figure 7.7 displays the availability for outdoor and indoor sites, illustrating the weakness of GPS in urban sites and the weakness of TPS in rural sites. In urban sites, the TPS success ratio is about 40% higher than that of GPS, a promising aspect of TPS. In the suburban and residential sites, both TPS and GPS perform well, while TPS suffers in rural sites due to blockage of TV signals by mountains as well as sparse TV coverage. For the indoor sites, GPS was incapable of delivering any fix except in certain wooden residential buildings. Because all other concrete buildings almost entirely block GPS signals, only TPS measurements were available in most cases and consequently the hybrid mode very closely follows the TPS mode. In outdoor sites the availability of the hybrid mode follows that of TPS in urban areas and GPS in rural areas.

The reader should note that the near 100% availability at all tested sites comes at the price of low position accuracy as shown in Figure 7.8. Generally, the outdoor accuracy improves as we move from dense urban areas to rural areas. The TPS accuracy results are worse than the GPS accuracy results and the hybrid mode accuracy is in the middle of TPS and GPS. The hybrid results are expected to be equivalent or better than the individual results and the preliminary results imply room for improvement. For indoor sites, the flat level of high position errors regardless of region

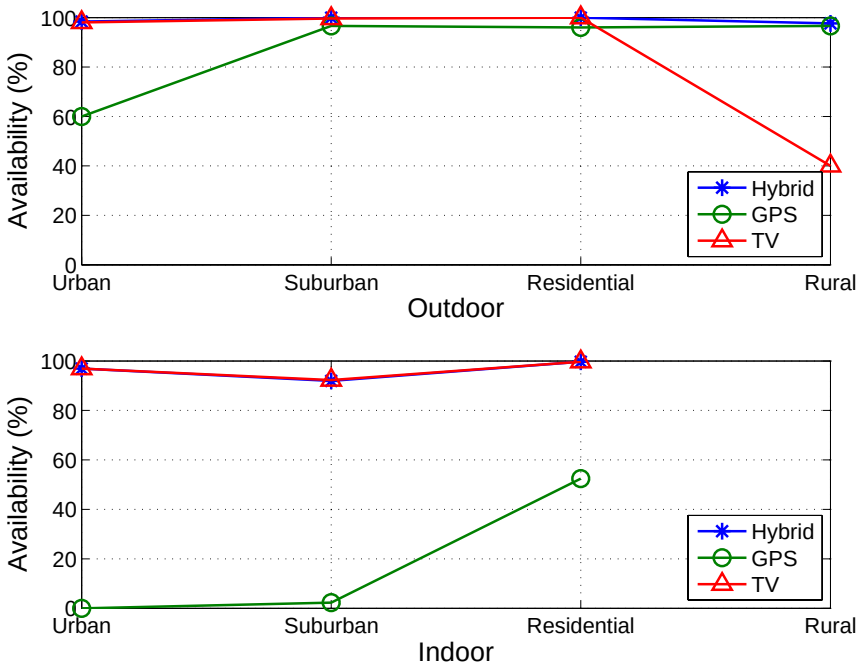

Figure 7.7: Preliminary availability results

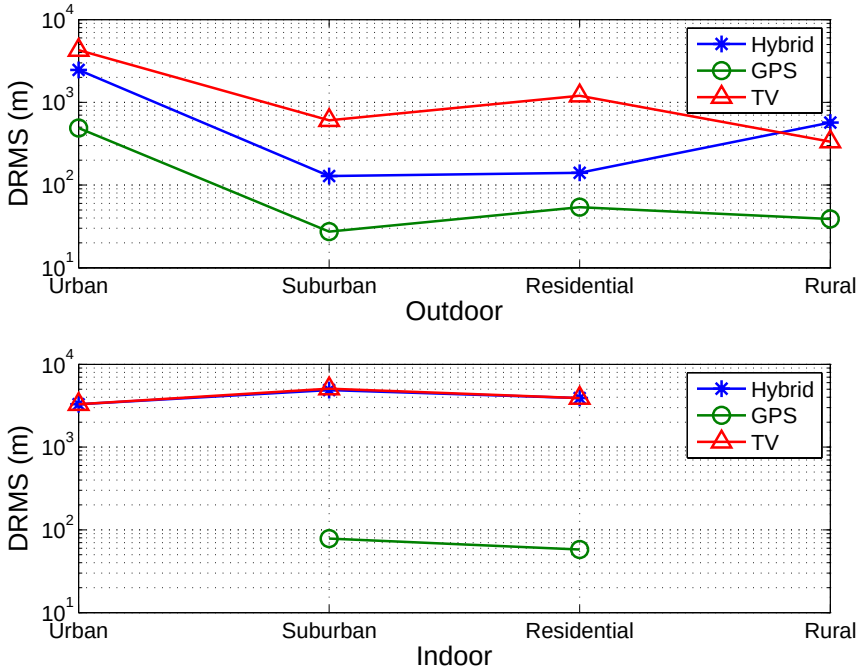

Figure 7.8: Preliminary (horizontal) accuracy results

proves again the existence of large outlying position errors. Otherwise the accuracy should have shown a more region-dependent pattern. Although GPS fixes are often not available, GPS estimates tend to be more accurate than TPS fixes.

These preliminary results without fault detection and exclusion by RAIM have shown high availability but failed to achieve high accuracy. The low accuracy results originate from large outlying pseudorange measurements which are not excluded from the position estimation process. The appropriate filtering of these outlying measurements is discussed in the following section.

7.3 Final Results with RAIM

This section presents position estimation results after the RAIM algorithms (see Chapter 6 for details) are applied. Instead of adopting a fixed error criteria, the RAIM algorithms are tuned in order to balance availability and accuracy. In addition to the RAIM, additional performance optimization efforts are described in this section.

7.3.1 RAIM Processing: χ^2, HPL, and MHSS

In Figure 7.9(a) (outdoor sites), Figure 7.9(b) (indoor sites), and Figure 7.10 (all sites), each point summarizes the hybrid position estimation results from all corresponding sites. These figures show a typical trade-off between availability and accuracy. Although both high accuracy and high availability are desired, there is a balance between them and it is necessary to find the best acceptable trade-off between these two, sometimes conflicting, goals. In the trade-off space, the south east region is most preferred with high availability and high accuracy but it is more likely that the choice needs to be made between either the south west or the north east regions. A tighter screening of range errors results in higher accuracy but with lower availability (south west region); a looser screening leads to higher availability but with lower accuracy (north east region).

Let us first visit the outdoor results in Figure 7.9(a). The trade-off curves of the

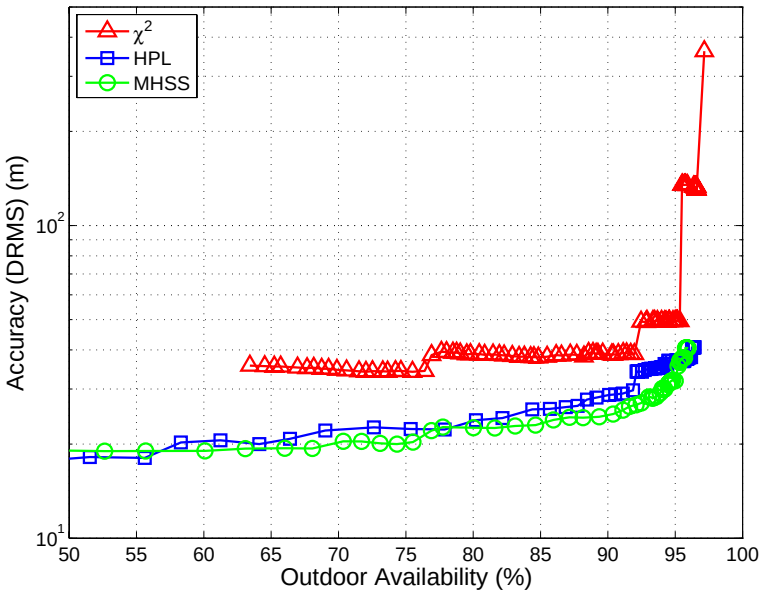

(a) Outdoor sites

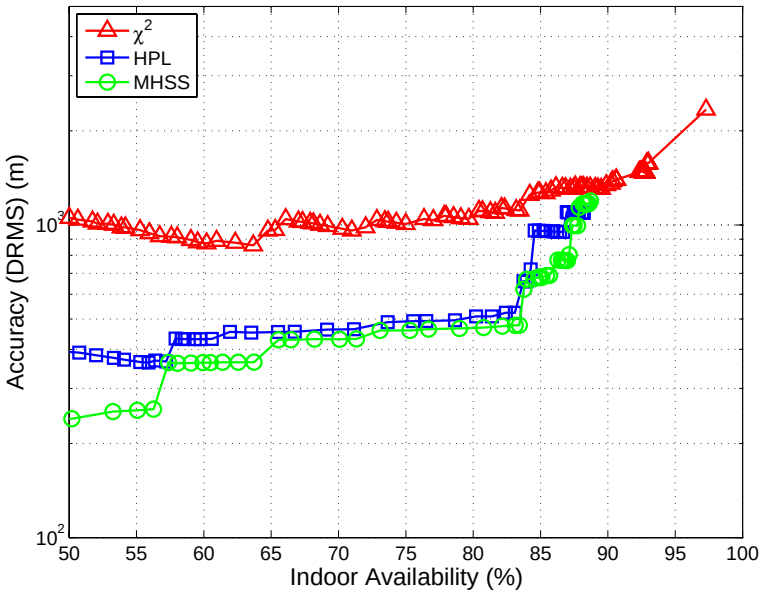

(b) Indoor sites

Figure 7.9: Trade-off between availability and accuracy in hybrid positioning (outdoors and indoors)

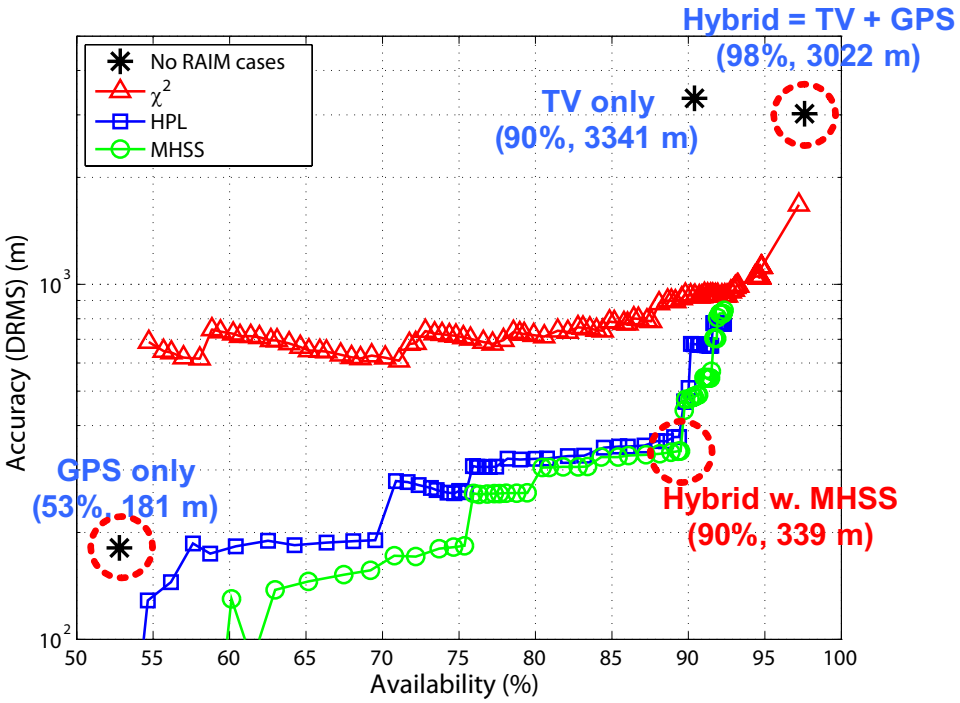

Figure 7.10: Trade-off between availability and accuracy in hybrid positioning (all sites)

HPL and MHSS RAIM methods are relatively flat while the χ^2 curve shows a sudden increase at its right end. Although the flat trade-off curves indicate that outdoor data are relatively free from outlying pseudorange errors, a small percentage of outliers can still cause a surge in position errors as shown in the case of the χ^2 test. In the HPL and MHSS tests, the RAIM parameters can be relaxed for high availability with a small accuracy loss outdoors. The indoor trade-off curves in Figure 7.9(b) show more dynamic variations with a larger gap between χ^2 and the rest. The ineffectiveness of χ^2 is clearly displayed by its flatness while other methods are able to improve accuracy as we move westward by tightening outlier screening. The HPL and the MHSS tests show almost stepwise accuracy improvement at 57% and 83% availability regions.

When the positioning device is not aware of whether a user is indoors or outdoors, the RAIM algorithms are also blind to this knowledge. Thus, a combined trade-off curve for all sites (see Figure 7.10) is used for the choice of the best trade-off point.

Table 7.3: Selected trade-off points between availability and accuracy (no RAIM, HPL, MHSS)

Processing Method		Overall		Outdoor		Indoor	
		%	(m)	%	(m)	%	(m)
GPS	No RAIM	52.8	181	87.3	247	18.2	68.9
	HPL	50.8	53.2	84.0	47.0	17.6	58.8
	MHSS	51.1	53.3	84.5	47.1	17.8	58.8
TPS	No RAIM	90.4	3341	84.4	2243	96.3	4158
	HPL	82.0	489	80.4	418	83.6	551
	MHSS	82.2	449	80.5	382	83.9	508
Hybrid	No RAIM	97.6	3022	99.0	1269	96.2	4082
	HPL	89.4	371	95.7	37.5	83.1	524
	MHSS	89.5	339	95.6	37.6	83.4	478

Due to the high level of indoor position errors, the combined curves follow the shape of the indoor curves more closely than those of the outdoor sites. In Figure 7.10, the "no RAIM" cases are at either end of the trade-off curves—low availability with high accuracy (the GPS mode, 53% and 181 m) or low accuracy with high availability (the hybrid mode, 98% and 3,022 m). Among various points on the trade-off curves, a reasonable choice would be the edge point around 90% availability (90% and 339 m) below which little gain in accuracy is achieved with the loss of availability and above which little gain in availability at the loss of accuracy. The availability and accuracy of 90% and 339 m are a balanced trade-off point compared to the no RAIM GPS case (53% and 181 m) and the no RAIM hybrid case (98% and 3,022 m). These trade-off points are highlighted by dotted circles in Figure 7.10.

The breakdown of this trade-off point into outdoor and indoor areas is given in Table 7.3. In the outdoor sites, by applying the MHSS RAIM, there is a substantial gain in accuracy from 1,269 m to 38 m with the loss of 3% availability (99% to 96%). This result reflects the existence of large but easily detectable outlying measurement errors. In the indoor sites, the accuracy gain is still significant (4,082 m to 478 m) but at a relatively high cost in terms of availability (96% to 83%).

7.3.2 Additional Optimization Efforts: Clusterization, Localization, and Position Filtering

The improvements by the RAIM alone still may not satisfy the needs of indoor users. So, a further improvement is sought through the following three methods: clusterization, RAIM localization (regional optimization), and position domain filtering (time averaging).

The first method is the clusterization of transmitters. Often TV transmitters are closely located to take advantage of a tall building or a high mountain. Then, these closely located transmitters are counted as one cluster and this grouping process is called clusterization. Because the number of clusters is an indicator of the geometric diversity of transmitters, a measurement set with less than four clusters is discarded in order to support geometric diversity. Exceptionally, three cluster cases are allowed if all three clusters include at least two consistent pseudorange measurements. The clusterization is a conservative approach because still most of the three cluster cases will be removed if any of the three clusters has a single measurement or disagreeing multiple measurements. With clusterization, the accuracy improves from 339 m to 209 m while the availability decreases from 90% to 84%.

The second method is the regional optimization of the RAIM. Apparently, the choice of RAIM parameters must be region dependent, since the trade-off curves are different from region to region. Thus, if the RAIM is optimized based on a trade-off curve per region or per site, the overall result improves over that of the blind RAIM as shown in Figure 7.11. While maintaining the same accuracy level as the clusterization, the availability again approaches 90%.

The last method is slightly different from the previous two methods in the sense that it uses position domain filtering instead of range domain filtering which includes all RAIM methods. Focusing on pedestrian users whose motion is under limited dynamics, each position estimate is expected to be correlated to one another and this correlation helps position domain filtering. The particular implementation of the position domain filtering in this analysis uses averaging in a five epoch window to avoid unnecessary exploitation of knowledge of user stationarity during the field

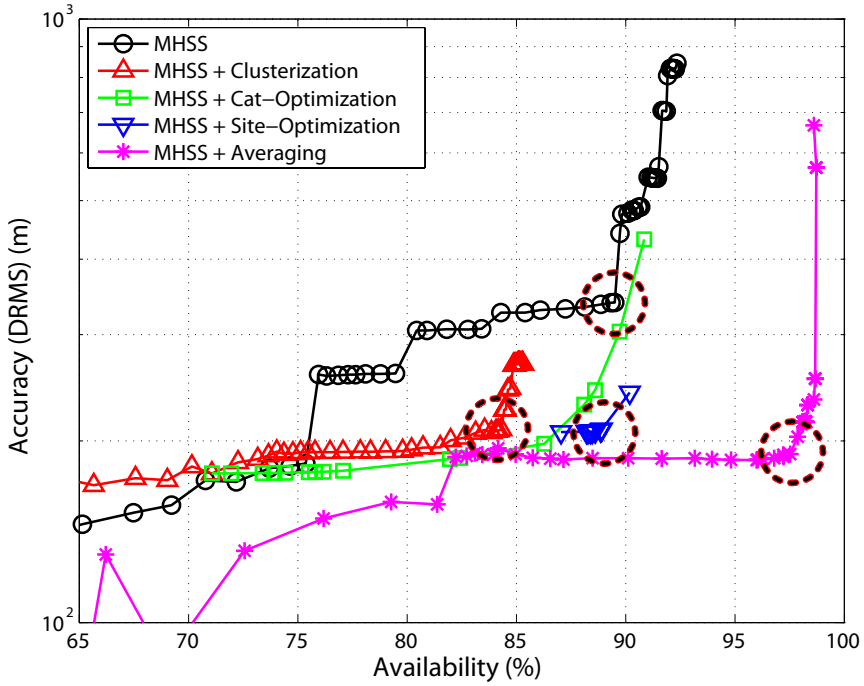

Figure 7.11: Availability and accuracy with optimization efforts

Table 7.4: Trade-off points between availability and accuracy (RAIM, localization, averaging)

Processing Method		Availability (%)	CEP (m)	DRMS (m)
GPS only		53	17	181
Hybrid	No RAIM	98	215	3022
	MHSS	90	83	339
	MHSS & Localization	89	73	208
	MHSS & Averaging	**97.6**	63	190

Table 7.5: Trade-off points between availability and accuracy in indoors and outdoors (RAIM, localization, averaging)

Processing Method		Outdoor			Indoor		
		%	CEP	DRMS	%	CEP	DRMS
GPS only		87	18	247	18	15	69
Hybrid	No RAIM	99	31	1269	96	400	4082
	MHSS	96	17	38	83	149	478
	MHSS & Localization	96	17	36	82	129	292
	MHSS & Averaging	**99.6**	14	26	**95.5**	111	268

test. Time averaging in the five epoch window (corresponding to approximately 50 seconds) is certainly applicable to most pedestrian users, moving or not. Also, if the current epoch estimate within the averaging window is unavailable or declared to be an outlier, the previous position estimate is maintained until the next valid position fix is available. With the position filtering, the availability reaches 98% (99.6% for outdoor and 95.5% for indoor) and the accuracy is 190 m (26 m for outdoor and 268 m for indoor). The position filtering may not work if the RAIM does not generate reliable position estimates after removing outlying pseudoranges, as shown at the right end of the trade-off curve for the position filtering.

Figure 7.11 presents multiple points of operation in practice. At the beginning of positioning without prior knowledge of user position, it is necessary to take a conservative approach, i.e., the clusterization, thus sacrificing availability. However, once the initial estimate is available, the RAIM parameter can be optimized according to

Table 7.6: Final availability and accuracy results

	Outdoor				Indoor		
	Urban	Sub.	Res.	Rural	Urban	Sub.	Res.
Availability (%)	99.4	100	100	99.0	99.6	87.7	99.0
DRMS (m)	46.7	11.9	16.0	7.4	407	198	103
67% CEP (m)	36.8	12.7	15.5	7.2	502	76.2	76.6
95% CEP (m)	79.5	22.4	25.3	13.7	691	317	227

a pre-surveyed localized RAIM parameter table for availability gain. Then, as confidence builds on position estimates, the position domain filtering starts to generate smoothed results. After all steps, the availability is 97.6% with an accuracy of 190 m in DRMS and 63 m in CEP (circular error probable, a median error) for all sites combined. For outdoors, it is 99.6% with 26 m in DRMS and 14 m in CEP. For indoor sites, the final availability is 95.5% with 268 m in DRMS and 111 m in CEP. Table 7.4 and Table 7.5 summarize the accuracy and availability trade-off for the various data processing methods applied here.

7.3.3 E911 Compliance

This section describes the E911 service in the Unites States and examines the E911 compliance of the hybrid GPS and TPS system. The E911 (emergency call) service is a government initiative in the United States for locating and rescuing persons in danger. The U.S. FCC (Federal Communication Commissions) requirements for E911 service dictates accuracy of 50 m for 67% CEP and 150 m for 95% CEP for mobile-based positioning and 100 m for 67% CEP and 300 m for 95% CEP for network-based positioning.

Table 7.6 summarizes the final availability and accuracy results (DRMS, 67% CEP, 95% CEP) in categorized areas. Focusing on the CEP measures, all outdoor results are well within the E911 requirements. However, indoor areas remain challenging. In particular, the accuracy results in the urban indoor sites show the challenges of indoor positioning in all three measures because there are both large biases and variances in the estimated position fixes.

Table 7.7: FCC E911 compliance ratio (compliant sites/total sites) in 67% CEP and 95% CEP (mobile-based)

	Outdoor				Indoor		
	Urban	Sub.	Res.	Rural	Urban	Sub.	Res.
67% CEP	4/6	4/4	8/8	5/5	1/4	1/5	3/5
95% CEP	5/6	4/4	8/8	5/5	1/4	2/5	3/5

The compliance of the hybrid GPS and TPS system to the E911 requirement is summarized in Table 7.7. The compliance ratio is defined to be the ratio of the number of compliant sites and the total number of sites. Overall, 21 out of 23 outdoor sites meet both the 67% CEP and 95% CEP requirements while 5 out of 14 indoor sites satisfy the requirements. For the network-based requirements which are less strict than the mobile-based requirements, all outdoor sites meet the requirements as well as half of the indoor sites. A detailed breakdown of 67% CEP and 95% CEP requirements is given in Table 7.7.

7.4 Summary

This chapter has presented the field test results of the hybrid GPS and TV positioning unit in indoor and outdoor; urban, suburban, residential, and rural areas. In urban canyons, there were three GPS satellites in view on average. This number shrank to zero for the urban indoor sites. In contrast, 15 TV channels were observed in the urban outdoor sites and 12 channels in urban indoor sites. These TV signals helped to fill the gap in positioning coverage in urban and indoor areas but the corresponding accuracy was often poor due to large outliers in the TV range measurements.

To improve accuracy, three types of RAIM algorithms were adopted to detect and exclude large outlying range measurements. The MHSS RAIM has been proven to be most effective by significantly improving position accuracy from (98% availability, 3,022 m accuracy) to (90%, 339 m). Further improvement to (89%, 208 m) has been achieved by RAIM localization in a given environment. Lastly, position domain filtering has enhanced the availability to (97.6%, 190 m). In practice, RAIM with

global paramaters is applied initially but as soon as the locale of the user is identified, RAIM can be adaptively configured to the type of environments. The position domain filtering becomes effective as more position estimates are accumulated.

If the results are divided into indoors and outdoors, the outdoor availability and accuracy result is (99.6%, 26 m); the indoor result is (95.5%, 268 m). While 26 m outdoor accuracy is a quite welcome result, 268 m indoors illustrates the difficulties of positioning in obstructed spaces, requiring further efforts toward improvement. Regarding the FCC E911 requirements, 91% of the outdoor sites are satisfactory but only 36% of indoor sites meet the requirements.

Despite severe environmental difficulties, significant enhancement in positioning coverage has been demonstrated by the hybrid GPS and TV positioning unit. In particular, the availability results have shown the potential of the integrated GPS and TPS system while at the same time the accuracy results have reminded us of the challenges in urban indoor areas.

Chapter 8

Conclusions and Future Work

This dissertation has investigated the feasibility and performance of the hybrid GPS and TV positioning system. With a prototype implementation of the hybrid system, the performance was tested through field trials and the position estimation process was optimized in order to achieve balance between availability and accuracy. The final availability and accuracy results have shown promising aspects of the hybrid GPS and TPS system as well as challenges in urban indoor areas. This chapter summarizes the main results from the hybrid positioning study and describes possible future work for further improvement.

8.1 Dissertation Contributions and Results

After highlighting the convergence of space and terrestrial signals, a summary of the dissertation contributions and results is presented in this section.

8.1.1 Convergence of Space and Terrestrial Signals

The goal of this hybrid positioning study is the enhancement of positioning coverage, in particular, in urban canyons and indoors. To achieve this goal, terrestrial TV signals are adopted as ranging sources for positioning and combined with GPS satellite signals. As depicted in Figure 8.1, conventional positioning systems such as GPS,

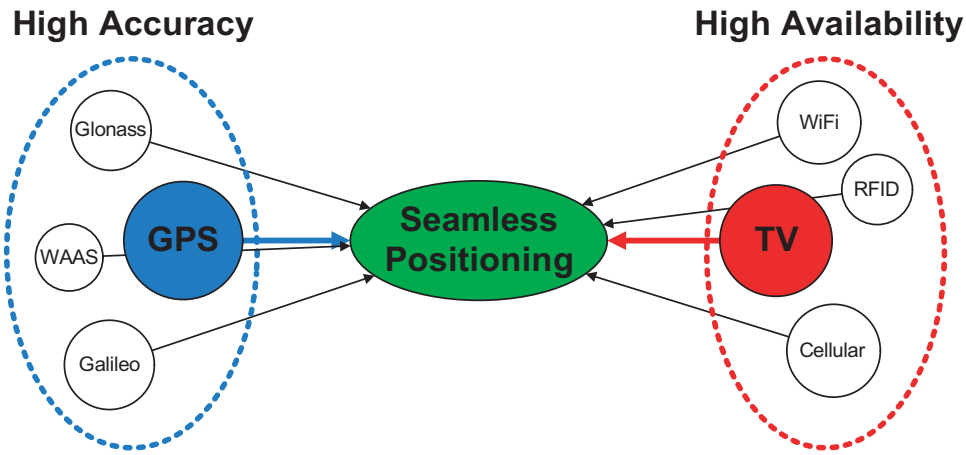

Figure 8.1: Road to seamless positioning: hybrid GPS and TV positioning

Glonass, Galileo, and augmentation systems such as WAAS (wide area augmentation system) command high accuracy but have limited availability in harsh urban and indoor environments. Since terrestrial transmitters are located near urban and indoor users, these radio devices have higher urban and indoor availability. Thus, the combined use of space-based ranging signals and land-based communication signals is proposed as a way to enhance positioning coverage beyond the conventional coverage areas. In this dissertation, GPS and TV signals were selected and the hybrid GPS and TPS system has been investigated.

8.1.2 Contributions

The major dissertation contributions for the hybrid GPS and TV positioning system include: assessment of robustness of TOA and TDOA positioning, design and implementation of the hybrid GPS and TV positioning system, design and implementation of the multi-fault tolerant RAIM algorithm, and verification and optimization of the hybrid positioning system through field tests.

First, the TOA based positioning and the TDOA based positioning were compared. Under ideal conditions, the equivalence proof of TOA and TDOA has been shown to be valid in the hybrid GPS and TPS system. Under non-ideal conditions,

TOA is slightly more robust than TDOA. Based on this comparison, the hybrid positioning is designed to be a TOA based positioning system.

Second, the hybrid GPS and TV positioning system was implemented. The hardware configuration included a GPS receiver and a TPS receiver and the software processing was implemented on the Matlab platform. The Matlab-based positioning algorithm is capable of TV pseudorange estimation and hybrid positioning using GPS and TV pseudorange measurements. On this platform the RAIM and other performance optimization methods were implemented and the field tests were conducted. As a part of the implementation efforts, an analytical performance analysis of the hybrid system was conducted as well as the investigation of clock stability and its impact on positioning accuracy.

Third, a multi-fault tolerant iterative RAIM has been proposed and implemented. The existing RAIM algorithms were compared and the MHSS RAIM has been shown to perform best. With modifications, these RAIM algorithms were reconfigured to detect and exclude multiple faults in range measurements. The field test results indeed contained a substantial number of outlying measurements, in particular, among TV range measurements. Significant accuracy improvements have been achieved by the proposed RAIM.

Lastly, the field tests were conducted in a variety of areas including indoors and urban canyons. The initial attempt of position estimation produced high availability but failed to achieve high accuracy. To balance availability and accuracy, optimization methods such as clusterization, RAIM localization, and position domain filtering were implemented and applied in addition to the multi-fault tolerant RAIM algorithm. The position estimation results were analyzed according to the applied processing methods and the corresponding regions such as indoors and outdoors.

8.1.3 Summary of Results

In the extensive field test campaign, raw range measurements were collected in a variety of locations around the San Francisco Bay Area including outdoor and indoor sites; urban, suburban, residential, and rural areas. Then the collected data were

Table 8.1: Availability and accuracy results from the field tests

	Outdoor	Indoor
Availability	99.6%	95.5%
Accuracy (DRMS)	26 m	268 m
Accuracy (CEP)	14 m	111 m

processed by the hybrid positioning system equipped with the proposed iterative RAIM algorithm for multi-fault tolerance against outliers found in the integrated range measurements.

The resulting availability showed significant enhancement in availability compared to the GPS only result. In the test locations, GPS provided 53% availability on average which means it worked only half the time. In particular, the GPS availability plummeted to 18% in indoor areas, unavailable in most indoor test sites with the exception of a few wooden houses. Then, at the same locations, the integrated GPS and TV positioning provided much higher availability of 99.6% outdoors and 95.4% indoors (see Table 8.1). At the outdoor sites, this was a combined result of GPS and TV pseudorange measurements, taking advantage of the high accuracy of GPS and high availability of TPS, generating high availability as well as high accuracy (14 m in CEP and 26 m in DRMS), while in indoor sites, this was, in many cases, TV only positioning, resulting in high availability but low accuracy (111 m in CEP and 268 m in DRMS).

The achievement of high availability in all areas satisfies the goal of the study, the enhancement of positioning coverage. On average, 98% availability is a substantial improvement from 53% GPS avaiability. However, the low indoor accuracy remains as future work to be discussed in the following section with recommendations to resolve it.

8.2 Infrastructural Investments

This section describes three possible future efforts regarding hybrid GPS and TV positioning. The first two suggestions are intended to solve the two remaining issues

from this dissertation: low accuracy in indoor areas and two excluded zero-availability indoor sites due to lack of measurements. The last recommendation, with broader implications, is a time and position reference system using integration of Loran and the TV positioning system which could be used as a backup to GPS in the case of a GPS failure.

8.2.1 Enhanced Signal Strength via Utilization of Data Segments

Low accuracy in indoor areas and two excluded zero-availability indoor sites are the result of severe multipath and low observability due to building obstructions in dense indoor areas. For example, one of the dropped indoor sites is a basement cafe in an eight story library building in downtown San Francisco where any form of radio signals are hard to detect. To survive in this type of deep indoor area, the foremost solution is securing stronger signal strength. Two suggestions are given in this and the next subsection.

In the current TV positioning system, only the repeated field synchronization codes are used for TV positioning which compose approximately 0.3% of the overall TV signals in time and power. The remaining unused 99.7% of TV signals are filled with data segments which are non-repeated video and audio data streams and thus normally not usable for positioning. However, with a dedicated TV tuner for each channel at monitor stations constantly capturing and sending broadcast signals to a positioning server, these can be used as ranging signals as well, providing substantial gain in signal strength. The user TV positioning device, currently searching only for field synchronization data lasting 77 μs and waiting another 24 ms before the next field synch, can capture and correlate TV signals without waiting. This continuous signal correlation enables more coherent and longer signal integration (more signal symbols but shorter in time) and consequently higher integration gain. In particular, the utilization of data segments is beneficial to a mobile user whose motion prevents longer integration.

8.2.2 Continuous Signal Monitoring

Another solution to the indoor positioning issues can be found from continuous signal monitoring. An array of TV tuners dedicated to individual channels at monitor stations provides the additional benefit of improved transmitter signal monitoring. With a small number of tuners, each TV channel cannot be monitored continuously, but with dedicated parallel TV tuners it becomes feasible. Then, any anomaly in TV transmitter signals can be detected. The consequent error propagation can then be effectively prevented since every measurement at user receivers will have a matching measurement from a monitor and the common bias can be removed accordingly.

8.2.3 A GPS backup: TV Positioning System Synchronized to Loran

The last recommendation for future work has broader implications. If Loran is used to synchronize either monitor stations for TV positioning or TV towers themselves, the TV positioning system can be used as a backup system to GPS, serving as an alternate time and position reference in the case of a GPS failure.

As we become more dependent on GPS day by day, we become more aware of the consequence of a GPS failure. There is a growing request for a backup to GPS to avoid disruption in transportation, financial, and communication infrastructures. But unfortunately and alarmingly, currently there is no clear alternative solution proposed or foreseen. If monitor stations in the TV positioning system are equipped with Loran receivers and synchronized to Loran timing or TV towers themselves are tied to Loran timing, the combined TV/Loran system can be the independent alternative time and position reference and could be available world-wide in places under Loran coverage. Moreover, since this is a combination of two very strong and widely available terrestrial signals, the hybrid TV/Loran system is very robust and immune to hostile jamming and interference. Thus, the proposed TV/Loran system is expected to provide redundancy, which we are lacking today, in global time and position reference with a modest investment in a short time frame.

Appendix A

Transmitter Position Estimation (GPS)

This section describes methods to estimate GPS satellite position. We start from a standard method for satellite position estimation and develop it into a case with limited measurements (modulo millisecond pseudorange). In handling modulo millisecond pseudorange, a user clock bias is one of the main error sources, as described in Chapter 3.

A.1 Calculation of Satellite Position

When a receiver is under favorable condition to have continuous reception of a satellite signal, it can parse a GPS signal and can recover the transmission time embedded in the signal. This can then be used to estimate the satellite position which will be a reference for trilateration to calculate the receiver position.

A.1.1 Range and Pseudorange

A range measurement in a TOA positioning system is the difference between reception time, t_{RX}, and transmission time, t_{TX}, when there are no clock biases.

$$r = t_{RX} - t_{TX} \tag{A.1}$$

where t_{RX} is the true reception time, t_{TX} is the true transmission time, and r is the true range between the transmitter and the receiver.

There are clock biases at both a transmitter and a receiver. Atmospheric delay will also add biases to the variables. To accommodate these biases, we define new variables, measured reception time, $\tilde{t}_{RX}$, and reported transmission time, $\tilde{t}_{TX}$, based on the time tag contained in a transmitted signal. Then the uncorrected pseudorange, $\tilde{\rho}$, is calculated as follows.

$$\tilde{\rho} = \tilde{t}_{RX} - \tilde{t}_{TX} \tag{A.2}$$

where

$$\begin{aligned}
\tilde{\rho} &= \text{uncorrected pseudorange} = \rho + I + T - B_{TX} \\
\tilde{t}_{RX} &= \text{measured reception time} = t_{RX} + b_{RX} \\
\tilde{t}_{TX} &= \text{reported transmission time} = t_{TX} + B_{TX}
\end{aligned}$$

$$\begin{aligned}
\rho &= \text{corrected pseudorange} = \tilde{\rho} - I - T + B_{TX} = r + b_{RX} \\
b_{RX} &= \text{receiver clock bias} \\
B_{TX} &= \text{transmitter clock bias} \\
I &= \text{ionospheric time delay} \\
T &= \text{tropospheric time delay}
\end{aligned}$$

For convenience, the variables are assumed to be in units of meters unless specified otherwise. Also, a tilde over a variable means an uncorrected raw measurement, a hat means an estimate, and no sign generally means a true value.

A.1.2 Correction in Transmission Time

To find the satellite position, X_{TX}, we need to know true transmission time, t_{TX}, which can be estimated based on reported transmission time, $\tilde{t}_{TX}$, and clock correction

parameters given in an ephemeris data set.

$$\tilde{t}_{TX} \rightarrow t_{TX} \rightarrow X_{TX} \tag{A.3}$$

The receiver provides the reception time, $\tilde{t}_{RX}$, and the pseudorange, $\tilde{\rho}$ in Equation (A.2), and we can reconstruct $\tilde{t}_{TX}$ from these two.

$$\tilde{t}_{TX} = \tilde{t}_{RX} - \tilde{\rho} \tag{A.4}$$

The reported transmission time contains a clock bias which includes a clock drift, a relativistic effect, and a transmitter group delay. The clock bias can be estimated by the clock correction parameters on the true transmission time but it does not vary much over a short period of time, and thus, we can approximate it on the reported transmission time, i.e., $B_{TX}(t_{TX}) \approx B_{TX}(\tilde{t}_{TX})$.

$$\hat{t}_{TX} = \tilde{t}_{TX} - \hat{B}_{TX} \tag{A.5}$$

where

$$\begin{aligned}
\hat{B}_{TX} &= a_{f_0} + a_{f_1}(t_{TX} - t_{EPH}) + a_{f_2}(t_{TX} - t_{EPH})^2 + t_{REL} - t_{GD} \\
&\approx a_{f_0} + a_{f_1}(\tilde{t}_{TX} - t_{EPH}) + a_{f_2}(\tilde{t}_{TX} - t_{EPH})^2 + t_{REL} - t_{GD} \\
(a_{f_0}, a_{f_1}, a_{f_2}) &= \text{clock correction parameters} \\
t_{EPH} &= \text{reference time of clock correction parameters} \\
t_{REL} &= \text{relativistic time} \\
t_{GD} &= \text{transmitter group delay}
\end{aligned}$$

A.1.3 Satellite Position Based on Ephemeris Data

Broadcast ephemeris data contains coordinate information to estimate satellite position at a given transmission time. For details refer to the GPS interface control document (ICD-GPS-200) [12].

A.1.4 Earth Rotation

During the time that transmitted signals from satellites are traveling to a receiver on the ground, Earth is rotating constantly at Earth's rotation rate, $\dot{\Omega}_e$. Therefore, when an Earth centered Earth fixed (ECEF) coordinate is used, the coordinates, i.e., the axes themselves, are rotating (see Figure A.1). The rotation angle, θ, is given as the product of Earth's rotation rate, $\dot{\Omega}_e$, and the approximate range, $\hat{r}$, in seconds and thus the calculated satellite position needs to be rotated back by $-\theta$ to compensate for the coordinate rotation. θ is not so sensitive to the range estimate, $\hat{r}$, and thus we can use the range from the satellite to a pre-known user position. Because Earth's rotation does not affect the satellite position in the z direction, only x and y directions require correction.

$$\begin{aligned} \begin{bmatrix} x_\theta \\ y_\theta \end{bmatrix} &= \begin{bmatrix} \cos\theta & -\sin\theta \\ \sin\theta & \cos\theta \end{bmatrix} \begin{bmatrix} x \\ y \end{bmatrix} \\ &\approx \begin{bmatrix} 1 & -\theta \\ \theta & 1 \end{bmatrix} \begin{bmatrix} x \\ y \end{bmatrix} \text{ (if } \theta \approx 0) \end{aligned} \tag{A.6}$$

where

$$\begin{aligned} \theta &= \text{Earth's rotation angle} = \dot{\Omega}_e \cdot \hat{r}[\text{rad}] \\ \dot{\Omega}_e &= \text{Earth's rotation rate} = 7.2921151467 \cdot 10^{-5}[\text{rad/s}] \\ \hat{r} &= \text{estimated range} \\ (x, y, z) &= \text{uncorrected satellite position [m]} \\ (x_\theta, y_\theta, z) &= \text{corrected satellite position [m]} \end{aligned}$$

A.1.5 Implementation

When a pseudorange and reception time are given, transmission time can be reconstructed and the remaining bias terms can be approximated based on GPS clock

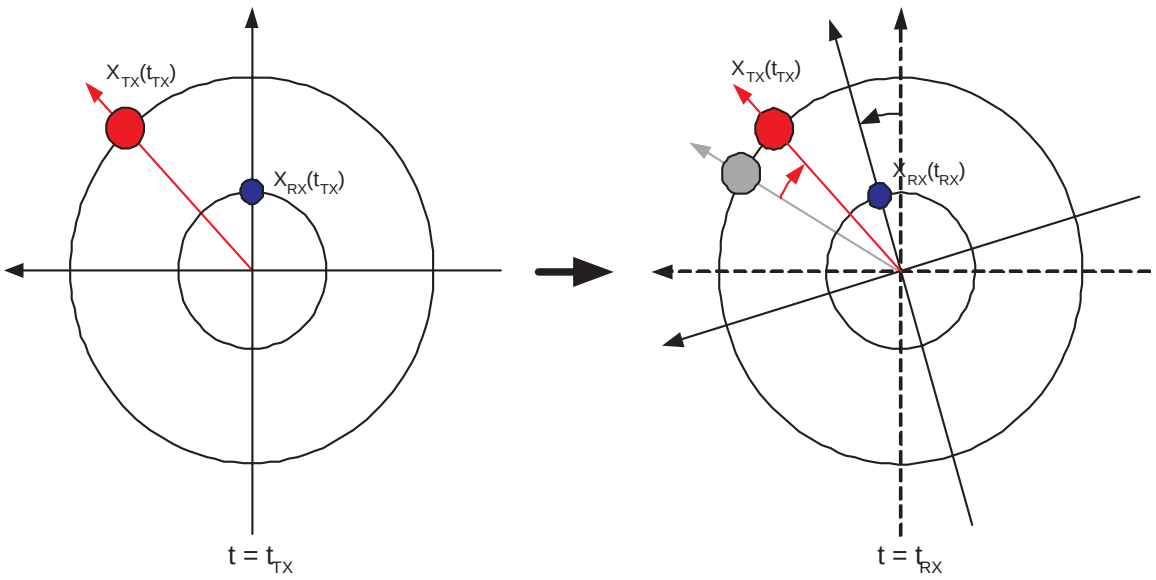

Figure A.1: Earth rotation during GPS signal travel time from satellite to user

correction model parameters. With corrected transmission time, satellite position can be calculated after compensating for Earth's rotation:

1. Reconstructing transmission time, $\tilde{t}_{TX} = \tilde{t}_{RX} - \tilde{\rho}$.
2. Calculating transmitter clock bias, $\hat{B}_{TX} = a_{f_0} + a_{f_1}(\tilde{t}_{TX} - t_{EPH}) + a_{f_0}(\tilde{t}_{TX} - t_{EPH})^2 + t_{REL} - t_{GD}$
3. Correcting transmission time, $\hat{t}_{TX} = \tilde{t}_{TX} - \hat{B}_{TX}$.
4. Calculating satellite position, $\hat{X}_{TX} = \hat{X}_{TX}(\hat{t}_{TX})$.
5. Considering Earth rotation, $\hat{X}_{TX,\theta} = R_\theta \hat{X}_{TX}$.

where

$$R_\theta = \begin{bmatrix} 1 & -\theta & 0 \\ \theta & 1 & 0 \\ 0 & 0 & 1 \end{bmatrix} \tag{A.7}$$

A.2 Dataless Estimation of Satellite Position

In urban or indoor areas, satellite signals often become very weak and cannot be received continuously. It is then difficult to parse GPS data and consequently the transmission time embedded in it. Due to the lack of transmission time, a pseudorange cannot be calculated because we only have reception time but not transmission time. However, if we use *a priori* knowledge of user position, $\tilde{X}_{RX}$, and the periodicity of the GPS PRN code with a 1 ms period, the pseudorange can be estimated under certain conditions. Because GPS data is not parsed at all, the scheme is called "Dataless Positioning."

A.2.1 Restoration of Pseudorange

In Equation (A.8), if the modulo 1 ms operation is taken on the left side, the transmission time can be removed because it only repeats every 1 ms. Then, the modulo 1 ms pseudorange, ρ_{mod}, becomes equal to the modulo 1 ms reception time, $\tilde{t}_{RX,mod}$.

$$\rho = \tilde{t}_{RX} - t_{TX} \rightarrow \rho_{mod} = \tilde{t}_{RX,mod} \tag{A.8}$$

Then, we only need to recover the integer part of the pseudorange, i.e., a multiple of ms, K, to restore the whole pseudorange, ρ. For simplicity, we assume the user clock bias to be zero. If the pre-known user position is within 150 km, equivalent to 0.5 ms from the current user position, i.e., $|\tilde{X}_{RX} - X_{RX}| < 150$ km, then the range from $\tilde{X}_{RX}$ and the range from X_{RX} are also within 150 km, i.e., $|\tilde{\rho} - r| < 0.5$ ms and K can be estimated from $\tilde{r}$ and ρ_{mod} in Equation (A.9).

$$\hat{K} = round(\hat{r} - \rho_{mod}) \tag{A.9}$$

Now, the pseudorange can be restored from $\hat{K}$ and ρ_{mod}.

$$\hat{\rho} = \rho_{mod} + \hat{K} \text{ [ms]} \tag{A.10}$$

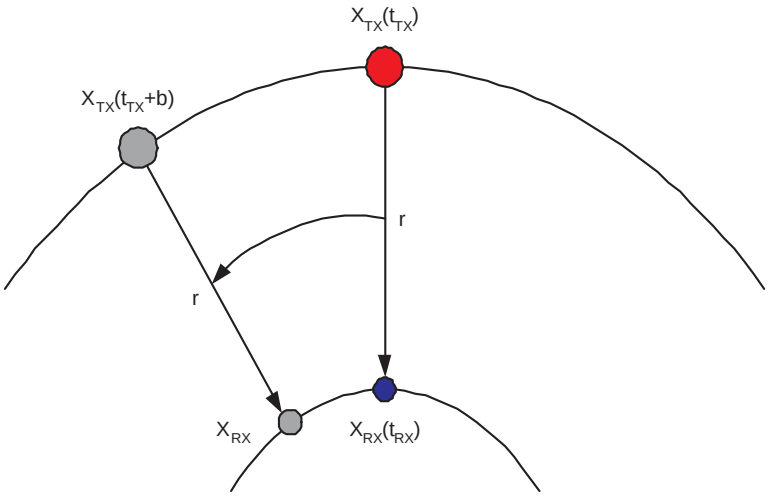

Figure A.2: Propagation of user clock bias to estimated satellite position and user position

A.2.2 User Clock Bias and Position Estimation Error

In the previous section, we assume that the user clock bias is zero but when it is not zero it causes error in the restoration of pseudoranges. Basically, the restoration process can only estimate the range, r, not the pseudorange, ρ, which contains the user clock bias, b. Thus, the pseudorange estimate, $\hat{\rho}$, in the previous section should have been called the range estimate, $\hat{r}$. Then, because it does not contain the user clock bias, the user clock bias is effectively delivered to the estimated transmission time in Equation (A.11).

$$\begin{aligned} \hat{t}_{TX} &= \tilde{t}_{RX} - \hat{r} \\ &= t_{TX} + b + (r - \hat{r}) \\ &\approx t_{TX} + b \text{ (if } \hat{r} \approx r) \end{aligned} \tag{A.11}$$

The error in the estimated transmission time is mostly generated by the user clock bias and it propagates to the satellite position estimation (see Figure A.2) and eventually

to the estimated user position.

$$\hat{t}_{TX} = t_{TX} + b \rightarrow \hat{X}_{TX}(t_{TX} + b) \rightarrow \hat{X}_{RX} \tag{A.12}$$

The error propagated to the user position is not directly proportional to the user clock bias because the satellites move in different directions and thus the errors in the satellite positions can nullify one another or accumulate depending on the satellite geometry.

A.3 Network-Aided Dataless Positioning

"Dataless Positioning" experiences positioning errors originating from the user clock bias, unless the clock bias is zero. Thus, reduction of the user clock bias is important for improvement of positioning accuracy. The reduction can be achieved via time synchronization between a receiver and a network. This is called "Network-Aided Dataless Positioning."

A.3.1 Network-Aided Time Synchronization

When a receiver is in contact with a network, there is a certain level of time synchronization between a user receiver and a base station transmitter at the network. Usually the clock at the base station is more accurate than the cheap user clock and is often synchronized to GPS time via an installed GPS receiver (for example, CDMA systems). The accurate timing and also frequency in a base station can be delivered to a user device for reduction of time and frequency biases. In general, a synchronized network such as a CDMA cellular system provides better timing accuracy than an asynchronous network such as a GSM system.

Time synchronization can be established through bi-directional communication between a receiver and a network time source. For higher accuracy, multiple transactions of time stamps are recommended to reduce error from network jitter and

latency.

$$\text{Network} \overset{\text{accurate time}}{\underset{\text{corrected time}}{\rightleftharpoons}} \text{Receiver}$$

Although uni-directional time transfer is feasible, it cannot provide timing accuracy sufficient for positioning purposes. While cellular systems use internal protocols to provide timing to users, in computer networks, the network time protocol (NTP) is most widely used [79], [80].

Even after the network-aided time synchronization, there is remaining timing error due to network jitter and latency which we assume to be bounded by a certain value, β. The bound, β, can be calculated based on the physical specification of a clock and the accuracy of network time transfer,

$$|b| < \beta \tag{A.13}$$

where β is the maximum clock bias. If other sources of range error are negligible compared to the clock bias, the difference between pseudorange, ρ, and range, r, is also bounded by β,

$$|\rho - r| < \beta. \tag{A.14}$$

A.3.2 Bounds on Range and Position Estimate by Cell-ID

Approximate user location is known when a user is in contact with a cellular network which is divided into multiple cells within specific areas. This is called the "Cell-ID" method and could provide a position estimate according to a cell size. Normally the cell size is much smaller than 100 km (a few kilometers in urban areas). This rough estimate of a user location can be used to bound a range estimation error. Usually for high elevation satellites, range estimation error is negligible compared to position estimation error. However, for low elevation satellites, range estimation error could

approach position estimation error.

$$|\hat{X}_{RX} - X_{RX}| < \alpha \rightarrow |\hat{r} - r| < \alpha \tag{A.15}$$

where X_{RX} is the user location, $\hat{X}_{RX}$ is the estimated user location, and α is the maximum position estimation error equivalent to the radius of a cell. $\hat{r}$ is the estimated range which is the range between a satellite and an estimated user location, $\hat{X}_{RX}$.

A.3.3 Pseudorange and Range Estimate

The bounds on the differences among range and pseudorange, and the range estimate, $\hat{r}$, are given in Equation (A.14) and (A.15). Based on these bounds, a bound on the difference between pseudorange and a range estimate, $\hat{r}$, can also be obtained.

$$|\rho - \hat{r}| < \alpha + \beta \tag{A.16}$$

where the range estimate, $\hat{r}$, is estimated from a Cell-ID and α and β are set by the specifications of a network and a receiver timing accuracy. The pseudorange is the only measured value and now is bounded by Equation (A.16). For example, we can assume α and β are 0.25 ms and then $|\rho - \hat{r}| < 0.5$ ms. Thus, ρ and $\hat{r}$ should be within 0.5 ms and even if we only have a modulo 1 ms pseudorange it can be restored to the whole pseudorange.

In the general case with specific α and β, we can restore the pseudorange in modulo M. For example, α and β are 0.4 ms and then $M = 2$.

$$M = ceil[2(\alpha + \beta)] \tag{A.17}$$

Then we can send the pseudorange in modulo 2 ms since there is no need to deliver the part of the pseudorange which can be estimated based on the rough user position. However, we should send the part of the pseudorange which cannot be recovered because of the uncertainty in the clock bias and the user position estimate. Those

uncertainties are represented by α and β.

A.3.4 Resolving Integer Ambiguity in Modulo M ms Pseudorange

A modulo M millisecond pseudorange is given as follows,

$$\rho_{mod} = \rho - K\,M \text{ [ms]} \tag{A.18}$$

where $0 \leq \rho_{mod} < M$ ms by definition. K is the integer part of the pseudorange divided by M ms, i.e., $K = floor(\rho/M)$. For example, if $M = 1$ (1 ms corresponds to 300 km) and $r = 20,000$ km (distance from a GPS satellite and a ground user), K is approximately 67 (20,000 km divided by 300 km). If the clock bias and the user location are bounded, $|\rho - \hat{r}| < \alpha + \beta$, K can be computed from the modulo pseudorange, ρ_{mod}, and the range estimate, $\hat{r}$.

$$\hat{K} = round(\frac{\hat{r} - \rho_{mod}}{M}) \tag{A.19}$$

where there is only one possible integer, $\hat{K}$, because of the bound in Equation (A.16) and the definition of M in Equation (A.17) which makes $K - 0.5 < \frac{\hat{r}-\rho_{mod}}{M} < K + 0.5$.

However, if the clock bias or the pre-known user location exceeds the expected bounds ($|\alpha + \beta| \geq 0.5$ ms), there could be an error in the restored pseudorange.

$$K - \alpha - \beta < \hat{K} < K + \alpha + \beta \rightarrow |K_b| \leq round(|\alpha + \beta|) \tag{A.20}$$

where K_b = integer error in restored pseudorange = $K - \hat{K}$. The integer error in the estimated pseudorange is then delivered to the estimated transmission time in Equation (A.21).

$$\begin{aligned} \hat{t}_{TX} &= \tilde{t}_{RX} - \hat{\rho} \\ &= t_{TX} + \rho - (\rho - K_b) \\ &= t_{TX} + K_b \end{aligned} \tag{A.21}$$

which affects the satellite position estimation and eventually the estimated user position.

$$\hat{t}_{TX} = t_{TX} + K_b \rightarrow \hat{X}_{TX}(t_{TX} + K_b) \rightarrow \hat{X}_{RX} \tag{A.22}$$

This is a similar result to that of the "Dataless Positioning". However, here the error term, K_b, is still bounded by α and β. For example, if α and β are 0.4 ms, then $K_b \in \{-1, 0, 1\}$. The subsequent maximum error in the estimated satellite position is 4 m and the error in the user position is expected to be much less than 4 m.

A.3.5 Implementation

The pseudorange in the modulo M ms format can be found from the reception time. The integer part of the pseudorange can then be estimated based on the user position estimate given by a Cell-ID. The estimation error in the integer part depends on the accuracy of time synchronization and the cell-size. A smaller cell size and more accurate time synchronization can guarantee less error in the integer resolving.

1. Retrieving the modulo M millisecond pseudorange, $\rho_{mod} = mod(\tilde{t}_{RX})_{M\text{ms}}$.
2. Range estimate, $\hat{r}$, based on the base station location.
3. Resolving the integer part of the pseudorange, $\hat{K} = round(\frac{\hat{r}-\rho_{mod}}{M})$.
4. Restoring pseudorange, $\hat{\rho} = \rho_{mod} + \hat{K}M$ ms.

This procedure is to be done for each satellite used for positioning.

Appendix B

TOA and TDOA in Asynchronous Networks

This section extends the proof of equivalence of TOA and TDOA in a single transmitter network to a combination of multiple networks. In other words, we are going to confirm that we can choose either TOA or TDOA methods regardless of whether ranging sources come from a single network or from multiple heterogeneous networks. "Asynchronously integrated networks" include the hybrid GPS and TV positioning system where GPS and TV networks are not synchronized to each other and contain separate clock biases.

Two sets of pseudorange measurements from two separate systems, System A and B, can be represented in the various combinations of the TOA and TDOA formats. These sets can be both in the TOA format, containing two unknown common receiver clock biases, b_A and b_B as in Equation (B.1), or in the TDOA format with no clock bias as in Equation (B.3). Alternately, one set is in the TOA format, while the other set is in the TDOA format, a hybrid of TOA and TDOA as in Equation (B.2). These

combinations are denoted as "TOA+TOA," "TOA+TDOA," and "TDOA+TDOA:"

$$\boldsymbol{W}\delta\boldsymbol{\rho} = \boldsymbol{W}\boldsymbol{G}\delta\boldsymbol{x} + \boldsymbol{W}\boldsymbol{v} \tag{B.1}$$

$$\boldsymbol{W}_{\mathrm{H}}\boldsymbol{H}\delta\boldsymbol{\rho} = \boldsymbol{W}_{\mathrm{H}}\boldsymbol{H}\boldsymbol{G}_{\mathrm{H}}\delta\boldsymbol{x}_{\mathrm{H}} + \boldsymbol{W}_{\mathrm{H}}\boldsymbol{H}\boldsymbol{v} \tag{B.2}$$

$$\boldsymbol{W}_{\mathrm{D}}\boldsymbol{D}\delta\boldsymbol{\rho} = \boldsymbol{W}_{\mathrm{D}}\boldsymbol{D}\boldsymbol{G}_{\mathrm{D}}\delta\boldsymbol{u} + \boldsymbol{W}_{\mathrm{D}}\boldsymbol{D}\boldsymbol{v} \tag{B.3}$$

where n_A and n_B transmitters are assumed for System A and System B, respectively. $\delta\boldsymbol{\rho} = [\delta\boldsymbol{\rho}_A^T, \delta\boldsymbol{\rho}_B^T]^T$, $\delta\boldsymbol{x} = [\delta\boldsymbol{u}^T, \delta b_A, \delta b_B]^T$, $\delta\boldsymbol{x}_{\mathrm{H}} = [\delta\boldsymbol{u}^T, \delta b_A]^T$, and $\boldsymbol{v} = [\boldsymbol{v}_A^T, \boldsymbol{v}_B^T]^T$. The geometry matrices are

$$\boldsymbol{G} = \begin{bmatrix} \boldsymbol{G}_{\mathrm{D}}^A & \mathbf{1} & \mathbf{0} \\ \boldsymbol{G}_{\mathrm{D}}^B & \mathbf{0} & \mathbf{1} \end{bmatrix} = \begin{bmatrix} \boldsymbol{G}_{\mathrm{D}} & \boldsymbol{E}_A & \boldsymbol{E}_B \end{bmatrix} = \begin{bmatrix} \boldsymbol{G}_{\mathrm{D}} & \boldsymbol{E} \end{bmatrix}$$

$$\boldsymbol{G}_{\mathrm{H}} = \begin{bmatrix} \boldsymbol{G}_{\mathrm{D}}^A & \mathbf{1} \\ \boldsymbol{G}_{\mathrm{D}}^B & \mathbf{0} \end{bmatrix} = \begin{bmatrix} \boldsymbol{G}_{\mathrm{D}} & \boldsymbol{E}_A \end{bmatrix}$$

$$\boldsymbol{G}_{\mathrm{D}} = \begin{bmatrix} \boldsymbol{G}_{\mathrm{D}}^A \\ \boldsymbol{G}_{\mathrm{D}}^B \end{bmatrix}$$

and the differencing matrices are:

$$\boldsymbol{H} = \begin{bmatrix} \boldsymbol{I} & \mathbf{0} \\ \mathbf{0} & \boldsymbol{D}_B \end{bmatrix} \text{ and } \boldsymbol{D} = \begin{bmatrix} \boldsymbol{D}_A & \mathbf{0} \\ \mathbf{0} & \boldsymbol{D}_B \end{bmatrix}$$

where $\boldsymbol{D}_A = [\boldsymbol{I}_{(n_A-1)\times(n_A-1)}, -\mathbf{1}_{(n_A-1)\times 1}]$ and $\boldsymbol{D}_B = [\boldsymbol{I}_{(n_B-1)\times(n_B-1)}, -\mathbf{1}_{(n_B-1)\times 1}]$, assuming that the last pseudoranges of each set of measurements have the smallest variance, without loss of generality. The weighting matrix, $\boldsymbol{W}$, is an $(n_A+n_B)\times(n_A+n_B)$ matrix for the TOA+TOA case, $\boldsymbol{W}_{\mathrm{H}}$ is an $(n_A+n_B-1)\times(n_A+n_B-1)$ matrix for the TOA+TDOA case, and $\boldsymbol{W}_{\mathrm{D}}$ is an $(n_A+n_B-2)\times(n_A+n_B-2)$ matrix for the TDOA+TDOA case.

The WLS solutions for Equation (B.1), (B.2), and (B.3) are given as follows, supposing measurement noise, $\boldsymbol{v}$, with a zero mean and a known covariance, $\boldsymbol{\Sigma}_{\boldsymbol{v}}$, where $\boldsymbol{v}_A$ and $\boldsymbol{v}_B$ are uncorrelated and thus, $\boldsymbol{\Sigma}_{\boldsymbol{v}} = diag(\boldsymbol{\Sigma}_{\boldsymbol{v}_A}, \boldsymbol{\Sigma}_{\boldsymbol{v}_B})$. The user variables are $\boldsymbol{\theta} = \delta\boldsymbol{x}$ for the TOA+TOA case, $\boldsymbol{\theta}_{\mathrm{H}} = \delta\boldsymbol{x}_{\mathrm{H}}$ for the TOA+TDOA case, and $\boldsymbol{\theta}_{\mathrm{D}} = \delta\boldsymbol{u}$

for the TDOA+TDOA case:

$$\begin{aligned}
\hat{\boldsymbol{\theta}}_{\text{TOA+TOA}} =& (\boldsymbol{W}\boldsymbol{G})^{\dagger}\boldsymbol{W}\delta\boldsymbol{\rho} \\
=& (\boldsymbol{G}^T\boldsymbol{\Sigma}_{\boldsymbol{v}}^{-1}\boldsymbol{G})^{-1}\boldsymbol{G}^T\boldsymbol{\Sigma}_{\boldsymbol{v}}^{-1}\delta\boldsymbol{\rho} \qquad \text{(B.4)} \\
\hat{\boldsymbol{\theta}}_{\text{H,TOA+TDOA}} =& (\boldsymbol{W}_{\text{H}}\boldsymbol{H}\boldsymbol{G}_{\text{H}})^{\dagger}\boldsymbol{W}_{\text{H}}\boldsymbol{H}\delta\boldsymbol{\rho} \\
=& [\boldsymbol{G}_{\text{H}}^T\boldsymbol{H}^T(\boldsymbol{H}\boldsymbol{\Sigma}_{\boldsymbol{v}}\boldsymbol{H}^T)^{-1}\boldsymbol{H}\boldsymbol{G}_{\text{H}}]^{-1} \\
& \times \boldsymbol{G}_{\text{H}}^T\boldsymbol{H}^T(\boldsymbol{H}\boldsymbol{\Sigma}_{\boldsymbol{v}}\boldsymbol{H}^T)^{-1}\boldsymbol{H}\delta\boldsymbol{\rho} \qquad \text{(B.5)} \\
\hat{\boldsymbol{\theta}}_{\text{D,TDOA+TDOA}} =& (\boldsymbol{W}_{\text{D}}\boldsymbol{D}\boldsymbol{G}_{\text{D}})^{\dagger}\boldsymbol{W}_{\text{D}}\boldsymbol{D}\delta\boldsymbol{\rho} \\
=& [\boldsymbol{G}_{\text{D}}^T\boldsymbol{D}^T(\boldsymbol{D}\boldsymbol{\Sigma}_{\boldsymbol{v}}\boldsymbol{D}^T)^{-1}\boldsymbol{D}\boldsymbol{G}_{\text{D}}]^{-1} \\
& \times \boldsymbol{G}_{\text{D}}^T\boldsymbol{D}^T(\boldsymbol{D}\boldsymbol{\Sigma}_{\boldsymbol{v}}\boldsymbol{D}^T)^{-1}\boldsymbol{D}\delta\boldsymbol{\rho} \qquad \text{(B.6)}
\end{aligned}$$

where $\boldsymbol{\Sigma}_{\boldsymbol{v}}$, $\boldsymbol{G}$, $\boldsymbol{G}_{\text{H}}$, and $\boldsymbol{G}_{\text{D}}$ are assumed to be full rank. The optimal weighting matrices are:

$$\boldsymbol{W}^* = \boldsymbol{\Sigma}_{\boldsymbol{v}}^{-1/2} \qquad \text{(B.7)}$$

$$\boldsymbol{W}_{\text{H}}^* = (\boldsymbol{H}\boldsymbol{\Sigma}_{\boldsymbol{v}}\boldsymbol{H}^T)^{-1/2} \qquad \text{(B.8)}$$

$$\boldsymbol{W}_{\text{D}}^* = (\boldsymbol{D}\boldsymbol{\Sigma}_{\boldsymbol{v}}\boldsymbol{D}^T)^{-1/2} \qquad \text{(B.9)}$$

The variances of the estimated user variables can be calculated accordingly.

$$\boldsymbol{\Sigma}_{\hat{\boldsymbol{\theta}}_{\text{TOA+TOA}}} = (\boldsymbol{G}^T\boldsymbol{\Sigma}_{\boldsymbol{v}}^{-1}\boldsymbol{G})^{-1} \qquad \text{(B.10)}$$

$$\boldsymbol{\Sigma}_{\hat{\boldsymbol{\theta}}_{\text{H,TOA+TDOA}}} = [\boldsymbol{G}_{\text{H}}^T\boldsymbol{H}^T(\boldsymbol{H}\boldsymbol{\Sigma}_{\boldsymbol{v}}\boldsymbol{H}^T)^{-1}\boldsymbol{H}\boldsymbol{G}_{\text{H}}]^{-1} \qquad \text{(B.11)}$$

$$\boldsymbol{\Sigma}_{\hat{\boldsymbol{\theta}}_{\text{D,TDOA+TDOA}}} = [\boldsymbol{G}_{\text{D}}^T\boldsymbol{D}^T(\boldsymbol{D}\boldsymbol{\Sigma}_{\boldsymbol{v}}\boldsymbol{D}^T)^{-1}\boldsymbol{D}\boldsymbol{G}_{\text{D}}]^{-1} \qquad \text{(B.12)}$$

We prove that position estimates from measurements in the TOA+TOA format, the TOA+TDOA format, and the TDOA+TDOA format are all equal,

$$\boxed{\hat{\boldsymbol{\theta}}_{\text{D,TOA+TOA}} \equiv \hat{\boldsymbol{\theta}}_{\text{D,TOA+TDOA}} \equiv \hat{\boldsymbol{\theta}}_{\text{D,TDOA+TDOA}}}$$

as well as their position variances,

$$\boxed{\boldsymbol{\Sigma}_{\hat{\boldsymbol{\theta}}_{\text{D,TOA+TOA}}} \equiv \boldsymbol{\Sigma}_{\hat{\boldsymbol{\theta}}_{\text{D,TOA+TDOA}}} \equiv \boldsymbol{\Sigma}_{\hat{\boldsymbol{\theta}}_{\text{D,TDOA+TDOA}}}}$$

for any noise distribution $\boldsymbol{\Sigma_v}$.

First, the equivalence between TOA+TOA and TDOA+TDOA is to be proved, with their covariance matrices derived from Equation (B.10) and (B.12). For a fair comparison, the covariance matrix for only position variables, $\boldsymbol{\Sigma}_{\hat{\boldsymbol{\theta}}_{\mathrm{D}}}$, needs to be obtained, having removed the clock biases related terms.

$$\begin{aligned}\boldsymbol{\Sigma}_{\hat{\boldsymbol{\theta}},\mathrm{TOA+TOA}} &= (\boldsymbol{G}^T\boldsymbol{\Sigma}_{\boldsymbol{v}}^{-1}\boldsymbol{G})^{-1} \\ &= \begin{bmatrix} \boldsymbol{G}_{\mathrm{D}}^T\boldsymbol{\Sigma}_{\boldsymbol{v}}^{-1}\boldsymbol{G}_{\mathrm{D}} & \boldsymbol{G}_{\mathrm{D}}^T\boldsymbol{\Sigma}_{\boldsymbol{v}}^{-1}\boldsymbol{E} \\ \boldsymbol{E}^T\boldsymbol{\Sigma}_{\boldsymbol{v}}^{-1}\boldsymbol{G}_{\mathrm{D}} & \boldsymbol{E}^T\boldsymbol{\Sigma}_{\boldsymbol{v}}^{-1}\boldsymbol{E} \end{bmatrix}^{-1} \\ &= \begin{bmatrix} \boldsymbol{\Sigma}_{\mathrm{D},11} & \boldsymbol{\Sigma}_{\mathrm{D},12} \\ \boldsymbol{\Sigma}_{\mathrm{D},21} & \boldsymbol{\Sigma}_{\mathrm{D},22} \end{bmatrix}\end{aligned} \tag{B.13}$$

The submatrices of $\boldsymbol{\Sigma}_{\hat{\boldsymbol{\theta}},\mathrm{TOA+TOA}}$ are given as

$$\begin{aligned}&\boldsymbol{\Sigma}_{\mathrm{D},11} \\ &= \left[\boldsymbol{G}_{\mathrm{D}}^T\boldsymbol{\Sigma}_{\boldsymbol{v}}^{-1}\boldsymbol{G}_{\mathrm{D}} - \boldsymbol{G}_{\mathrm{D}}^T\boldsymbol{\Sigma}_{\boldsymbol{v}}^{-1}\boldsymbol{E}(\boldsymbol{E}^T\boldsymbol{\Sigma}_{\boldsymbol{v}}^{-1}\boldsymbol{E})^{-1}\boldsymbol{E}^T\boldsymbol{\Sigma}_{\boldsymbol{v}}^{-1}\boldsymbol{G}_{\mathrm{D}}\right]^{-1} \\ &= \left\{\boldsymbol{G}_{\mathrm{D}}^T\left[\boldsymbol{\Sigma}_{\boldsymbol{v}}^{-1} - \boldsymbol{\Sigma}_{\boldsymbol{v}}^{-1}\boldsymbol{E}(\boldsymbol{E}^T\boldsymbol{\Sigma}_{\boldsymbol{v}}^{-1}\boldsymbol{E})^{-1}\boldsymbol{E}^T\boldsymbol{\Sigma}_{\boldsymbol{v}}^{-1}\right]\boldsymbol{G}_{\mathrm{D}}\right\}^{-1} \\ &= \left\{\boldsymbol{G}_{\mathrm{D}}^T\begin{bmatrix}\boldsymbol{P}_A & \boldsymbol{0} \\ \boldsymbol{0} & \boldsymbol{P}_B\end{bmatrix}\boldsymbol{G}_{\mathrm{D}}\right\}^{-1} \\ &= (\boldsymbol{G}_{\mathrm{D}}^T\boldsymbol{P}_{\mathrm{D}}\boldsymbol{G}_{\mathrm{D}})^{-1} = \boldsymbol{\Sigma}_{\hat{\boldsymbol{\theta}}_{\mathrm{D}},\mathrm{TOA+TOA}}\end{aligned} \tag{B.14}$$

$$\boldsymbol{\Sigma}_{\mathrm{D},12} = -\boldsymbol{\Sigma}_{\mathrm{D},11}\boldsymbol{G}_{\mathrm{D}}^T\boldsymbol{\Sigma}_{\boldsymbol{v}}^{-1}\boldsymbol{E}(\boldsymbol{E}^T\boldsymbol{\Sigma}_{\boldsymbol{v}}^{-1}\boldsymbol{E})^{-1} = \boldsymbol{\Sigma}_{\mathrm{D},21}^T \tag{B.15}$$

$$\begin{aligned}\boldsymbol{\Sigma}_{\mathrm{D},22} &= (\boldsymbol{E}^T\boldsymbol{\Sigma}_{\boldsymbol{v}}^{-1}\boldsymbol{E})^{-1} + (\boldsymbol{E}^T\boldsymbol{\Sigma}_{\boldsymbol{v}}^{-1}\boldsymbol{E})^{-1}\boldsymbol{E}^T\boldsymbol{\Sigma}_{\boldsymbol{v}}^{-1}\boldsymbol{G}_{\mathrm{D}} \\ &\times \boldsymbol{\Sigma}_{\mathrm{D},11}\boldsymbol{G}_{\mathrm{D}}^T\boldsymbol{\Sigma}_{\boldsymbol{v}}^{-1}\boldsymbol{E}(\boldsymbol{E}^T\boldsymbol{\Sigma}_{\boldsymbol{v}}^{-1}\boldsymbol{E})^{-1}\end{aligned} \tag{B.16}$$

where $\boldsymbol{P}_{\mathrm{D}} = diag(\boldsymbol{P}_A, \boldsymbol{P}_B)$, $\boldsymbol{P}_A = \boldsymbol{\Sigma}_{\boldsymbol{v}_A}^{-1} - \frac{\boldsymbol{\Sigma}_{\boldsymbol{v}_A}^{-1}\boldsymbol{1}\boldsymbol{1}^T\boldsymbol{\Sigma}_{\boldsymbol{v}_A}^{-1}}{\boldsymbol{1}^T\boldsymbol{\Sigma}_{\boldsymbol{v}_A}^{-1}\boldsymbol{1}}$, and $\boldsymbol{P}_B = \boldsymbol{\Sigma}_{\boldsymbol{v}_B}^{-1} - \frac{\boldsymbol{\Sigma}_{\boldsymbol{v}_B}^{-1}\boldsymbol{1}\boldsymbol{1}^T\boldsymbol{\Sigma}_{\boldsymbol{v}_B}^{-1}}{\boldsymbol{1}^T\boldsymbol{\Sigma}_{\boldsymbol{v}_B}^{-1}\boldsymbol{1}}$. Because $\boldsymbol{E}$ is orthogonal to $\boldsymbol{D}$, $\boldsymbol{P}_{\mathrm{D}} = \boldsymbol{D}^T(\boldsymbol{D}\boldsymbol{\Sigma}_{\boldsymbol{v}}\boldsymbol{D}^T)^{-1}\boldsymbol{D}$ as shown in Section 5.1. $\boldsymbol{\Sigma}_{\mathrm{D},11}$ is the error covariance matrix corresponding to $\boldsymbol{\theta}_{\mathrm{D}}$ for the TOA+TOA method,

equal to that of the TDOA+TDOA method, $\boldsymbol{\Sigma}_{\hat{\boldsymbol{\theta}}_{\mathrm{D}},\mathrm{TDOA+TDOA}}$.

$$\begin{aligned}\boldsymbol{\Sigma}_{\hat{\boldsymbol{\theta}}_{\mathrm{D}},\mathrm{TDOA+TDOA}} &= \left[\boldsymbol{G}_{\mathrm{D}}^{T}\boldsymbol{D}^{T}(\boldsymbol{D}\boldsymbol{\Sigma}_{\boldsymbol{v}}\boldsymbol{D}^{T})^{-1}\boldsymbol{D}\boldsymbol{G}_{\mathrm{D}}\right]^{-1} \\ &= (\boldsymbol{G}_{\mathrm{D}}^{T}\boldsymbol{P}_{\mathrm{D}}\boldsymbol{G}_{\mathrm{D}})^{-1} \\ &= \boldsymbol{\Sigma}_{\hat{\boldsymbol{\theta}}_{\mathrm{D}},\mathrm{TOA+TOA}} \end{aligned} \tag{B.17}$$

This proves the equivalence of the position variances of TOA+TOA and TDOA+ TDOA. Their position solutions are given in Equation (B.4) and (B.6).

$$\begin{aligned}\hat{\boldsymbol{\theta}}_{\mathrm{TOA+TOA}} &= (\boldsymbol{G}^{T}\boldsymbol{\Sigma}_{\boldsymbol{v}}^{-1}\boldsymbol{G})^{-1}\boldsymbol{G}^{T}\boldsymbol{\Sigma}_{\boldsymbol{v}}^{-1}\delta\boldsymbol{\rho} \\ &= \begin{bmatrix}\boldsymbol{\Sigma}_{\mathrm{D},11} & \boldsymbol{\Sigma}_{\mathrm{D},12} \\ \boldsymbol{\Sigma}_{\mathrm{D},21} & \boldsymbol{\Sigma}_{\mathrm{D},22}\end{bmatrix}\begin{bmatrix}\boldsymbol{G}_{\mathrm{D}}^{T} \\ \boldsymbol{E}^{T}\end{bmatrix}\boldsymbol{\Sigma}_{\boldsymbol{v}}^{-1}\delta\boldsymbol{\rho} \end{aligned} \tag{B.18}$$

Again, only the elements of the TOA+TOA solution related to $\boldsymbol{\theta}_{\mathrm{D}}$ is concerned here. $\boldsymbol{\Sigma}_{\mathrm{D},11}$ and $\boldsymbol{\Sigma}_{\mathrm{D},12}$ are given in Equation (B.14) and (B.15).

$$\begin{aligned}&\hat{\boldsymbol{\theta}}_{\mathrm{D,TOA+TOA}} \\ &= (\boldsymbol{\Sigma}_{\mathrm{D},11}\boldsymbol{G}_{\mathrm{D}}^{T} + \boldsymbol{\Sigma}_{\mathrm{D},12}\boldsymbol{E}^{T})\boldsymbol{\Sigma}_{\boldsymbol{v}}^{-1}\delta\boldsymbol{\rho} \\ &= (\boldsymbol{G}_{\mathrm{D}}^{T}\boldsymbol{P}_{\mathrm{D}}\boldsymbol{G}_{\mathrm{D}})^{-1}\boldsymbol{G}_{\mathrm{D}}^{T} \\ &\times \left[\boldsymbol{\Sigma}_{\boldsymbol{v}}^{-1} - \boldsymbol{\Sigma}_{\boldsymbol{v}}^{-1}\boldsymbol{E}(\boldsymbol{E}^{T}\boldsymbol{\Sigma}_{\boldsymbol{v}}^{-1}\boldsymbol{E})^{-1}\boldsymbol{E}^{T}\boldsymbol{\Sigma}_{\boldsymbol{v}}^{-1}\right]\delta\boldsymbol{\rho} \\ &= (\boldsymbol{G}_{\mathrm{D}}^{T}\boldsymbol{P}_{\mathrm{D}}\boldsymbol{G}_{\mathrm{D}})^{-1}\boldsymbol{G}_{\mathrm{D}}^{T}\boldsymbol{P}_{\mathrm{D}}\delta\boldsymbol{\rho} \end{aligned} \tag{B.19}$$

$$= \hat{\boldsymbol{\theta}}_{\mathrm{D,TDOA+TDOA}} \tag{B.20}$$

which proves the equivalence of the position solutions of TOA+TOA and TDOA+ TDOA.

Second, we prove the equivalence of TOA+TDOA and TDOA+TDOA. Their

covariance matrices can be derived from Equation (B.11) and (B.12).

$$\begin{aligned}
\boldsymbol{\Sigma}_{\hat{\boldsymbol{\theta}}_{\mathrm{D}},\mathrm{TOA+TDOA}} &= [\boldsymbol{G}_{\mathrm{H}}^T \boldsymbol{H}^T (\boldsymbol{H}\boldsymbol{\Sigma}_{\boldsymbol{v}}\boldsymbol{H}^T)^{-1}\boldsymbol{H}\boldsymbol{G}_{\mathrm{H}}]^{-1} \\
&= (\boldsymbol{G}_{\mathrm{H}}^T \boldsymbol{P}_{\mathrm{H}} \boldsymbol{G}_{\mathrm{H}})^{-1} \\
&= \begin{bmatrix} \boldsymbol{G}_{\mathrm{D}}^T \boldsymbol{P}_{\mathrm{H}} \boldsymbol{G}_{\mathrm{D}} & \boldsymbol{G}_{\mathrm{D}}^T \boldsymbol{P}_{\mathrm{H}} \boldsymbol{E}_A \\ \boldsymbol{E}_A^T \boldsymbol{P}_{\mathrm{H}} \boldsymbol{G}_{\mathrm{D}} & \boldsymbol{E}_A^T \boldsymbol{P}_{\mathrm{H}} \boldsymbol{E}_A \end{bmatrix}^{-1} \\
&= \begin{bmatrix} \boldsymbol{\Sigma}_{\mathrm{H},11} & \boldsymbol{\Sigma}_{\mathrm{H},12} \\ \boldsymbol{\Sigma}_{\mathrm{H},21} & \boldsymbol{\Sigma}_{\mathrm{H},22} \end{bmatrix}
\end{aligned} \tag{B.21}$$

where

$$\begin{aligned}
\boldsymbol{P}_{\mathrm{H}} &= \begin{bmatrix} \boldsymbol{\Sigma}_{\boldsymbol{v}_A}^{-1} & \boldsymbol{0} \\ \boldsymbol{0} & \boldsymbol{P}_B \end{bmatrix} \\
&= \boldsymbol{\Sigma}_{\boldsymbol{v}}^{-1} - \boldsymbol{\Sigma}_{\boldsymbol{v}}^{-1}\boldsymbol{E}_B(\boldsymbol{E}_B^T\boldsymbol{\Sigma}_{\boldsymbol{v}}^{-1}\boldsymbol{E}_B)^{-1}\boldsymbol{E}_B^T\boldsymbol{\Sigma}_{\boldsymbol{v}}^{-1} \\
&= \boldsymbol{H}^T(\boldsymbol{H}\boldsymbol{\Sigma}_{\boldsymbol{v}}\boldsymbol{H}^T)^{-1}\boldsymbol{H}
\end{aligned} \tag{B.22}$$

because $\boldsymbol{E}_B \perp \boldsymbol{H}$. $\boldsymbol{\Sigma}_{\mathrm{H},11}$ is the error covariance matrix corresponding to $\boldsymbol{\theta}_{\mathrm{D}}$ and is equivalent to that of the TDOA+TDOA method, $\boldsymbol{\Sigma}_{\hat{\boldsymbol{\theta}}_{\mathrm{D}},\mathrm{TDOA+TDOA}}$.

$$\begin{aligned}
\boldsymbol{\Sigma}_{\mathrm{H},11} &= \boldsymbol{\Sigma}_{\hat{\boldsymbol{\theta}}_{\mathrm{D}},\mathrm{TOA+TDOA}} \\
&= \left\{\boldsymbol{G}_{\mathrm{D}}^T\left[\boldsymbol{P}_{\mathrm{H}} - \boldsymbol{P}_{\mathrm{H}}\boldsymbol{E}_A(\boldsymbol{E}_A^T\boldsymbol{P}_{\mathrm{H}}\boldsymbol{E}_A)^{-1}\boldsymbol{E}_A^T\boldsymbol{P}_{\mathrm{H}}\right]\boldsymbol{G}_{\mathrm{D}}\right\}^{-1} \\
&= \left\{\boldsymbol{G}_{\mathrm{D}}^T\left[\boldsymbol{\Sigma}_{\boldsymbol{v}}^{-1} - \boldsymbol{\Sigma}_{\boldsymbol{v}}^{-1}\boldsymbol{E}(\boldsymbol{E}^T\boldsymbol{\Sigma}_{\boldsymbol{v}}^{-1}\boldsymbol{E})^{-1}\boldsymbol{E}^T\boldsymbol{\Sigma}_{\boldsymbol{v}}^{-1}\right]\boldsymbol{G}_{\mathrm{D}}\right\}^{-1} \\
&= (\boldsymbol{G}_{\mathrm{D}}^T\boldsymbol{P}_{\mathrm{D}}\boldsymbol{G}_{\mathrm{D}})^{-1} \\
&= \boldsymbol{\Sigma}_{\hat{\boldsymbol{\theta}}_{\mathrm{D}},\mathrm{TDOA+TDOA}}
\end{aligned} \tag{B.23}$$

$$\boldsymbol{\Sigma}_{\mathrm{H},12} = -\boldsymbol{\Sigma}_{\mathrm{H},11}\boldsymbol{G}_{\mathrm{D}}^T\boldsymbol{P}_{\mathrm{H}}\boldsymbol{E}_A(\boldsymbol{E}_A^T\boldsymbol{P}_{\mathrm{H}}\boldsymbol{E}_A)^{-1} \tag{B.24}$$

Equation (B.23) proves the equivalence of the position covariances of TOA+TDOA

and TDOA +TDOA. Their position solutions are given in Equation (B.5) and (B.6).

$$\begin{aligned}\hat{\boldsymbol{\theta}}_{\mathrm{D,TOA+TDOA}} &= (\boldsymbol{\Sigma}_{\mathrm{H},11}\boldsymbol{G}_{\mathrm{D}}^{T} + \boldsymbol{\Sigma}_{\mathrm{H},12}\boldsymbol{E}_{A}^{T})\boldsymbol{P}_{\mathrm{H}}\delta\boldsymbol{\rho} \\ &= (\boldsymbol{G}_{\mathrm{D}}^{T}\boldsymbol{P}_{\mathrm{D}}\boldsymbol{G}_{\mathrm{D}})^{-1}\boldsymbol{G}_{\mathrm{D}}^{T}\boldsymbol{P}_{\mathrm{D}}\delta\boldsymbol{\rho} \\ &= \hat{\boldsymbol{\theta}}_{\mathrm{D,TDOA+TDOA}} \end{aligned} \tag{B.25}$$

which proves the equivalence of the position solutions of TOA+TDOA and TDOA+ TDOA.

Regarding $\boldsymbol{\theta}_{\mathrm{H}}$, TOA+TOA and TOA+TDOA can be shown to be equivalent

$$\boxed{\hat{\boldsymbol{\theta}}_{\mathrm{H,TOA+TOA}} \equiv \hat{\boldsymbol{\theta}}_{\mathrm{H,TOA+TDOA}}}$$

$$\boxed{\boldsymbol{\Sigma}_{\hat{\boldsymbol{\theta}}_{\mathrm{H}},\mathrm{TOA+TOA}} \equiv \boldsymbol{\Sigma}_{\hat{\boldsymbol{\theta}}_{\mathrm{H}},\mathrm{TOA+TDOA}}}$$

with similar steps to that of the proof for $\boldsymbol{\theta}_{\mathrm{D}}$.

Appendix C

Monotonic Decrease of Position Variance

In positioning, the variance of position estimates monotonically decreases as the number of range sources increases. This is particularly important when we are introducing significantly more ranging sources—in addition to the existing GPS and Glonass satellites—such as Galileo satellites and terrestrial ranging sources like television stations, WiFi transmitters, and cellular networks [4]. The pseudorange measurements from these additional sources, regardless of their quality, are always beneficial to position estimation, as long as the mean and covariance of measurement noises are known. In this paper, instead of the rather complicated existing proof [62], we present a straightforward and intuitive proof of this monotonicity, based on the negative definiteness of the difference between position variance matrices. We first divide the position variance for n ranging sources into the position variance for $n-1$ ranging sources and residual terms, and then prove the negative definiteness of the residual terms.

Assuming perfect knowledge of the covariance matrix, $\boldsymbol{\Sigma}_{\boldsymbol{v},n}$, of measurement noise, $\boldsymbol{v}$, the position variance, $\boldsymbol{\Sigma}_{\hat{\boldsymbol{\theta}},n}$, is given as follows for n ranging sources. Without loss of generality, it is assumed that $\boldsymbol{\Sigma}_{\hat{\boldsymbol{\theta}},n}$ is positive definite.

$$\boldsymbol{\Sigma}_{\hat{\boldsymbol{\theta}},n} = (\boldsymbol{G}_n^T \boldsymbol{\Sigma}_{\boldsymbol{v},n}^{-1} \boldsymbol{G}_n)^{-1} \tag{C.1}$$

where $\hat{\boldsymbol{\theta}}$ is the weighted least square estimate of user variables, $\boldsymbol{\theta}$, which are usually user position and a receiver clock bias, and $\boldsymbol{G}_n$ is the geometry matrix of transmitters. $\boldsymbol{\Sigma}_{\hat{\boldsymbol{\theta}},n}$ can be expressed as the function of the position variance for $n-1$ ranging sources, $\boldsymbol{\Sigma}_{\hat{\boldsymbol{\theta}},n-1}$, and a residual matrix, $\boldsymbol{A}$, in Equation (C.2).

$$\begin{aligned}\boldsymbol{\Sigma}_{\hat{\boldsymbol{\theta}},n} &= (\boldsymbol{G}_{n-1}^T \boldsymbol{\Sigma}_{\boldsymbol{v},n-1}^{-1} \boldsymbol{G}_{n-1} + \boldsymbol{G}_n^T \boldsymbol{A} \boldsymbol{G}_n)^{-1} \\ &= (\boldsymbol{\Sigma}_{\hat{\boldsymbol{\theta}},n-1}^{-1} + \boldsymbol{G}_n^T \boldsymbol{A} \boldsymbol{G}_n)^{-1} \qquad \text{(C.2)} \\ &= \boldsymbol{\Sigma}_{\hat{\boldsymbol{\theta}},n-1} - \boldsymbol{\Sigma}_{\hat{\boldsymbol{\theta}},n-1} \boldsymbol{G}_n^T \\ &\quad \times (\boldsymbol{A}^{-1} + \boldsymbol{G}_n \boldsymbol{\Sigma}_{\hat{\boldsymbol{\theta}},n-1} \boldsymbol{G}_n^T)^{-1} \boldsymbol{G}_n \boldsymbol{\Sigma}_{\hat{\boldsymbol{\theta}},n-1} \qquad \text{(C.3)}\end{aligned}$$

Then, by the Woodbury formula, $\boldsymbol{\Sigma}_{\hat{\boldsymbol{\theta}},n-1}$ is taken out of the inverse, and separated from the residual term, $\boldsymbol{\Sigma}_{\hat{\boldsymbol{\theta}},n-1} \boldsymbol{G}_n^T (\boldsymbol{A}^{-1} + \boldsymbol{G}_n \boldsymbol{\Sigma}_{\hat{\boldsymbol{\theta}},n-1} \boldsymbol{G}_n^T)^{-1} \boldsymbol{G}_n \boldsymbol{\Sigma}_{\hat{\boldsymbol{\theta}},n-1}$ in Equation (C.3).

Because the residual term is in a quadratic form, its positive definiteness can be determined by $(\boldsymbol{A}^{-1} + \boldsymbol{G}_n \boldsymbol{\Sigma}_{\hat{\boldsymbol{\theta}},n-1} \boldsymbol{G}_n^T)^{-1}$. First, since $\boldsymbol{\Sigma}_{\hat{\boldsymbol{\theta}},n-1}$ is positive definite, so is $\boldsymbol{G}_n \boldsymbol{\Sigma}_{\hat{\boldsymbol{\theta}},n-1} \boldsymbol{G}_n^T$. Second, because it is unknown whether or not $\boldsymbol{A} > 0$, $\boldsymbol{A}$ needs to be interpreted with the given noise covariance matrices. $\boldsymbol{A}$ is defined to be the difference between $\boldsymbol{\Sigma}_{\boldsymbol{v},n}^{-1}$ and $\boldsymbol{\Sigma}_{\boldsymbol{v},n-1}^{-1}$.

$$\boldsymbol{A} = \begin{bmatrix} \boldsymbol{A}_{11} & \boldsymbol{A}_{12} \\ \boldsymbol{A}_{21} & \boldsymbol{A}_{22} \end{bmatrix} = \boldsymbol{\Sigma}_{\boldsymbol{v},n}^{-1} - \begin{bmatrix} \boldsymbol{\Sigma}_{\boldsymbol{v},n-1}^{-1} & \boldsymbol{0} \\ \boldsymbol{0} & 0 \end{bmatrix}$$

where $\boldsymbol{\Sigma}_{\boldsymbol{v},n}^{-1}$ and $\boldsymbol{\Sigma}_{\boldsymbol{v},n-1}^{-1}$ are related such that

$$\boldsymbol{\Sigma}_{\boldsymbol{v},n} = \begin{bmatrix} \boldsymbol{\Sigma}_{\boldsymbol{v},11} & \boldsymbol{\Sigma}_{\boldsymbol{v},12} \\ \boldsymbol{\Sigma}_{\boldsymbol{v},21} & \boldsymbol{\Sigma}_{\boldsymbol{v},22} \end{bmatrix} \text{ and } \boldsymbol{\Sigma}_{\boldsymbol{v},n-1} = \boldsymbol{\Sigma}_{\boldsymbol{v},11}$$

Thus, the components of $\boldsymbol{A}$ can be retrieved as functions of $\boldsymbol{\Sigma}_{\boldsymbol{v},11}, \boldsymbol{\Sigma}_{\boldsymbol{v},12}, \boldsymbol{\Sigma}_{\boldsymbol{v},21}$, and

$\boldsymbol{\Sigma}_{\boldsymbol{v},22}$.

$$\begin{aligned}
\boldsymbol{A}_{11} &= -\boldsymbol{\Sigma}_{\boldsymbol{v},11}^{-1} + [\boldsymbol{\Sigma}_{\boldsymbol{v},11}^{-1} + \boldsymbol{\Sigma}_{\boldsymbol{v},11}^{-1}\boldsymbol{\Sigma}_{\boldsymbol{v},12} \\
&\quad \times (\boldsymbol{\Sigma}_{\boldsymbol{v},22} - \boldsymbol{\Sigma}_{\boldsymbol{v},21}\boldsymbol{\Sigma}_{\boldsymbol{v},11}^{-1}\boldsymbol{\Sigma}_{\boldsymbol{v},12})^{-1}\boldsymbol{\Sigma}_{\boldsymbol{v},21}\boldsymbol{\Sigma}_{\boldsymbol{v},11}^{-1}] \\
&= \boldsymbol{\Sigma}_{\boldsymbol{v},11}^{-1}\boldsymbol{\Sigma}_{\boldsymbol{v},12}\boldsymbol{A}_{22}\boldsymbol{\Sigma}_{\boldsymbol{v},21}\boldsymbol{\Sigma}_{\boldsymbol{v},11}^{-1} \\
\boldsymbol{A}_{12} &= -\boldsymbol{\Sigma}_{\boldsymbol{v},11}^{-1}\boldsymbol{\Sigma}_{\boldsymbol{v},12}(\boldsymbol{\Sigma}_{\boldsymbol{v},22} - \boldsymbol{\Sigma}_{\boldsymbol{v},21}\boldsymbol{\Sigma}_{\boldsymbol{v},11}^{-1}\boldsymbol{\Sigma}_{\boldsymbol{v},12})^{-1} \\
&= -\boldsymbol{\Sigma}_{\boldsymbol{v},11}^{-1}\boldsymbol{\Sigma}_{\boldsymbol{v},12}\boldsymbol{A}_{22} = \boldsymbol{A}_{21}^{T} \\
\boldsymbol{A}_{22} &= (\boldsymbol{\Sigma}_{\boldsymbol{v},22} - \boldsymbol{\Sigma}_{\boldsymbol{v},21}\boldsymbol{\Sigma}_{\boldsymbol{v},11}^{-1}\boldsymbol{\Sigma}_{\boldsymbol{v},12})^{-1}
\end{aligned}$$

If we denote $\alpha = \boldsymbol{A}_{22}$ and $\boldsymbol{\beta} = \boldsymbol{\Sigma}_{\boldsymbol{v},11}^{-1}\boldsymbol{\Sigma}_{\boldsymbol{v},12}$ to simplify the expressions, $\boldsymbol{A}_{11} = \boldsymbol{\beta}\alpha\boldsymbol{\beta}^T$ and $\boldsymbol{A}_{12} = \boldsymbol{A}_{21}^T = -\boldsymbol{\beta}\alpha$, where α is a positive scalar because $\boldsymbol{A}_{22}$ is a 1×1 matrix and $\boldsymbol{\Sigma}_{\boldsymbol{v},n} > 0$ and $\boldsymbol{\Sigma}_{\boldsymbol{v},n}^{-1} > 0$. For $\boldsymbol{A}$ to be positive semi-definite, $\boldsymbol{x}^T\boldsymbol{A}\boldsymbol{x}$ should be nonnegative for any nonzero $n \times 1$ vector, $\boldsymbol{x} = [\boldsymbol{x}_1^T x_2]^T$, where $\boldsymbol{x}_1$ is an $(n-1) \times 1$ vector and x_2 is a scalar.

$$\begin{aligned}
&\boldsymbol{x}^T\boldsymbol{A}\boldsymbol{x} \\
&= \boldsymbol{x}_1^T\boldsymbol{A}_{11}\boldsymbol{x}_1 + x_2\boldsymbol{A}_{21}\boldsymbol{x}_1 + \boldsymbol{x}_1^T\boldsymbol{A}_{12}x_2 + x_2\boldsymbol{A}_{22}x_2 \\
&= \boldsymbol{x}_1^T\boldsymbol{\beta}\alpha\boldsymbol{\beta}^T\boldsymbol{x}_1 + x_2(-\alpha\boldsymbol{\beta}^T)\boldsymbol{x}_1 + \boldsymbol{x}_1^T(-\boldsymbol{\beta}\alpha)x_2 + x_2\alpha x_2 \\
&= \alpha\left(\boldsymbol{x}_1^T\boldsymbol{\beta}\boldsymbol{\beta}^T\boldsymbol{x}_1 - x_2\boldsymbol{\beta}^T\boldsymbol{x}_1 - \boldsymbol{x}_1^T\boldsymbol{\beta}x_2 + x_2^2\right) \\
&= \alpha(\boldsymbol{\beta}^T\boldsymbol{x}_1 - x_2)^T(\boldsymbol{\beta}^T\boldsymbol{x}_1 - x_2) \\
&\geq 0
\end{aligned} \tag{C.4}$$

Because $\boldsymbol{A}$ is shown to be positive semi-definite as is $\boldsymbol{A}^{-1}$, the residual in Equation (C.3) is negative definite.

$$-\boldsymbol{\Sigma}_{\hat{\boldsymbol{\theta}},n-1}\boldsymbol{G}_n^T(\boldsymbol{A}^{-1} + \boldsymbol{G}_n\boldsymbol{\Sigma}_{\hat{\boldsymbol{\theta}},n-1}\boldsymbol{G}_n^T)^{-1}\boldsymbol{G}_n\boldsymbol{\Sigma}_{\hat{\boldsymbol{\theta}},n-1} < 0 \tag{C.5}$$

Therefore, the difference between position variances are always negative definite

$$\boldsymbol{\Sigma}_{\hat{\boldsymbol{\theta}},n} < \boldsymbol{\Sigma}_{\hat{\boldsymbol{\theta}},n-1} \tag{C.6}$$

for $n > 4$, because at least four measurements are required for three dimensional positioning. Consequently, their traces are in the same order [66], [67].

$$tr(\mathbf{\Sigma}_{\hat{\boldsymbol{\theta}},n}) < tr(\mathbf{\Sigma}_{\hat{\boldsymbol{\theta}},n-1}) \tag{C.7}$$

The square root sums of these traces are called weighted dilution of precision (WDOP) [62]. Since WDOP is a scaler from range domain errors to position domain errors, lower WDOP indicates lower position errors. Thus, WDOP also follows the monotonic decrease of the traces.

$$\text{WDOP}_n < \text{WDOP}_{n-1} \tag{C.8}$$

Equation (C.6), (C.7), and (C.8) have proved the negative definiteness of position variance and the monotonic decrease of WDOP with respect to the number of ranging sources.

Appendix D

Glossary

AGPS Assisted GPS or Aided GPS

AOA Angle of Arrival

ATSC American Television Standard Committee

BOC Binary Offset Code

CDF Cumulative Distribution Function

CDMA Code Division Multiple Access

CEP Circular Error Probable, a median horizontal positioning error

CORS Continuously Operating Reference Stations

DME Distance Measurement Equipment

DOP Dilution of Precision

DRMS Distance Root Mean Squared error

DVB Digital Video Broadcasting

FCC Federal Communications Commission

FDMA Frequency Division Multiple Access

GBAS Ground Based Augmentation System

GCR Ghost Canceling Reference, time referencing signal for analog television

GEO Geostationary Earth Orbit

GNSS Global Navigation Satellite Systems

GPRS GSM Packet Radio System

GPS Global Positioning System

GSM Global System for Mobile communication

HAL Horizontal Alert Limit

HDOP Horizontal Dilution of Precision

HPL Horizontal Protection Level

ILS Instrument Landing System

INS Inertial Navigation System

ISDB Integrated Services Digital Broadcasting

ISM Industrial, Scientific, and Medical bands

LAI Location Area Identifier, user coordinates from the GSM network

LEO Low Earth Orbit

LLA Latitude, Longitude and Altitude

Loran LOng RAnge Navigation system

MEO Medium Earth Orbit

MHSS Multi-Hypothesis Solution Separation

MLS Microwave Landing System

NGS U.S. National Geodetic Survey

NTSC National Television Standard Committee

OCXO Oven Compensated Crystal Oscillators

PAL Phase Alternating Line

PCS Personal Communication Service

QZSS Quasi-Zenith Satellite System

RAIM Receiver Autonomous Integrity Monitoring

RF Radio Frequency

RFID Radio Frequency Identification

RMS Root Mean Squared error

RSSI Received Signal Strength Indicator

SBAS Space Based Augmentation System

SECAM color sequential with memory

TACAN Tactical Air Navigation

TCXO Temperature Compensated Crystal Oscillators

TDMA Time Division Multiple Access

TOA Time of Arrival

UHF Ultra High Frequency

VDOP Vertical Dilution of Precision

VHF Very High Frequency

VOR VHF Omnidirectional Range

VSB Vestigial Sideband Modulation

Bibliography

[1] J. Do, M. Rabinowitz, and P. Enge, "Robustness of TOA and TDOA Positioning underSub-Optimal Weighting Conditions," *IEEE TAES (Transactions on Aerospace and Electronic Systems)*, Vol. 43, No. 3, pp. 1177–1180, July 2007

[2] J. Do, M. Rabinowitz, and P. Enge, "Multi-Fault Tolerant RAIM Algorithm for Hybrid GPS/TV Positioning," *Proc. ION National Technical Meeting*, pp. 788–797, San Diego, January 2007

[3] J. Do, M. Rabinowitz, and P. Enge, "Performance of Hybrid Positioning System Combining GPS and Television Signals," *Proc. IEEE/ION Position Location and Navigation Symposium*, pp. 556–564, San Diego, April 2006

[4] J. Do, M. Rabinowitz, and P. Enge, "Performance of TOA and TDOA in a non-homogeneous transmitter network combining GPS and terrestrial signals," *Proc. ION National Technical Meeting* 2006, pp. 642–649, Monterey, January 2006

[5] J. Do, M. Rabinowitz, and P. Enge, "Linear Time-of-Arrival Estimation in a Multipath Environment by Inverse Correlation Method," *Proc. ION Annual Meeting*, pp. 720-725, Cambridge, June 2005

[6] J. Do, D. Akos, and P. Enge, "L and S bands spectrum survey in the San Francisco bay area," *Proc. IEEE Position Location and Navigation Symposium (PLANS) 2004*, pp. 566–572, April 2004

[7] P. Enge, D. Akos, J. Do, J. Simoneau, L. P. Wilson, and V. Seetharam, "Measurements of Man-Made Spectrum Noise Floor," *National Aeronautics and Space Administration*, CR-2004-213551, November 2004

[8] Federal Communication Commission (FCC) Office of Engineering and Technonology Policy and Rules Division, "FCC online table of frequency allocations," *Federal Communication Commission*, 47 C.F.R. 2.106, May 2007

[9] Steven Cherry, "Total Recall," *IEEE Spectrum*, November 2005

[10] Per Enge et al., "Terrestrial radionavigation technologies," *ION Navigation*, Vol. 42, No. 1, 1995

[11] G. Linn Roth et al., "Enhanced or eLoran for time and frequency applications," *IEEE Proc. Frequency Control Symposium and Exposition*, pp. 816–823, Aug. 2005

[12] ARINC research corp., *ICD-GPS-200: Navstar GPS Space Segment/Navigation User Interfaces*, El Segundo, 2000

[13] B. Parkinson and J. Spilker, *Global Positioning System: Theory and Applications.* AIAA, 1996

[14] P. Misra and P. Enge, *Global Positioning System: Signals, Measurements, and Performance.* Massachusetts: Ganga-Jamuna Press, 2006

[15] E. D. Kaplan, *Understanding GPS Principles and Applications,* Boston: Artech House, 1996.

[16] B. C. Barker et al., "Overview of the GPS M Code Signal," *Proc. ION National Technical Meeting*, pp. 542–549, Anaheim, January 2000

[17] R. D. Fontana et al., "The New L2 Civil Signal," *Proc. International Technical Meeting of the Satellite Division of the Institute of Navigation ION GPS 2001*, pp. 617–631, Salt Lake City, September 2001

[18] European Space Agency / Galileo Joint Undertaking, *Galileo Open Service Signal In Space Interface Control Document (OS SIS ICD) Draft 0*, 2006

[19] Grace Xingxin Gao et al., "GNSS Over China: The Compass MEO Satellite Codes," *InsideGNSS*, July/August issue, pp. 36–43, July 2007

[20] D. G. Luenberger, *Linear and nonliner programming,* Menlo Park, California, second edition, 1987

[21] M. Rabinowitz and J.J. Spilker, Jr., "A new positioning system using television synchronization signals," *IEEE Trans. Broadcasting*, Vol. 51, No. 1, pp. 51–61, March 2005

[22] M. Rabinowitz and J.J. Spilker, Jr., "Is a next generation positioning technology necessary," *Rosum white paper*, June 2002

[23] J.J. Spilker, Jr., "DTV Monitor System Unit," *Rosum Internal Memorandum*, May 2001.

[24] J.J. Spilker, Jr., "Position location range and SNR performance," *Rosum Internal Memorandum*, April 2001.

[25] J.J. Spilker, Jr., "Location performance comparison GPS vs. DTV," *Rosum Internal Memorandum*, December 2001.

[26] D. A. Burgess and M. Rabinowitz, "A review of error sources," *Rosum Internal Memorandum*, March 2003.

[27] Advanced Television Systems Committee (ATSC) Technology Group on Distribution (T3), "ATSC digital television standard with amendment No. 1," ATSC Document A/53, September 1995.

[28] European Broadcasting Union, "Digital video broadcasting (DVB), framing structure, channel coding and modulation for digital terrestrial television," ETSI EN 300 744 v1.3.1, January 2001.

[29] 3GPP Technical Specification Group (TSG), Services and System Aspects, TS 22.071, "Location Services (LCS); Service description; Stage 1 (Release 7)," v7.4.0, December 2005

[30] 3GPP2 C.S0022-A Version 1.0, "Position Determination Service for cdma2000 Spread Spectrum Systems," March 2004

[31] W. Buchanan, J. Munoz, R. Manson, and K. Raja, "Analysis and migration of location-finding methods for GSM and 3G networks," *IEE Proc. 5th IEE International Conference on 3G Mobile Communication Technologies*, pp. 352–358, 2004

[32] D. Porcino, "Location of third generation mobile devices: a comparison between terrestrial and satellite positioning systems," *IEEE Proc. 53rd VTC*, Vol. 4, pp. 2970–2974, May 2001

[33] R. Yamasaki, A. Ogino, T. Tamaki, T. Uta, N. Matsuzawa, and T. Kato, "TDOA location system for IEEE 802.11b WLAN," *IEEE Proc. WCNC*, Vol. 4, pp. 2338–2343, Mar. 2005

[34] P. Bahl and V. N. Padmanabhan, "RADAR: An in-building RF-based user location and tracking system," *IEEE Proc. infocom*, Vol. 2, pp. 775–784, Mar. 2000

[35] Department of Commerce, *Radio Frequency Identification: Opportunities and Challenges in Implementation*, Washington D.C., April 2005

[36] D. W. Allan, M. A. Weiss, and J. L. Jespersen, "A Frequency-Domain View of Time-Domain Characterization of Clocks and Time and Frequency Distribution Systems," *Proceedings of the Fourty-Fifth Annual Symposium on Frequency Control*, pp. 667–678, May 1991.

[37] D. W. Allan, et al., *The Science of Timekeeping*, HP Application Note 1289, 1997

[38] B. E. Blair, *Time and Frequency: Theory and Fundamentals*, pp. 153–191, National Bureau of Standards, 1974.

[39] P. Lesage and C. Audoin, "Characterization and Measurement of Time and Frequency Stability," *Radio Science*, Vol. 14, No. 4, pp. 521–539, 1979.

[40] A. Leon-Garcia, *Probability and Random Processes for Electrical Engineering*, pp. 403–449, Massachusetts, Addison-Wesley, 1994.

[41] J. S. Cho, "Terrestrial-DMB adds color to Korean lifestyle," *The Korea Times*, February 12, 2006

[42] L. R. Weill, "Multipath Mitigation Using Modernized GPS Signals: How Good Can It Get?" *Proc. ION GPS* 2002, pp. 493–505, Sept. 2002

[43] I. P. Kirsteins, "High Resolution Time Delay Estimation," *IEEE Proc. ICASSP* 87, pp. 451–454, Apr. 1987

[44] D. W. Tufts and R. Kumaresan, "Estimation of Frequencies of Multiple Sinusoids: Making linear prediction perform like maximum likelihood," *Proc. IEEE*, Vol. 70, pp. 975–989, Sept. 1982.

[45] R. J. Vaccaro, T. Manickam, C. S. Ramalingam, R. Kumaresan, D. W. Tufts, "Least-Squares Time-of-Arrival Estimation for Transient Signals in a Multipath Environment," *IEEE Proc. Asilomar Conference* 1991, Vol. 2, pp. 1098–1102, Nov. 1991.

[46] J. Werb and C. Lanzl, "Designing a positioning system for finding things and people indoors," *IEEE Spec.*, Vol. 35, No. 9, pp 71–78, September 1998

[47] Frank van Diggelan, "Indoor GPS technology," *CTIA Wireless-Agenda*, Dallas, May 2001

[48] N.F. Krasner, G. Marshall, W. Riley, "Position determination using hybrid GPS/cellphone ranging," *Proc. International Technical Meeting of the Satellite Division of the Institute of Navigation ION GPS 2002*, pp. 165–176, Portland, September, 2002

[49] Jimmy LaMance et al, "Assisted GPS: a low infrastructure approach," *GPS World*, March 2002

[50] Snaptrack, "Location Technologies for GSM, GPRS and UMTS networks," 2003

[51] Z. Biacs et al., "The Qualcomm/Snaptrack wireless GPS hybrid positioning system and results from initial commercial deployments," *Proc. International Technical Meeting of the Satellite Division of the Institute of Navigation ION GPS 2002*, pp. 378–384, Portland, September, 2002

[52] J. Carroll, "Performance analysis of an integrated GPS/Loran-C tracking system," *Proc. National Technical Meeting of the Institute of Navigation*, pp. 615–628, Monterey, January 2006

[53] W. Lindlohr and D. Wells, "GPS design using undifferenced carrier beat phase observations," *Manuscripta Geodaetica* 1985, Vol. 10, pp. 255–295

[54] B. Schaffrin and E. Grafarend, "Generating classes of equivalent linear models by nuisance parameter elimination: Application to GPS observations," *Manuscripta Geodaetica* 1986, Vol. 11, pp. 262–271

[55] D. H. Shin, S. B. Son, and T. K. Sung, "DOP relationship between the TOA and the TDOA positioning," *Proc. ION Annual Meeting* 2000, pp. 436–442, June 2000

[56] C. Park, I. Kim, G. I. Jee, and J. G. Lee, "Relationships between positioning error measures in global positioning system," *AIAA Journal of Guidance, Control, and Dynamics*, Vol. 20, No. 5, pp. 1045–1047, 1997

[57] C. Park and I. Kim, "Comments on—Relationship between dilution of precision for point positioning and for relative positioning with GPS," *IEEE Trans. Aerospace and Electronic Systems*, Vol. 36, No. 1, pp. 73–74, Jan. 2000

[58] R. O. Nielsen, "Relationship between dilution of precision for point positioning and for relative positioning with GPS," *IEEE Trans. Aerospace and Electronic Systems*, Vol. 33, No. 1, pp. 333–337, Jan. 1997

[59] P. J. G. Teunissen, "A proof of Nielsen's conjecture on the GPS dilution of precision," *IEEE Trans. Aerospace and Electronic Systems*, Vol. 34, No. 2, pp. 693–695, Apr. 1998

[60] P. J. Duffett-Smith and P. Hansen, "Precise time transfer in a mobile radio terminal," *Proc. ION National Technical Meeting* 2005, pp. 1101–1106, San Diego, Jan 2005

[61] S. M. Kay, *Fundamentals of Statistical Signal Processing: Estimation Theory.* New Jersey: Prentice Hall, 1993

[62] H. Sairo, D. Akopian, and J. Takala, "Weighted dilution of precision as quality measure in satellite positioning," *IEE Proc. Radar Sonar Navig.*, Vol. 150, No. 6, pp. 430–436, Dec. 2003

[63] J. D. Bard and F. M. Ham, "Time difference of arrival dilution of precision and applications," *IEEE Trans. Signal Processing*, Vol. 47, No. 2, pp. 521–523, Feb. 1999

[64] C. Park, I. Kim, J. G. Lee, and G. I. Jee, "A satellite selection criterion incorporating the effect of elevation angles in GPS positioning," *Control Eng. Pract.*, Vol. 4, No. 12, pp. 1741–1746, 1996

[65] United States Coast Guard Navigation Center, *Navstar GPS User Equipment Introduction, Public Release Version.* United States Coast Guard Navigation Center, Sept. 1996.

[66] G. Strang and K. Borre, *Linear Algebra, Geodesy, and GPS.* Massachusetts: Wellesley-Cambridge Press, 1997

[67] R. A. Horn and C. R. Johnson, *Matrix Analysis.* Cambridge: Cambridge University Press, 1987

[68] R. G. Brown, "A baseline GPS RAIM scheme and a note on the equivalence of three RAIM methods," *ION Navigation*, Vol. 39, No. 3, Fall 1992.

[69] R. G. Brown, "GPS RAIM: calculation of threshold and protection radius using chi-square methods—a geometric approach," *RTCA*, 491-94/SC159-584, December 1994.

[70] B. Pervan, S. Pullen, and J. Christie, "A multiple hypothesis approach to satellite navigation integrity," *ION Navigation*, Vol. 45, No. 1, Spring 1998.

[71] A. Enu, J. Blanch, and T. Walter, "Galileo-GPS RAIM for vertical guidance," *Proc. ION National Technical Meeting* 2006, pp. 432–440, Monterey, January 2006.

[72] M. Sturza, "Navigation system integrity monitoring using redundant measurements," *ION Navigation*, Vol. 35, No. 4, Winter 1988-89.

[73] F. van Diggelen and A. Brown, "Mathematical aspects of GPS RAIM," *IEEE Proc. Position Location and Navigation Symposium (PLANS) 2004*, pp. 733–738, April 1994 .

[74] R. J. Kelly, "The linear model, RNP, and the near-optimum fault detection and exclusion algorithm," *Global Positioning System: Papers Published in NAVIGATION Volume V*, Alexandria: The Institute of Navigation, 1998.

[75] Novatel, "GPS Position Accuracy Measures," *APN-029*, Rev 1, December 2003.

[76] T. M. Cover and J. A. Thomas, *Elements of Information Theory.* New York: Wiley, 1991.

[77] B. Sklar, *Digital Communications Fundamental and Applications.* New Jersey: Prentice Hall, 2001.

[78] T. Rappaport, *Wireless Communications Principles and Practice.* New Jersey: Prentice Hall, 1999.

[79] D. L. Mills, "Network Time Protocol (Version 3) Specification, Implementation and Analysis. Request for Comments 1305," ,1992

[80] D. L. Mills, "Network Time Protocol Version 4 Reference and Implementation Guide," *Technical Report 06-6-1 University of Delaware*, June 2006